Spring 1-1-2012

Critical Dynamics in Complex Excitable Networks

Daniel Benjamin Larremore
University of Colorado at Boulder, daniel.larremore@colorado.edu

Critical Dynamics in Complex Excitable Networks

by

Daniel B. Larremore

B.S., Washington University in St. Louis, 2005

M.S., University of Colorado, 2009

A thesis submitted to the

Faculty of the Graduate School of the

University of Colorado in partial fulfillment

of the requirements for the degree of

Doctor of Philosophy

Department of Applied Mathematics

2012

This thesis entitled:
Critical Dynamics in Complex Excitable Networks
written by Daniel B. Larremore
has been approved for the Department of Applied Mathematics

Prof. Juan G. Restrepo

Prof. James Meiss

Date

The final copy of this thesis has been examined by the signatories, and we find that both the content and the form meet acceptable presentation standards of scholarly work in the above mentioned discipline.

Larremore, Daniel B. (Ph.D., Applied Mathematics)

Critical Dynamics in Complex Excitable Networks

Thesis directed by Prof. Juan G. Restrepo

We study the effect of network structure on the dynamical response of networks of coupled discrete-state excitable elements to two distinct types of stimulus. First, we consider networks which are stochastically stimulated by an external source. Such systems have been used as toy models for the dynamics of some human sensory neuronal networks and neuron cultures. The collective dynamics of such systems depends on the topology of the connections in the network. Here we develop a general theoretical approach to study the effects of network topology on dynamic range, which quantifies the range of stimulus intensities resulting in distinguishable network responses. We find that the largest eigenvalue of the weighted network adjacency matrix governs the network dynamic range. Specifically, a largest eigenvalue equal to one corresponds to a critical regime with maximum dynamic range. This result appears to hold for random, all-to-all, and scale free topologies, and is robust to the inclusion of time delays and refractory states. We gain deeper insight into the effects of network topology using a nonlinear analysis in terms of additional spectral properties of the adjacency matrix. We find that homogeneous networks can reach a higher dynamic range than those with heterogeneous topology. Second, we consider networks stimulated only once at a single node, with dynamics allowed to evolve without additional stimulus. Each realization of such a process will create a cascade of activity of varying duration and size. We analyze the distributions of cascade size and duration in complex networks resulting from a single nodal excitation, finding that when the largest eigenvalue is equal to one, so-called "critical avalanches" are power-law distributed in size, with exponent -3/2, and power-law distributed in duration, with exponent -2. We employ techniques from dynamical systems to recover the differences among avalanches started at different network nodes, also deriving distributions for avalanches in subcritical and supercritical regimes.

Dedication

This work is dedicated, with love and respect, to my grandparents, Dr. Sidney and Ruth Weiss, and Ted and Billie Larremore, who brought imagination, warmth, and a love of mathematics into my life, and taught me how to be a *mensch*.

Acknowledgements

I would first and foremost like to thank Professor Juan Gabriel Restrepo. He has been supportive and encouraging from the first day that I walked into his office. I feel lucky to have had the opportunity to learn how he approaches ideas and problems, and I optimistically hope that perhaps some of his cleverness will take root in my future work.

I would also like to thank my parents for everything they have done, keeping me well fed in every sense, from day one.

Daniel Noven and Saverio Spagnolie deserve a special acknowledgement, for without their timely and wise intervention, I would be a lawyer by now.

Over the years, I have been helped by many of my peers, including Daniel Kaslovsky, Ryan Lewis, Sebastian Skardal, Dane Taylor, and Brock Mosovsky. Thank you all for being superb friends and colleagues. I would also like to thank Dr. Jim Curry, Anne Dougherty, and Adam Norris, for being fantastically nice people. When I see any of you in the halls of the Department, you make me feel like a family.

Finally, Laura, thank you for being a source of reassurance and love. I am looking forward to collaborating on a great many things with you.

Contents

Chapter

1 Introduction 1

1.1 Introduction to complex networks 1

1.1.1 Adjacency matrix 4

1.1.2 Degree distribution 4

1.1.3 Degree correlations 6

1.1.4 Network models 10

1.1.5 The Perron-Frobenius Theorem 14

1.2 Excitable dynamics on complex networks 16

1.2.1 Biological neuron models 17

1.2.2 Description of the model 20

1.2.3 Neuronal network dynamics in the literature 22

1.3 Publication Note 27

2 Predicting criticality and dynamic range in complex networks:

effects of topology 28

2.1 Introduction 28

2.2 Model Dynamics 29

2.3 Perturbative analysis 33

2.4 Numerical Simulations 37

2.5 Impact on Dynamic Range 40
2.6 Discussion 43
2.7 Appendix: approximation of product by exponential 45

3 Effects of network topology, transmission delays, and refractoriness on the response of coupled excitable systems to a stochastic stimulus 47
3.1 Introduction 48
3.2 Background 49
3.3 Generalized Kinouchi-Copelli model 51
3.3.1 Description of the model 51
3.3.2 Model dynamics 52
3.4 Analysis 53
3.4.1 Steady-state response 53
3.4.2 Perturbative approximations 55
3.4.3 Dynamics near the critical regime 57
3.4.4 Relation to previous results 58
3.5 Dynamic Range 59
3.6 Numerical experiments 61
3.6.1 Construction of networks 61
3.6.2 Results of numerical experiments 63
3.6.3 Validity of the approximation $Ap \propto u$ 67
3.7 Discussion 70

4 Statistical Properties of Avalanches in Networks 74
4.1 Formulation 76
4.2 Distribution of Avalanche Durations 77
4.2.1 Subcritical Networks ($\lambda < 1$) 79
4.2.2 Supercritical networks ($\lambda > 1$) 80

4.2.3 Critical Networks ($\lambda = 1$) 82
4.3 Distribution of Avalanche Sizes 83
4.4 Numerical Experiments 89
4.5 Discussion 94
4.6 Appendix: probability of finite avalanche durations 98
4.7 Appendix: $\lambda > 1 \rightarrow \lambda_D < 1$ 100

5 Concluding Remarks 102
5.1 Summary of Main Results 102
5.2 Key assumptions and their roles 103
5.3 Opportunities for future research 104

Bibliography 107

Figures

Figure

1.1 A collection of recipes may be represented as a network of ingredients in different ways. By convention nodes are shown as circles and links as lines or arrows. If multiple links are allowed, the network is not simple (upper right). If multiple links (and self-links) are not allowed, and all links are of equal strength the network is simple and unweighted (bottom left). If multiple links and self-links are not allowed, but some links are stronger than others (represented by the bold link), the network is simple and weighted. Since links in all three networks have no direction (or are bi-directional), all three networks are undirected. The decision of which type of network to use depends on the intended use of the network. To aid the eye, we have colored the two recipes so the reader may more easily see from which recipe each link is derived. 3

1.2 Complex networks are networks whose topologies are non-trivial. An example of a complex network is shown (top) as well as two networks that are not complex: a ring (left) and a lattice (right). 5

1.3 For unweighted networks, the in- and out-degree of a node are the integer numbers of incoming and outgoing links, respectively. In the diagram above, an unweighted network is shown with in-degree inside each node and out-degree next to each node. The nodes are labeled with letters which correspond to rows and columns in the adjacency matrix. The networks is directed and so the adjacency matrix need not be symmetric, as shown. The row sum and column sum corresponding to node a are shown, demonstrating Eq. (1.3). 7

1.4 Diagram showing examples of the types of links that one might observe in networks with particular η and ρ values. (a) node in- and out-degree are anti correlated, (b) node in- and out-degree are correlated, (c) in-degree at node n is correlated with out-degree at node m, and (d) in-degree at node n is anti-correlated with out-degree at node m. Figure reproduced from [1]. 9

1.5 In an implementation of the Erdős-Rényi model (top), each of the possible links (dashed lines) is chosen to exist independently with some probability p (top left). Chosen links are placed in the network (top right) resulting in a draw from the ensemble of networks with N nodes and expected number of links Np. In an implementation of the configuration model (bottom), each node is given a number of "stubs" corresponding to its intended degree (bottom left, solid lines). Pairs of stubs are chosen randomly to be connected (bottom left, grey sketch lines) resulting in a draw from the ensemble of networks with N nodes and degree sequence K (bottom right). 13

1.6 A network diagram (top right) and corresponding adjacency matrix (top left) are shown, along with the eigenvalue and corresponding eigenvectors (to four digits of accuracy) guaranteed by the Perron-Frobenius (PF) theorem [2]. The conditions of the theorem apply because (i) the entries of the adjacency matrix are non-negative and (ii) any node in the network is accessible from any other node in the network via a directed path which guarantees an irreducible matrix. Note that the eigenvalue is real and positive, and the eigenvector entries are strictly positive. 15

1.7 Spectrum of a 500×500 unweighted network adjacency matrix corresponding to an Erdős-Rényi random network with $p = 0.1$, reproduced from Ref. [3] 16

1.8 The Hodgkin-Huxley model as published in the final paper of their 1951–1952 series [4] describes the relationship between current I, capacitance C, and voltage V, where subscripts correspond to sodium (Na), potassium (K), and leak (l). All instances of α, β, and $\bar{g}$ are constants which Hodgkin and Huxley estimated exhaustively from experimental data. They were awarded a Nobel Prize in Medicine in 1963 along with John Eccles who made enormous advancements regarding the neuronal synapse. . . 18

1.9 The states of the version of the Greenberg-Hastings Cellular automaton (bottom) studied in the chapters below are meant to mimic discretized states of a neuron (top). 21

1.10 Recordings of many cascades of spontaneous activity in slices of neonatal rat cortex show a fascinating organization when viewed as a histogram of cascade sizes, measured both by number of recording electrodes stimulated (D) and by accumulated potential in microVolts (F). On the log-log scale, the red dotted line is a reference for a power law, exponent $-3/2$. The colors correspond to different subsampling of the total number of electrodes, as shown in the diagram inset (D). Figure reproduced from figure 4 of [5]. 24

2.1 Schematic illustration of the definition of dynamic range in the active network case. The baseline and saturation values are F_0 and F_1, respectively. Two threshold values, denoted by F_{low} and F_{high}, respectively, are used to determine the range of values of η defined as the *dynamic range* Δ. 32

2.2 Dynamic range (Δ) is maximized when the mean degree (σ, Eq. (2.3)) is equal to one in excitable Erdős-Rényi random networks without degree correlations, reproduced from [6]. 34

2.3 (a) Response F vs. stimulus η for power law networks with exponent $\gamma = 2.5$ and no correlation between k^{in} and k^{out}. Eq. (2.13) (lines) captures much of the behavior of the simulation (circles), particularly for low levels of η and F, as expected from approximating Eq. (2.2). (b) Dynamic range Δ is maximized at $\lambda = 1$ in both simulation results (circles) and Eq. (2.11) (line). This result compares quite favorably in trend with the dynamic range result for Erdős-Rényi random networks [6] reproduced in Fig. 2.2 and the dynamic range result for in vitro measurements of the dynamic range of slices of neonatal rat cortex [7] reproduced in Fig. 2.4. 39

2.4 Dynamic range (Δ) is maximized when the in vitro neonatal rat cortex is stimulated in the absence of drugs (black symbols). When drugs are added which suppress excitatory neurons, dynamic range decreases (blue symbols). Similarly, dynamic range decreases when drugs are added whic suppress inhibitory neurons (red symbols). The horizontal axis κ is a statistical measure devised *ad hoc* in [7] to measure deviation away from the critical state in which neuronal avalanches occur. Figure reproduced from [7]. 41

2.5 $F_{\eta\to 0}$ obtained from direct numerical simulation of the Kinouchi-Copelli model (symbols) plotted against $\langle d\rangle$ (a, b) and λ (c). Blue solid lines result from iterating Eq. (2.2) and green dashed lines result from Eq. (2.12). Small arrows show where $\lambda = 1$ predicts a phase transition. (a) A set of random networks (category 3) showing that criticality occurs at $\lambda = 1$ (arrow), but not $\langle k\rangle = 1$. (b) Criticality in scale free networks (category 4) with node degree correlation also occurs at $\lambda = 1$ (arrow), but not $\langle k\rangle = 1$. (c) Category 5 networks are tuned through criticality by changing assortativity, without changing the degree distributions and fixed $\langle k\rangle = 1$. 42

2.6 For power-law degree distributions with $\lambda = 1$, peak dynamic range increases monotonically with network homogeneity, as measured by power law exponent γ. Simulations (circles) agree well with our predictions [Eq. (2.18); line]. 44

3.1 Semi-log plots of data from five simulations (symbols) testing a variety of situations in order to show the robustness of Eq. (3.17) (lines) to various sets of conditions: (1) Random network; $\lambda = 1$; mixed refractory states, $m_i \in \{1, 2, 3\}$; no delays; (2) Random network; $\lambda = 0.7$; no refractory states, $m_i = m = 1$; mixed delays, $\tau_{ij} \in \{0, 1, 2, 3\}$; (3) Scale free network; $\lambda = 0.8$; disassortative rewiring; no refractory states, $m_i = m = 1$; no delays; (4) Scale free network; $\lambda = 1.2$; uniform refractory states, $m_i = m = 2$; no delays; (5) Scale free network; $\lambda = 1.0$; mixed refractory states, $m_i \in \{1, 2, 3, 4\}$; mixed delays, $\tau_{ij} \in \{0, 1, 2\}$; (6) Scale free network; $\lambda = 1.2$; uniform refractory states, $m_i = m = 1$; no delays. The plots show excellent agreement between prediction and simulation at many points in parameter space. . . 62

3.2 Simulation data for networks with power-law degree distribution comprising 10^4 nodes (symbols) and numerical solution of Eq. 3.17 (lines). (a) Stimulus vs response predictions agree well in the regime where $Ap \approx su$, as discussed in section 3.6.3. Eigenvalues range from 0.2 to 0.9 (blue squares), exactly 1.0 (red diamonds), and from 1.1 to 1.8 (black circles). (b) Dynamic range predictions capture maximization at $\lambda = 1$ as well as the non-critical behavior. 65

3.3 Phase transitions of $F_{\eta \to 0}$ for different refractory states, m for simulations (symbols) and Eq. (3.17) (lines). Inset: Eq. (3.21) predicts that phase transitions should scale by $\langle m + 1/2 \rangle^{-1}$, confirmed by rescaling data from the larger plot accordingly. 66

3.4 Simulation data (symbols) compare reasonably with the prediction of the perturbative approximation close to saturation, Eq. 3.23, for different refractory states. $\delta\eta$ was chosen to be the difference between $\eta = 10^0$ and $\eta = 10^{-0.1}$, corresponding to the two rightmost data points of each simulation. 68

3.5 Time series (solid lines) for initial growth of signals within four active networks, with growth rates from Eq. (3.23) shown (dotted lines). The timesteps shown on the horizontal axis have been shifted to display multiple results together, but not rescaled or distorted. In less than 100 timesteps, all networks tested exhausted the exponential growth regime. N=100000 nodes and $\eta = 10^{-6}$, for (1) $\lambda = 1.1$, $\tau = 0$, (2) $\lambda = 1.2$, $\tau = 0$, (3) $\lambda = 1.1$, $\tau \in \{0, 1, 2, 3\}$, (4) $\lambda = 1.2$, $\tau \in \{0, 1, 2, 3\}$. 69

3.6 Plots of normalized Ap_i vs su_i for scale-free networks, with eigenvalues 0.6 (blue, top row), 1.0 (red, middle row), and 1.2 with assortative mixing (black, bottom row) at stimulus levels $\eta = 10^{-5}, 10^{-3}$,and 1 for the left, middle, and center columns respectively. Agreement is very good for critical and active cases, with more noise in the quiescent case due to less incoming stimuli over the duration of the simulation. 71

4.1 An example avalanche is shown, where circles represent nodes, arrows represent links, and numbers inside nodes correspond to the time step at which each node is activated. Starting from a single excited node, labeled 1, the avalanche spreads to two other nodes, labeled 2, and so on. Note that the presence of a link does not guarantee the transmission of excitation. The example avalanche above lasts for five time steps and excited a total of six nodes in addition to the initial node, so $d = 5$ and $x = 7$. 78

4.2 Histograms of avalanche durations shown above for networks of $N = 10^5$ nodes with power law degree distribution, exponent $\gamma = 3.5$ with Perron-Frobenius eigenvalues of $\lambda = 0.9$ (left), $\lambda = 1.0$ (center) and $\lambda = 1.1$ (right). Symbols show the number of avalanches having duration d from a single simulation of 10^6, $2 \cdot 10^6$, and 10^6 avalanches, respectively, from left to right. Dashed lines provide a reference for the theoretical predictions described in Eqs. (4.7), (4.23), and (4.13). Note that the vertical position of the dashed lines was chosen arbitrarily. Due to predictions of exponential decay for the sub- and super-critical cases, the left and right plots are plotted on a log-linear scale, while the center plot is plotted on a log-log scale to show the power-law decay. Infinite duration avalanches in the supercritical case (right) are not displayed in the figure. 86

4.3 Histograms of avalanche sizes shown above for networks of $N = 10^5$ nodes with power law degree distribution, exponent $\gamma = 3.5$ with Perron-Frobenius eigenvalues of $\lambda = 0.9$ (left), $\lambda = 1.0$ (center) and $\lambda = 1.1$ (right) on a log-log scale. Symbols show the number of avalanches having size x from a single simulation of 10^6, $2 \cdot 10^6$, and 10^6 avalanches, respectively, from left to right. Dashed lines provide a reference for the theoretical prediction $x^{-3/2} \exp(-x/x^*)$ described in Eqs. (4.44) and (4.45). Note that the vertical position of the dashed lines was chosen arbitrarily. Infinite size avalanches in the supercritical case (right) are not represented in the data set. Agreement between theoretical prediction and measurement is excellent despite finite sample size noise. 87

4.4 A comparison of predicted duration decay rates (Eq. (4.7) and Eq. (4.13)) (solid line), and numerical simulations (solid circles) plotted against λ, the largest eigenvalue of the network adjacency matrix. Agreement is excellent for both the subcritical and supercritical numerical simulations. 91

4.5 Testing the prediction that avalanche size x is distributed as $x^{-3/2} \exp(-x/x^*)$, we compare the theoretical prediction of x^* (solid line) with x^* estimated via regression on the largest 10% of avalanches from numerical simulations (solid circles, dashed line). Inset, identical data on a magnified domain around $\lambda = 1$. Agreement is excellent for λ near 1, and decreasingly accurate for much larger or smaller λ. 92

4.6 When the Perron-Frobenius eigenvalue λ is larger than one, there is a non-zero probability of an avalanche starting at node n having infinite duration, as predicted by Eq. (4.9). Here we average the finite fraction of avalanches originating from node n over all nodes, showing excellent agreement between the fraction predicted by averaging Eq. (4.9) (solid line) and fraction measured from simulation (solid circles). 95

4.7 Testing the node-specific prediction of Eq. (4.7), avalanches were simulated on a subcritical ($\lambda = 0.95$) and disassortative ($\rho = 0.8$) Erdős Rényi random network with $N = 10^4$ nodes. In the large plot, the fraction of avalanches originating at node n that last longer than 30 time steps, $f_n(30)$ is plotted against the corresponding entry in the right Perron-Frobenius eigenvector, v_n. In the inset, the same values $f_n(30)$ are plotted against the corresponding out-degree k_n^{out}. The eigenvector entry v_n does a significantly better job than out-degree k_n^{out} of predicting the duration of avalanches originating at node n in disassortative networks (shown) and for assortative networks (not shown). 96

5.1 Diagram of a cortical "microcolumn" (left) and cell types with diagram of their differing structure (right), reproduced from [8]. Roman numerals (left) correspond to layers of the cortex. This particular microcolumn diagram can be found in the primary visual cortex of macaque monkeys. 105

5.2 A Nissl-stained slice of human cortex (upper bank of superior temporal sulcus) shows striations which correspond to microcolumns spanning multiple cortical layers, reproduced from [8]. Magnification is $\times 40$. 105

Chapter 1

Introduction

This thesis is composed of five chapters which focus on critical dynamics on complex excitable networks and the relationship between dynamics and network structure. The first chapter consists of two parts. First, we offer a brief background on the subject of complex networks in general, meant for the reader wishing to gain familiarity with terminology and techniques used in later chapters. Second, we provide a description of the excitable systems analyzed in the following chapters. Since the theory developed here is motivated by experimental developments in neuroscience, this section is appropriately set in the context of biological neuron models and includes a description of the relevant literature. The second, third, and fourth chapters cover original research on mathematical models of critical dynamics on complex excitable networks. The fifth chapter discusses these results in the broader contexts of mathematics and neuroscience, highlighting potential future investigations.

1.1 Introduction to complex networks

A network consists of a set of N *nodes* (or vertices) and a set of M *links* (or edges), where each link represents a connection between a pair of nodes. For example, a link $l = \{n, m\}$ is a connection l from node n to node m. In networks where links don't have a specific direction, links are considered as unordered pairs of nodes and we call such networks *undirected*. In networks where links may only point in one direction, links are considered as ordered pairs of nodes, and we call such networks *directed*. If only one link is allowed from node n to node m (no multiple connections) and node n may not link to node n (no self connections), the network is called *simple*.

These definitions can be made more accessible by using a few straightforward demonstrations, where we take observed relationships and use them to construct a network. First consider a network made from the ingredients and recipes in a cookbook. Each ingredient is a node, and when two ingredients appear in the same recipe together we make a link between those ingredients. Such a network would be undirected, because if sugar appears in a common recipe with flour, flour necessarily appears in that same recipe with sugar. If we allow only one link to be created despite multiple mutual appearances of ingredients, the network is simple. If ingredients are allowed to link to each other multiple times, the network is not simple. These two cases are shown in Fig. 1.1. Second, consider a network of business card exchanges between attendees at a conference. Each attendee is a node, and when one attendee John gives another attendee Jane his business card, we make a link from John to Jane, but not from Jane to John. Such a network would be directed because if John gives Jane his card, Jane need not also give John her card.

Additionally, it is often the case that not all links are equal in strength. For example, consider the network of ingredients from the cookbook discussed above. Despite capturing all of the pairwise common occurrences of every ingredient, it may not capture the fact that flour and sugar appear together many more times than flour and bacon. In order to account for this difference, each link may be given a *weight* corresponding to some property of the connection between the elements. Depending on their context, weights may be drawn from a variety of sets, including integer, real, positive, and negative. In the recipe ingredients example, we might choose positive integer values for weights so that the final link weight corresponds to the total number of times the two connected ingredients appear together. This case is also shown in Fig. 1.1. Networks in which links possess weight are called *weighted* whereas networks in which links either exist or they don't are called *unweighted*, or sometimes binary.

Complex networks are networks whose topologies are non-trivial. For example, neither the ring network (nodes connected in a ring) nor a regular 2D lattice are complex networks, but the network formed by the ingredients in the cookbook described above is complex, as shown in Fig. 1.2. Generally, in this thesis, we will describe networks as being complex in order to assure the reader

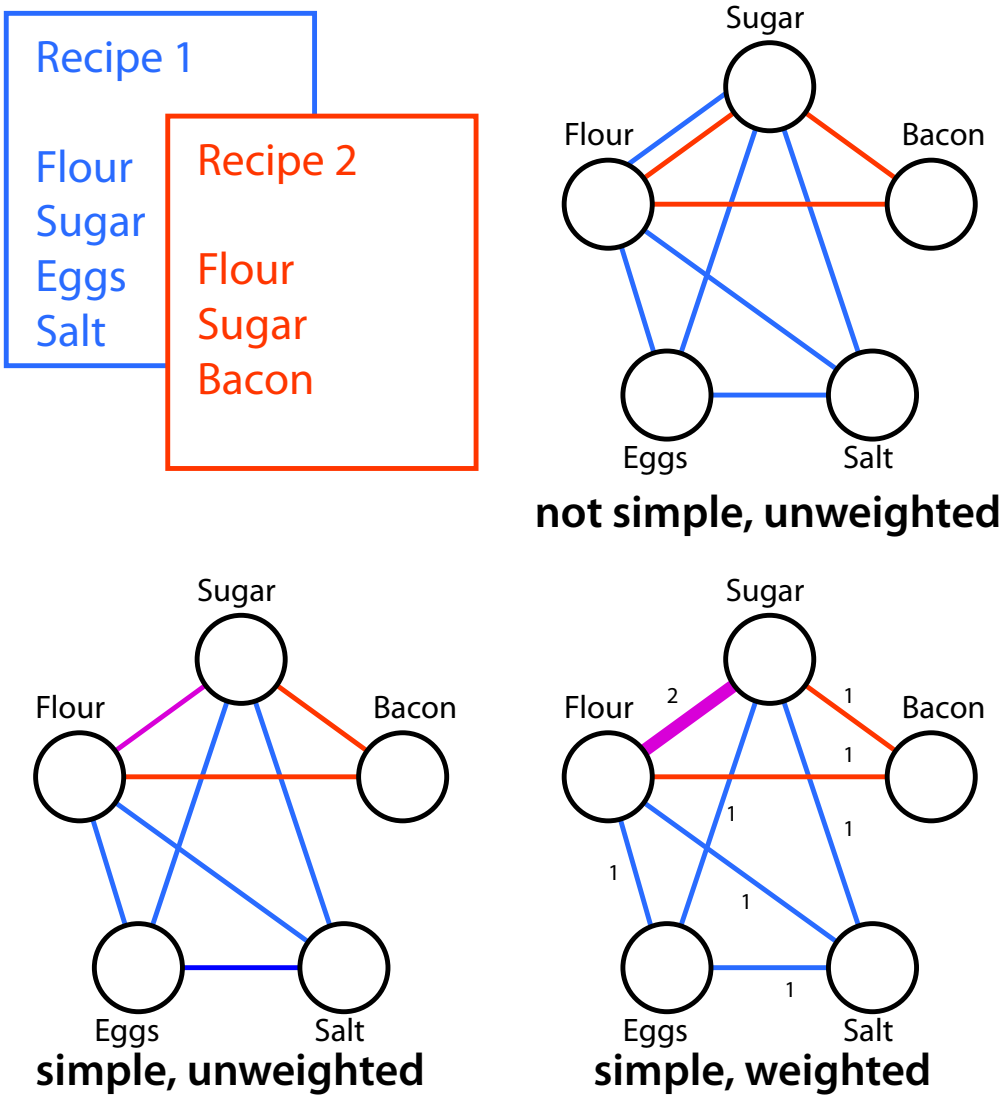

Figure 1.1: A collection of recipes may be represented as a network of ingredients in different ways. By convention nodes are shown as circles and links as lines or arrows. If multiple links are allowed, the network is not simple (upper right). If multiple links (and self-links) are not allowed, and all links are of equal strength the network is simple and unweighted (bottom left). If multiple links and self-links are not allowed, but some links are stronger than others (represented by the bold link), the network is simple and weighted. Since links in all three networks have no direction (or are bi-directional), all three networks are undirected. The decision of which type of network to use depends on the intended use of the network. To aid the eye, we have colored the two recipes so the reader may more easily see from which recipe each link is derived.

that we have not assumed any simple or regular topological features. Unless otherwise specified, the reader may assume networks to be complex and simple—irregular topology, without multiple or self-connections. (Readers unfamiliar with network vocabulary should divest themselves of the notion that simple and complex are opposites or mutually exclusive, in the context of networks). In the subsections below, we highlight some of the methods which have been developed by others to handle such complexity.

1.1.1 Adjacency matrix

Given a network of N nodes, an *adjacency matrix* is a convenient and useful representation. We define the elements of the adjacency matrix A as

$$A_{nm} = \begin{cases} 1 & \text{if there is a link from node } m \text{ to node } n \\ 0 & \text{otherwise} \end{cases} \tag{1.1}$$

It is worth noting that the elements of A may be defined with indices reversed arbitrarily. Here we choose this convention for consistency with particular previous papers [6]. Strictly speaking, Eq. (1.1) is therefore a matrix showing which nodes are "adjacent" and therefore consists of only zeroes and ones. However, we will hereafter refer to the matrix described in Eq. (1.1) as the *unweighted adjacency matrix*, preferring to reserve *adjacency matrix* for the weighted version,

$$\begin{aligned} A_{nm} &\neq 0 \quad \text{if there is a link from node } m \text{ to node } n \\ A_{nm} &= 0 \quad \text{otherwise,} \end{aligned} \tag{1.2}$$

where the non-zero entries of A will take on values appropriate to the network at hand. Therefore, intuitively, binary networks are represented by adjacency matrices of ones and zeroes. Note also that for undirected networks $A_{nm} = A_{mn}$ and therefore adjacency matrices for undirected networks are symmetric, $A = A^T$.

1.1.2 Degree distribution

The *in-degree* of a node is the number of links ending at that node, and the *out-degree* of a node is the number of links originating at that node. In terms of the adjacency matrix, these nodal

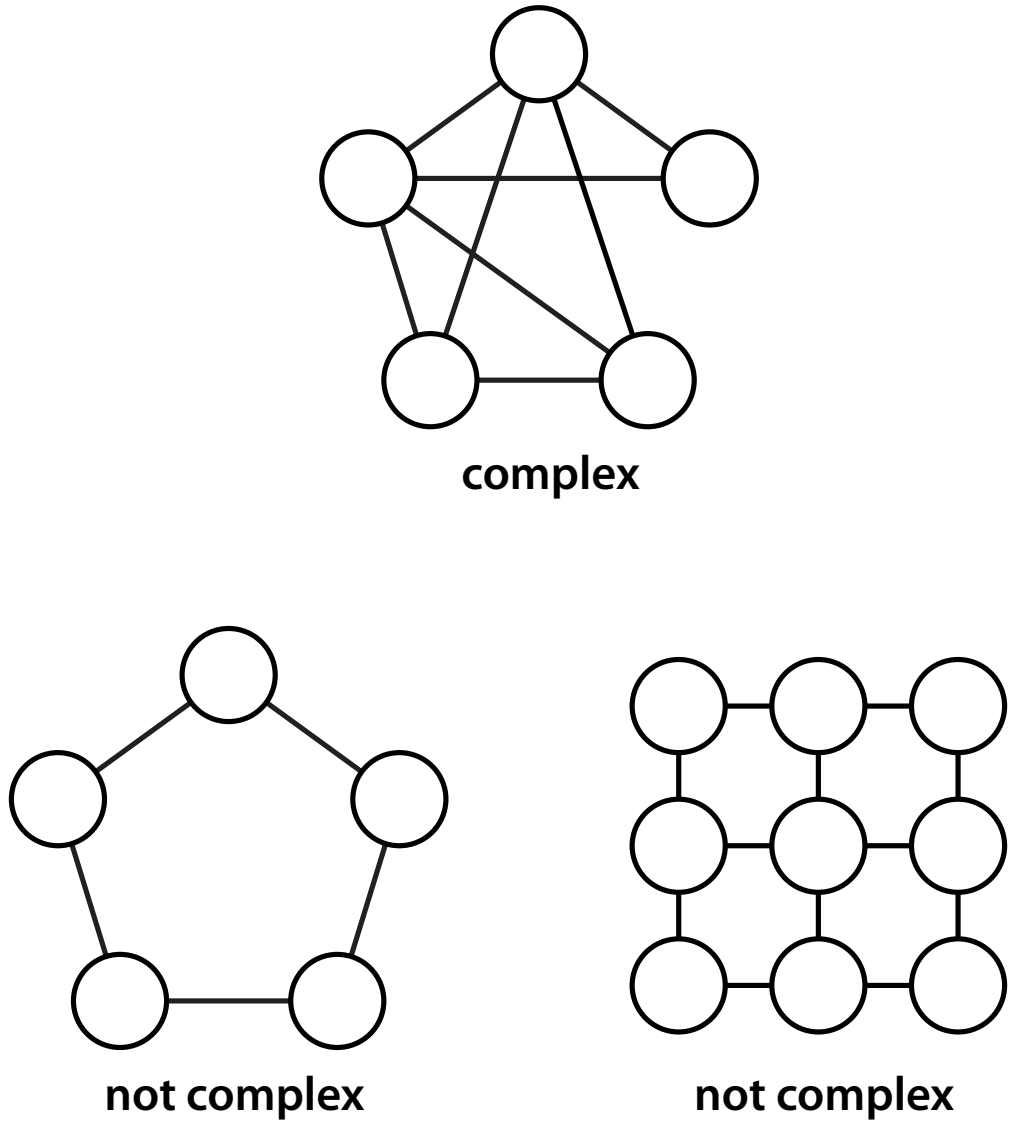

Figure 1.2: Complex networks are networks whose topologies are non-trivial. An example of a complex network is shown (top) as well as two networks that are not complex: a ring (left) and a lattice (right).

degrees, which we call k^{in} and k^{out} are defined for each node n as

$$k_n^{in} = \sum_{m=1}^{N} A_{nm} \qquad\qquad k_n^{out} = \sum_{m=1}^{N} A_{mn}. \tag{1.3}$$

When a network is unweighted, the in- and out-degrees correspond to the integer numbers of links ending and starting at a node, respectively. On the other hand, when a network is weighted, the in- and out-degrees—also called the in-strength and out-strength—correspond to the sum of incoming weights and sum of outgoing weights, respectively, at a node. Figure 1.3 shows an example of an unweighted directed network with k^{in} and k^{out} indicated. We define the *mean degree* of the network as

$$\langle k \rangle = N^{-1} \sum_{n=1}^{N} k_n^{in} = N^{-1} \sum_{n=1}^{N} k_n^{out} \tag{1.4}$$

where either version of the equation can be used since $\langle k \rangle$ amounts to the average value of the network adjacency matrix, element-wise, regardless of whether that average is represented by an average of in- or out-degrees as an intermediate step.

While an adjacency matrix provides a complete description of all the nodes and links in a network, the sequences of in-degrees $k_1^{in}, k_2^{in}, ..., k_N^{in}$ and out-degrees $k_1^{out}, k_2^{out}, ..., k_N^{out}$ provide an incomplete but nonetheless meaningful description. By creating histograms a network's in- and out-degree sequences, we can observe the *degree distributions* of the network, which are often quite interesting, because they may suggest that the underlying network was (or sometimes wasn't!) created by a particular process. In Sec. 1.1.4, we will discuss the creation of networks in the context of degree distributions, using particular degree distributions as a target property to be achieved during network construction, rather than a property to be measured from an observed network.

1.1.3 Degree correlations

Since we have established that an adjacency matrix provides a complete description of all nodes and links in the network, and the in- and out-degree distributions provide an incomplete but nonetheless useful description, we may find middle-ground between the two by examining degree

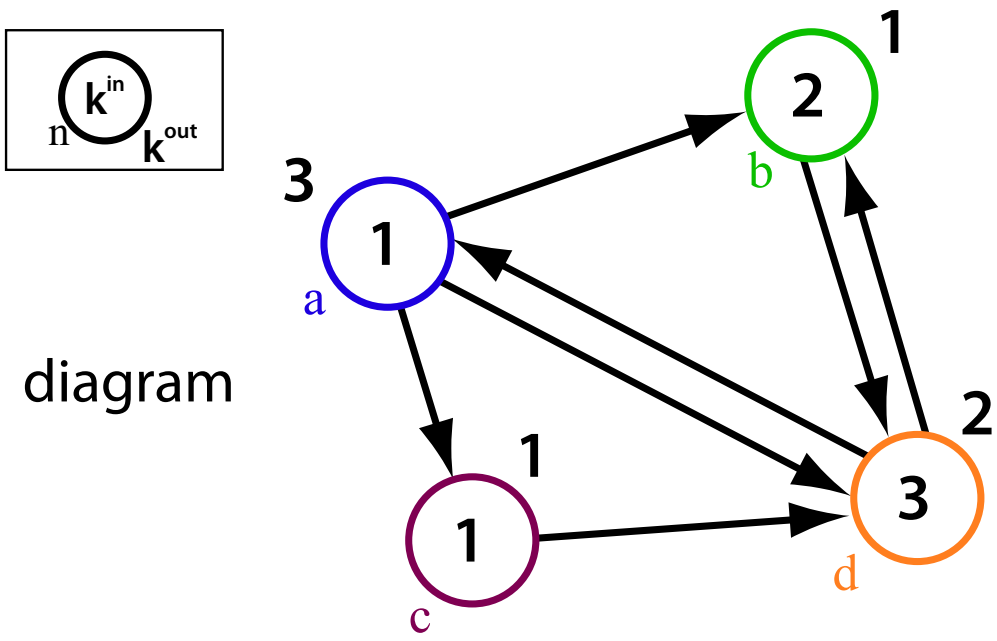

	a	b	c	d	
a	0	0	0	1	1
b	1	0	0	1	
c	1	0	0	0	
d	1	1	1	0	
	3				

adjacency matrix

Figure 1.3: For unweighted networks, the in- and out-degree of a node are the integer numbers of incoming and outgoing links, respectively. In the diagram above, an unweighted network is shown with in-degree inside each node and out-degree next to each node. The nodes are labeled with letters which correspond to rows and columns in the adjacency matrix. The networks is directed and so the adjacency matrix need not be symmetric, as shown. The row sum and column sum corresponding to node a are shown, demonstrating Eq. (1.3).

correlations within the network. While there are many types of descriptions available, we will highlight two important types of correlations here: nodal degree correlations, and edge degree correlations. For reference, diagrams of both types of degree correlations are shown in Fig. 1.4, which may help to understand the definitions below.

Nodal degree correlations are correlations between the in-degree and out-degree of a randomly chosen node. From a network's degree sequences, one may estimate the probability that a randomly chosen node has a particular in- and out-degree, $P(k^{in}, k^{out})$. If each node's in-degree and out-degree are independent of each other, then

$$P(k^{in}, k^{out}) = P_{in}(k^{in})P_{out}(k^{out}). \tag{1.5}$$

However, if in-degree and out-degree are correlated, the joint degree distribution $P(k^{in}, k^{out})$ will not be equal to the product of the marginal distributions as in Eq. (1.5). In this case, one may be interested in the full joint degree distribution, but a more streamlined measure is the correlation coefficient for nodal degree correlations,

$$\eta = \frac{\langle k^{in}k^{out}\rangle}{\langle k^{in}\rangle\langle k^{out}\rangle} = \frac{\langle k^{in}k^{out}\rangle}{\langle k\rangle^2}, \tag{1.6}$$

where $\langle\cdot\rangle$ denotes an average over nodes. When in- and out-degrees are independent $\eta = 1$, and $\eta > 1$ ($\eta < 1$) when in- and out-degrees are positively (negatively) correlated. Examples are shown in Fig. 1.4 (a) and (b). Alternatively, the Pearson correlation coefficient is also often useful,

$$r_{node} = \frac{\langle (k^{in} - \langle k\rangle)(k^{out} - \langle k\rangle)\rangle}{\sqrt{\langle (k^{in} - \langle k\rangle)^2\rangle}\sqrt{\langle (k^{out} - \langle k\rangle)^2\rangle}}. \tag{1.7}$$

When in- and out-degrees are independent, $r_{node} = 0$, and $r_{node} > 0$ ($r_{node} < 0$) when in- and out-degrees are positively (negatively) correlated. In the following chapters, we favor η over r_{node} for convenience, but we note that r_{node} is a shifted and renormalized form of η, and thus they measure the same property but express it on different scales.

Edge degree correlations are correlations between the in- and out-degree at the end of a randomly chosen link. In particular, for a link from node n to node m, we can look for correlations

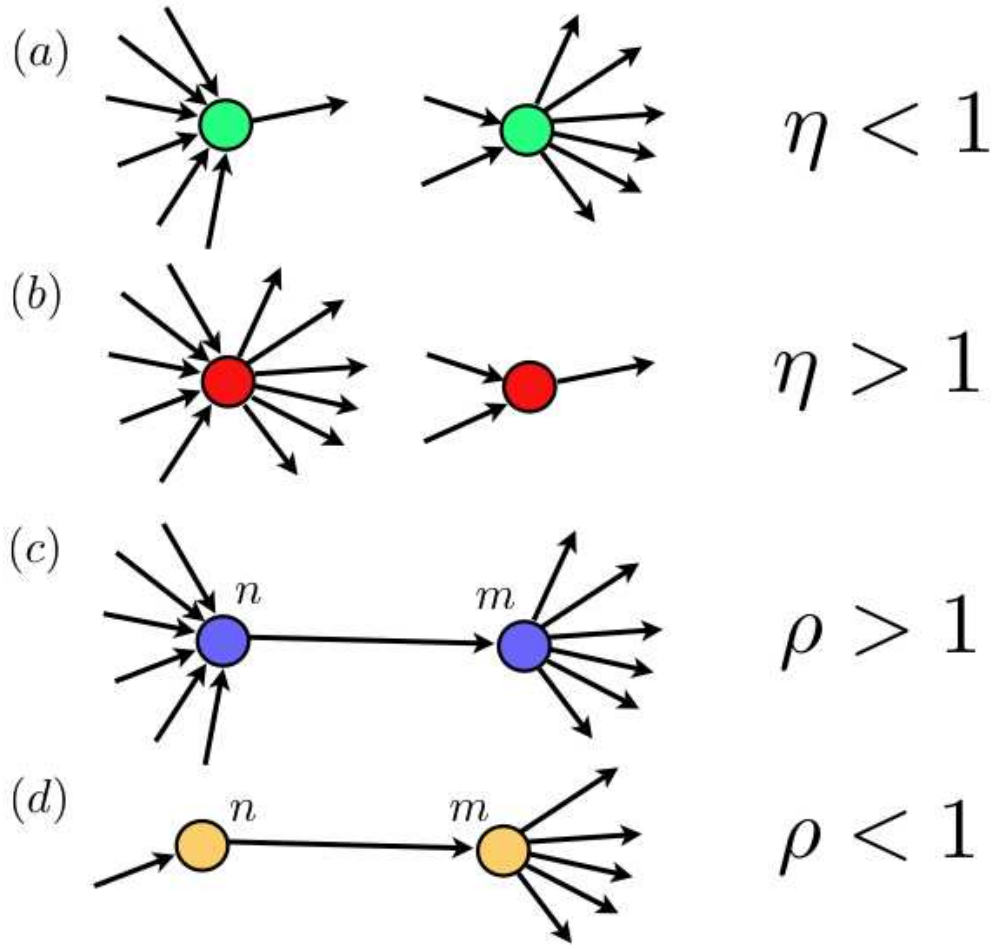

Figure 1.4: Diagram showing examples of the types of links that one might observe in networks with particular η and ρ values. (a) node in- and out-degree are anti correlated, (b) node in- and out-degree are correlated, (c) in-degree at node n is correlated with out-degree at node m, and (d) in-degree at node n is anti-correlated with out-degree at node m. Figure reproduced from [1].

between the in-degree at n and the out-degree at m. In similar construction to Eq. (1.6), edge degree correlations can be measured by the coefficient

$$\rho = \frac{\langle k_n^{in} k_m^{out} \rangle_e}{\langle k^{in} \rangle_e \langle k^{out} \rangle_e}, \tag{1.8}$$

where $\langle \cdot \rangle_e$ denotes an average over edges. The average over edges may be easily evaluated as

$$\langle x_{nm} \rangle_e = \frac{\sum_{n,m} A_{nm} x_{nm}}{\sum_{n,m} A_{nm}}. \tag{1.9}$$

In the absence of edge degree correlation, $\rho = 1$, and $\rho > 1$ ($\rho < 1$) for positive (negative) correlation. Examples are shown in Fig. 1.4 (c) and (d).

Both nodal and edge degree correlations are featured in the chapters that follow. As a vocabulary note, nodal degree correlations are sometimes called *degree-degree correlations* and edge degree correlations are sometimes called *assortative mixing by degree*.

1.1.4 Network models

In the chapters that follow, theoretical predictions are made regarding dynamics on networks characterized by different properties. For example, chapter 2 predicts dynamics on networks with a particular degree distribution, as well as on networks with node degree correlations and edge degree correlations. In order to simulate dynamics, one must construct a network with particular properties with confidence that the constructed network is a "typical" specimen of the totality of networks with the desired properties. Here, we formalize this concept using the *network ensemble* framework, and describe the *Erdős-Rényi model* and the *configuration model* used to sample two particular ensembles of interest.

Given a property, a network ensemble is a probability space in which each event is a network with the property, paired with the probability that such a network occurs. In order to create a network with the given property, we must draw a sample from the ensemble and so reframed, the problem becomes one of properly drawing a sampling the ensemble, which is what is meant in the paragraph above by generating a "typical" specimen. Many network models may be put into this framework:

(1) Networks with a given number of nodes N and links m,

(2) Networks with an expected degree sequence,

(3) Networks with a given number of nodes N and expected number of links m,

(4) Networks with a given degree sequence,

and many others. In the chapters that follow, we will be primarily concerned with the types (3) and (4) listed above. Networks with a given number of nodes N and expected number of links m are a type of random network and may be generated by the Erdős-Rényi model. They are therefore often referred to as Erdős-Rényi random networks. Networks with a given degree sequence may be generated by the configuration model.

The Erdős-Rényi random graph model is the ensemble of simple networks with N nodes where the probability of choosing a graph G with m edges is $P(G) = p^m(1-p)^{\binom{N}{2}-m}$. $\binom{N}{2}$ is the total possible number of edges, so $P(G)$ corresponds to placing each link independently with probability p. Given N nodes, and a probability of one node connecting to each of the others p, then the expected number of connections at each node is $\mathrm{E}[k] = p(N-1)$. In practice, one may choose a desired number of directed links m, fix $p = m/(N(N-1))$, and place each of the possible links in the network with probability p. For undirected networks, $p = 2m/(N(N-1))$ should be used since there are half as many possible links as in the undirected case. A diagram of construction by this method is shown in Fig. 1.5, top. There is a rich and interesting literature corresponding to Erdős-Rényi random networks in which m is small. In such sparse networks, it is often the case that not all nodes are linked to the others and so not all the nodes are connected in a *giant component*, a connected component whose size (number of member nodes) is of the same order as N. For the cases considered in the following chapters, however, there are an order of magnitude more links than nodes. For sufficiently large N or small m, such networks will have approximately Poisson degree distribution [9].

In what follows, we describe the configuration model for undirected networks, which may be extended to directed networks. The configuration model is the ensemble of simple networks with

a particular degree sequence $K = \{k_1, k_2, ..., k_N\}$, with uniform probability. While conceptually straightforward, in practice there may be no simple graphs with a given sequence K. For example, the sequence $K = \{3, 1\}$ is impossible because it requires node 1 to connect to itself. Similarly, the sequence $K = \{2, 1\}$ is impossible because after connecting nodes 1 and 2, it is clear that node 1 must connect to another node, but there are no other candidates available. By extending this simple example, we may restrict our study to cases where the sum of the elements of K is even, and no element in K is larger than $(N - 1)$. In fact, a sequence K is called a *graphic sequence* if it can serve as the degree sequence of some graph [10]. A sequence $\{k_1, k_2, ..., k_N\}$ is graphic if and only if the sum of degrees is even and the sequence obeys

$$\sum_{n=1}^{r} k_n \leq r(r-1) + \sum_{n=r+1}^{N} \min(r, k_n) \tag{1.10}$$

The next challenge is how to actually construct graphs with degree sequence K with uniform probability. In order to do so, we imagine each of the N nodes where node n has k_n "stubs", or half-links. Then, we pick uniformly random pairs of unmatched stubs and connect them. After this process is complete, if there are no self-connections or double-links, the process is finished. A diagram of construction by this method is shown in Fig. 1.5, bottom. Though not described here, it may be reasoned that the fraction of nodes with multiple edges generated by this process is approximately,

$$f \approx \frac{1}{2N} \left(\frac{\langle k^2 \rangle - \langle k \rangle}{\langle k \rangle^2} \right)^2 \tag{1.11}$$

where we have assumed a large network size N [1]. Problematically, for particular degree sequences such as those drawn from a power law distribution, $k_n \sim k^{-\gamma}$, $\langle k^2 \rangle$ tends to infinity as network size increases for $\gamma < 3$, meaning that successfully completing the protocol described above for large networks is improbable. There are two common solutions. First, one may repeat the protocol above until a simple network is found, which is called the *repeated configuration model*. Second, one may generate a single network by the protocol above, but then erase any redundant links, thus simplifying the network, which is called the *erased configuration model*. Note that the erased configuration model results in a network with a degree sequence other than K. In particular, those

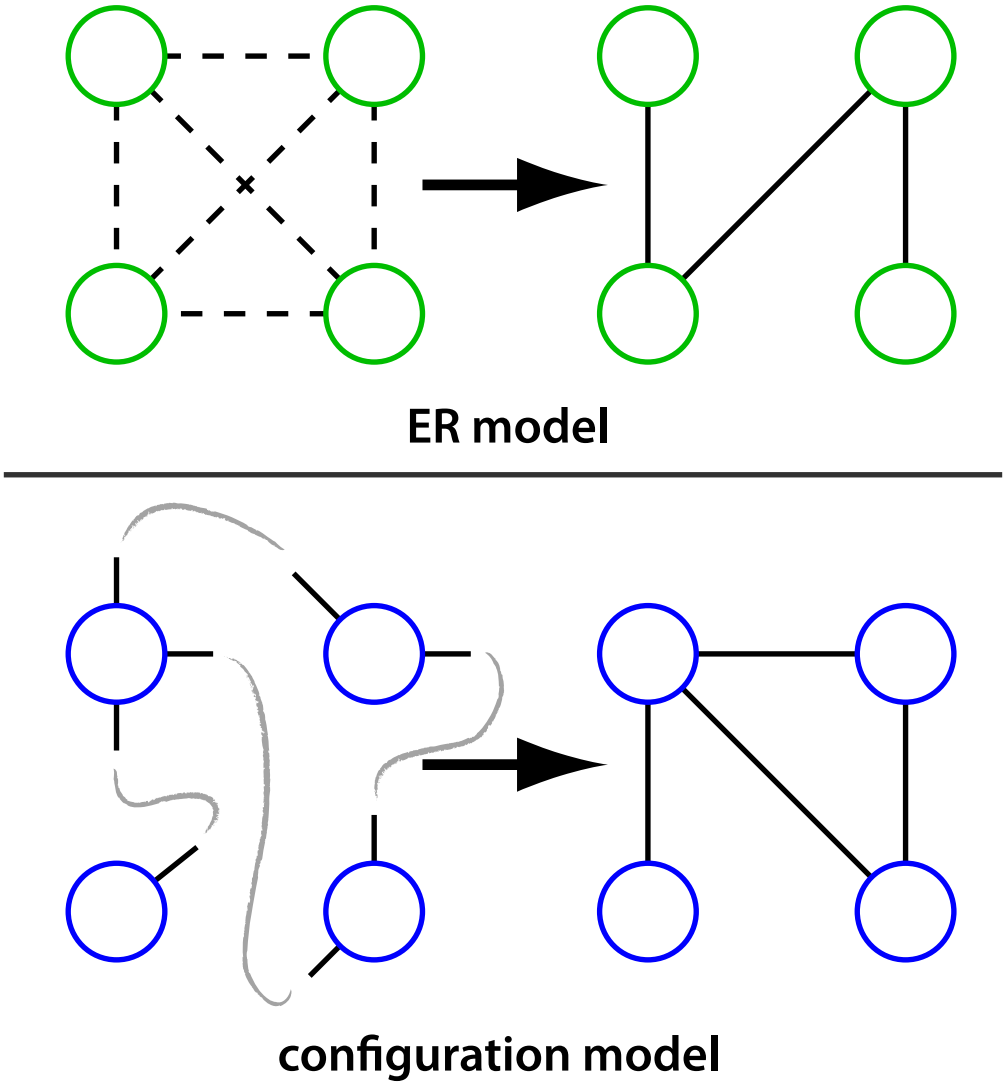

Figure 1.5: In an implementation of the Erdős-Rényi model (top), each of the possible links (dashed lines) is chosen to exist independently with some probability p (top left). Chosen links are placed in the network (top right) resulting in a draw from the ensemble of networks with N nodes and expected number of links Np. In an implementation of the configuration model (bottom), each node is given a number of "stubs" corresponding to its intended degree (bottom left, solid lines). Pairs of stubs are chosen randomly to be connected (bottom left, grey sketch lines) resulting in a draw from the ensemble of networks with N nodes and degree sequence K (bottom right).

nodes with a high probability of having generated redundant connections—nodes of high desired degree—are likely to be more restricted in their final degree than nodes of low desired degree. Quantification of this effective restriction is possible [1] but not presented here.

1.1.5 The Perron-Frobenius Theorem

> **Theorem (Perron-Frobenius):** *Let A be a $N \times N$ non-negative and irreducible matrix. Then there exists a simple positive eigenvalue λ of A which has an associated eigenvector u with positive entries, and which has a larger magnitude than the other eigenvalues of A. Furthermore, u is the only eigenvector of A with positive entries.*

There are many proofs of the Perron-Frobenius theorem which can be found in the review [2], of which the geometric proof found in reference [11] is particularly accessible in the candidate's opinion. Rather than present a proof here, we instead comment on implications of this theorem for the spectra of network adjacency matrices.

First we show that the theorem applies to network adjacency matrices: (i) as long as network weights are non-negative, then the resulting adjacency matrix will be non-negative, and (ii) an irreducible adjacency matrix will be formed from a fully-connected network—a network in which any node is reachable from any other node via a directed path. Though never explicitly stated, we consider only fully-connected networks.

Many times in the chapters that follow, we will make reference to the Perron-Frobenius eigenvalue λ as the *largest eigenvalue* or *dominant eigenvalue*. Since it arises naturally in the analysis in the following chapters, and other eigenvalues do not arise, we will also sometimes refer to λ as simply the eigenvalue of the network adjacency matrix, with u and v being the right and left eigenvectors of the adjacency matrix, where $Au = \lambda u$ and $A^T v = \lambda v$. Since the entries of A are non-negative, so are the entries of A^T, and thus the theorem implies that both v and u have strictly positive entries. Figure 1.6 shows a network to which the theorem's conditions can be visually confirmed, along with the Perron-Frobenius eigenvalue and eigenvectors.

In each of the following chapters, we find that λ plays an important role in governing dy-

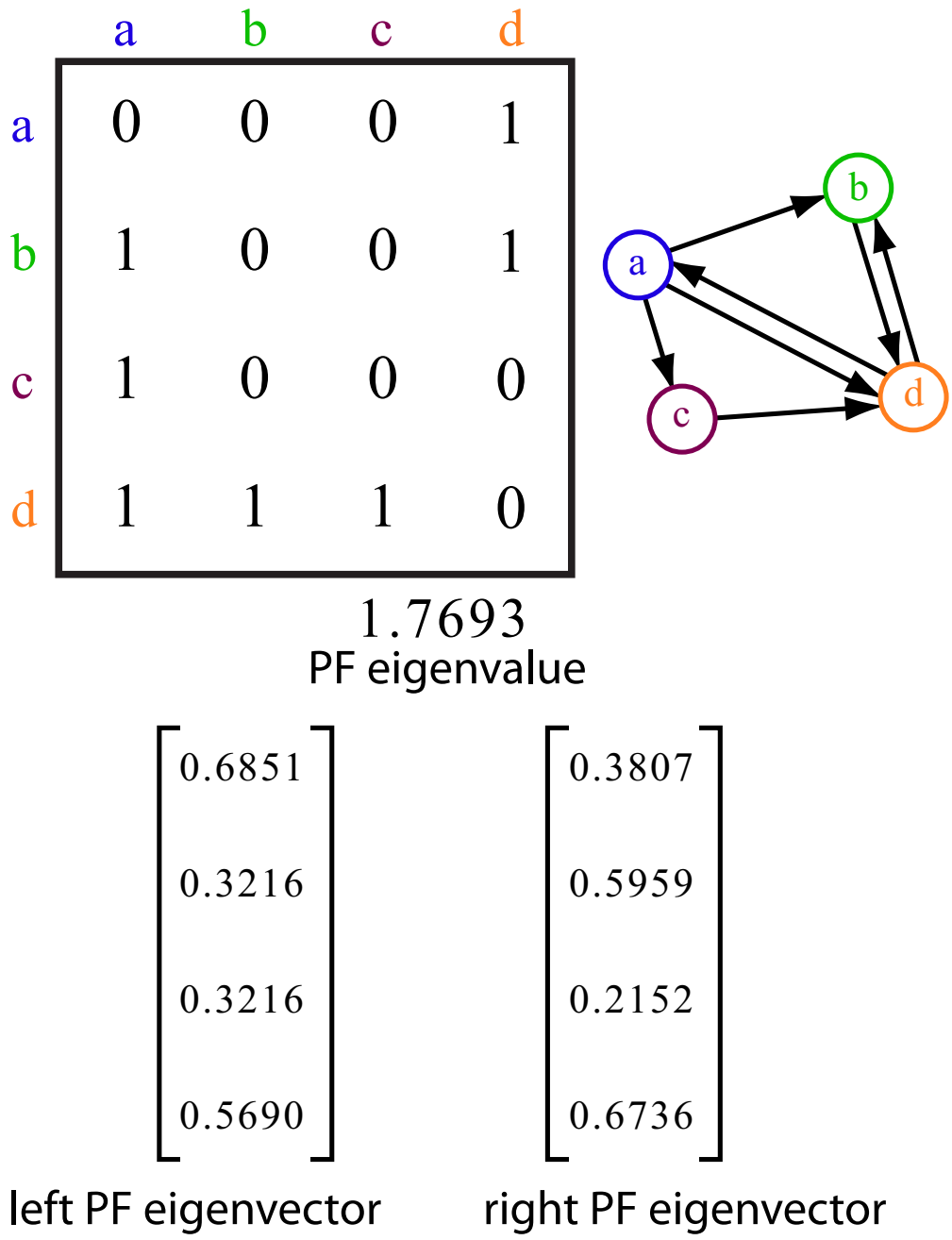

Figure 1.6: A network diagram (top right) and corresponding adjacency matrix (top left) are shown, along with the eigenvalue and corresponding eigenvectors (to four digits of accuracy) guaranteed by the Perron-Frobenius (PF) theorem [2]. The conditions of the theorem apply because (i) the entries of the adjacency matrix are non-negative and (ii) any node in the network is accessible from any other node in the network via a directed path which guarantees an irreducible matrix. Note that the eigenvalue is real and positive, and the eigenvector entries are strictly positive.

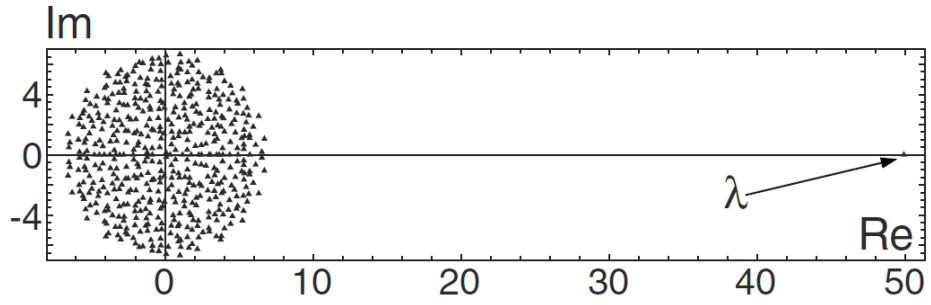

Figure 1.7: Spectrum of a 500×500 unweighted network adjacency matrix corresponding to an Erdős-Rényi random network with $p = 0.1$, reproduced from Ref. [3]

namics, and find that the entries of u and v have significant bearing on node-specific properties of the dynamics. It may, at various points, seem as though we ignore the rest of the spectrum of the adjacency matrix in favor of just the largest eigenvalue, for which there is good reason. In many cases, the largest eigenvalue is well separated from the rest of the spectrum, as shown in Fig. 1.7, reproduced from [3].

1.2 Excitable dynamics on complex networks

Coupled dynamical systems are not new to mathematics and there exist many systems of coupled equations which could be considered excitable. A subset of those are directly inspired by excitable systems observed in the physics and biology communities. Here, we discuss a class of excitable systems derived from observation of biological neurons. *Biological neuron models* are intended to capture some aspect of the operation of a biological neuron, a name which differentiates them from so-called *artificial neuron models*, which are used in artificial neural networks and are selected for their computational properties. To be clear, here we only consider biological neuron models, despite the fact that such models vary widely in their ability to reproduce the full variety of biological phenomena.

1.2.1 Biological neuron models

The history of biological neuron models is fascinating, and began in 1933 when the zoologist—and soon-to-become neuroscientist—John Zachary Young discovered that squid (specifically *loligo*) have a "giant axon" which has a large diameter—0.5 mm or more. An axon is part of a nerve cell (neuron), and this giant axon is many orders of magnitude larger than the axons of typical neurons. Physiologically, this increased axon size is important for the squid, allowing it to react extremely quickly to a threatening stimulus by jetting away rapidly [12], but was also important for Young, who was able to make significant and detailed measurements about the giant axon owing in "no small part" to its massive size. Less than 20 years later, in a series of papers published 1951–1952, Alan Lloyd Hodgkin and Andrew Huxley leveraged Young's extensive work to propose and validate a model for the electrical characteristics of the squid's giant axon, consisting of a system of coupled ordinary differential equations [4], for which they received a Nobel prize. These equations, now called the Hodgkin-Huxley model, are shown in Fig. 1.8 in their original 1952 form. They describe the interrelationship between current I, capacitance C, and voltage V.

In 1961 Richard Fitzhugh proposed a two-dimensional simplification to the Hodgkin-Huxley model [13], and in 1962 Jin-ichi Nagumo *et al.* described a prototype of the simplified system [14], and so the simplified two-dimensional form of the Hogkin-Huxley model became known as the Fitzhugh-Nagumo model,

$$\begin{aligned} \dot{v} &= v - v^3 - w + I_{\text{external}} \\ \tau\dot{w} &= v - a - bw \end{aligned} \tag{1.12}$$

where v may be called the *excitable variable* and w the *recovery variable*. The authors originally called it the Bonhoeffer-van der Pol oscillator, due to the fact that substituting $a = b = 0$ into Eq. (1.12) recovers the well-known van der Pol oscillator. Of great importance to mathematical neuroscientists, Fitzhugh was the first to use phase-plane analysis to understand the behavior of a neuron model. Since then, there have been many derived models proposed which intend to describe the behavior of a biological neuron. For a thorough and modern review, see [15].

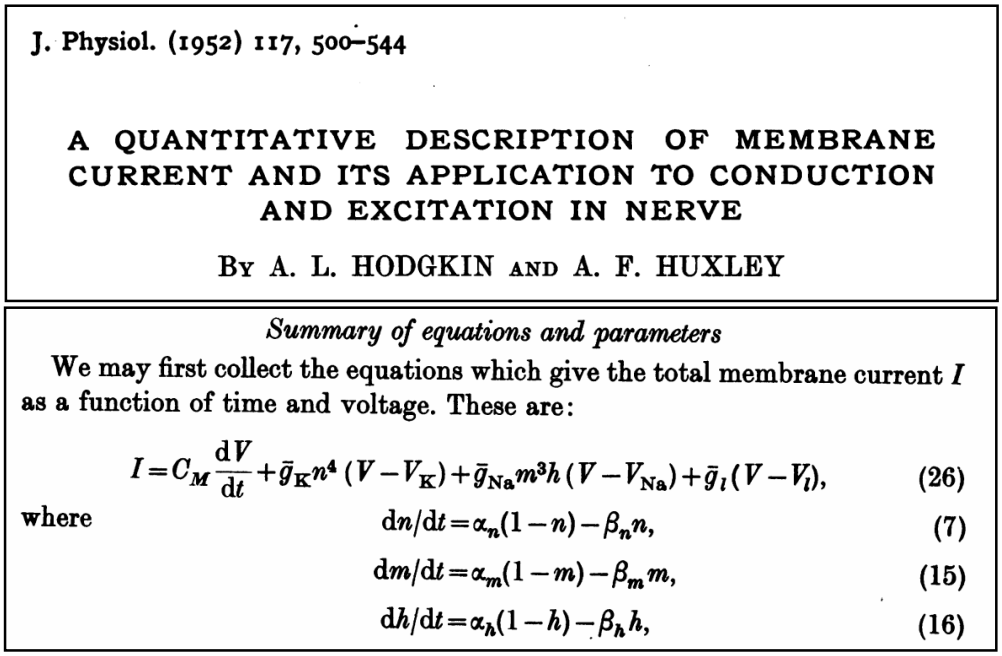

J. Physiol. (1952) 117, 500–544

A QUANTITATIVE DESCRIPTION OF MEMBRANE CURRENT AND ITS APPLICATION TO CONDUCTION AND EXCITATION IN NERVE

By A. L. HODGKIN and A. F. HUXLEY

Summary of equations and parameters

We may first collect the equations which give the total membrane current I as a function of time and voltage. These are:

$$I = C_M \frac{dV}{dt} + \bar{g}_K n^4 (V - V_K) + \bar{g}_{Na} m^3 h (V - V_{Na}) + \bar{g}_l (V - V_l), \quad (26)$$

where

$$dn/dt = \alpha_n (1 - n) - \beta_n n, \quad (7)$$

$$dm/dt = \alpha_m (1 - m) - \beta_m m, \quad (15)$$

$$dh/dt = \alpha_h (1 - h) - \beta_h h, \quad (16)$$

Figure 1.8: The Hodgkin-Huxley model as published in the final paper of their 1951–1952 series [4] describes the relationship between current I, capacitance C, and voltage V, where subscripts correspond to sodium (Na), potassium (K), and leak (l). All instances of α, β, and $\bar{g}$ are constants which Hodgkin and Huxley estimated exhaustively from experimental data. They were awarded a Nobel Prize in Medicine in 1963 along with John Eccles who made enormous advancements regarding the neuronal synapse.

The commonality among all the biological neuron models is that they capture the inherent excitability of the neuron: if a perturbation in one of its variables exceeds a particular threshold, the system will exhibit a characteristic excursion through phase space until returning to equilibrium, just as when a neuron receives a sufficiently strong stimulus it will emit or "fire" an action potential and then return to a resting state. Since the excursion corresponds directly to an "excitation" we call the system excitable. Depending on which neuron properties are important to the modeler, the form of this excursion may vary significantly [15]. The model we use in the chapters that follow, described in full detail in section 1.2.2, is simplified to include only three discrete states, resting, excited, and recovering, which may be occupied by the system in discrete time steps. This oversimplification is intentional and is based on the following premise: we may more easily study the effect of network topology when individual node dynamics are allowed to be so drastically simplified.

Thus, we choose not a beautiful and complex model such as the Hodgkin-Huxley, but instead an extremely simple and importantly *tractable* model: the Greenberg-Hastings cellular automaton. While the reader may be unconvinced, we will comment extensively on the surprising effectiveness of this simple model in reproducing biological phenomena in chapter 5. The following quotation from Fitzhugh's 1961 paper [13] regarding his own model Eq. (1.12) is particularly apt:

> *Its solution does not, to be sure, give an accurate fit to curves obtained from many physical oscillators. The equation was intended rather to represent the qualitative properties of a wide class of such oscillators, its algebraic form being chosen to be as simple as possible.*

We will thus consider a simple dynamical system placed on each node of a large and complex network. Since each node is excitable, the network in its entirety may be considered a large and complex dynamical system, and thus is called an *excitable network*.

Before proceeding to a description of the model, we note that excitable networks arise in contexts other than neuroscience. In fact, many biological, social, or engineered systems may be studied in the context of excitable networks. For example, the spread of a virus through a

population of computers or organisms may be viewed just so, where an infection is an excitation and the transmission of the virus to others is captured in the network coupling [16]. In the context of genetics, the inheritance of a genetic trait from ancestors may also be thought of this way, where the excited state corresponds to possession of the trait, and passing on the trait to offspring is captured in the network coupling [17]. Here, to maintain a strong connection to the forefront of neuroscience, we have developed theory which is applicable to cutting-edge research in neuronal networks, but may also be of use in more general fields. The techniques developed for analysis of these systems, may certainly be applied to fields other than neuroscience, where appropriate.

1.2.2 Description of the model

In all of the research presented in this thesis, we will analyze a generalized version of the Kinouchi-Copelli model [6] which uses as its excitable nodes the Greenberg-Hastings cellular automaton [18]. The dynamics of each automaton are adjusted to mimic the excitable dynamics of a single neuron with resting, excited, and refractory states, as shown in Figure 1.9, below. The Kinouch-Copelli model also includes possibly heterogeneous distributions of time delays on links and refractory periods on nodes. The model is as follows:

- There are N excitable elements, labeled $i = 1, \ldots, N$.
- At discrete times $t = 0, 1, ...,$ each element i can be in one of $m_i + 1$ states, x_i^t. The state $x_i^t = 0$ is the resting state, $x_i^t = 1$ is the excited state, and there may be additional refractory states $x_i^t = 2, 3, ..., m_i$.
- If element i is in the resting state at time t, $x_i^t = 0$, it can be excited in the next time step, $x_i^{t+1} = 1$, by another excited element j with delay τ_{ij} (i.e., if $x_j^{t-\tau_{ij}} = 1$) with probability A_{ij}, or independently by an external stimulus with probability η.
- The elements that are excited or in a refractory state, $x_i^t \geq 1$, will deterministically make a transition to the next refractory state if one is available, or return to the resting state otherwise (i.e., $x_i^{t+1} = x_i^t + 1$ if $1 \leq x_i^t < m_i$, and $x_i^{t+1} = 0$ if $x_i^t = m_i$).

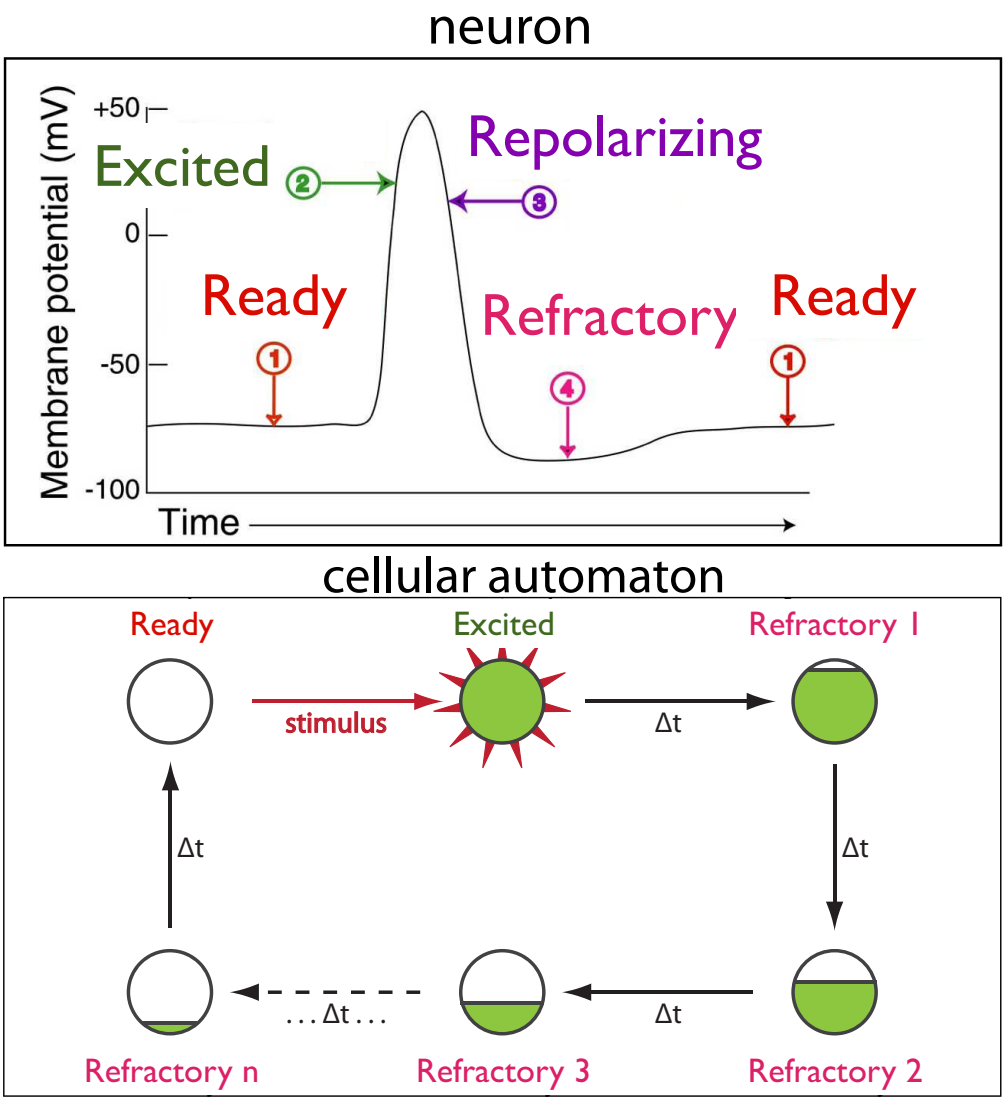

Figure 1.9: The states of the version of the Greenberg-Hastings Cellular automaton (bottom) studied in the chapters below are meant to mimic discretized states of a neuron (top).

- The coupling network, encoded by the matrix with entries A_{ij}, is allowed to have complex topology.

In chapter 2, we will analyze these dynamics in networks where nodes have no refractory states ($m_i = 0$) and links have no time delays ($\tau_{ij} = 0$). In chapter 3, we will analyze dynamics in networks with a variety of refractory states at each node and a variety time delays on the links. In chapter 4, we will remove the external stimulus entirely ($\eta = 0$) and instead study cascades of excitation originating from a single excited node.

1.2.3 Neuronal network dynamics in the literature

The dynamics of networks of interconnected neurons has been studied over many decades (for a review, see [19, 20]). Findings have been extensive, fascinating, and ongoing, brought on by increases in research funding, resolution of imaging and measurement techniques, and improved computational abilities.

However, recent experimental studies in cultured and acute cortical slices [5, 21] have opened a new avenue of research, suggesting that some neuronal networks operate at a critical regime that maximizes information processing. These experiments by Dietmar Plenz and collaborators showed that neuronal activity is characterized by temporally localized bursts, also called *neuronal avalanches*, that last a few milliseconds and whose size is power-law distributed. Figure 1.10 is reproduced from [5] showing histograms constructed from recordings of a slice of neonatal rat cortex spontaneously firing in a dish. Fascinatingly, the histogram data are distributed according to a power law with exponent $-3/2$ when measured by the both the total number of electrodes stimulated and the total potential of the cascade. Many additional observations of such patterns have been published [21, 7, 22, 23].

These observations can be modeled by a branching process in which a neuron activates, on average, only 1 additional neuron [24, 25, 7]. This model predicts the observed power law distribution of avalanche size and, remarkably, the numerical value of the observed power law exponent [24]. It has been hypothesized that the critical nature of this branching process (i.e.,

activating, on average, only 1 additional neuron) is helpful in maximizing information processing, which has also been demonstrated experimentally [7, 26, 22].

A related quantity of importance for certain neuronal networks is the dynamic range, the range of stimulus over which there is significant variation in the collective response of the network. For neuronal networks associated to sensory input, it is reasonable to assume that having a large dynamic range is beneficial. In particular, it is known that olfactory [27] and auditory [28] systems can have a dynamic range spanning various orders of magnitude. In a 2006 paper by Osame Kinouchi and Mauro Copelli it was shown in a simple model of neuronal networks that the dynamic range is maximized when the network operates at criticality [6]. Ref. [6] considers a system which we call the Kinouchi-Copelli model in the previous section: a network of Greenberg-Hastings cellular automata [18], one of the simplest excitable systems, subject to continuous stochastic external stimulation. Considering an Erdős-Rényi random graph and using a mean field approximation, Ref. [6] shows that the dynamic range is maximized when the average branching ratio σ of the network is 1 (meaning that a neuron activates, on average, only 1 additional neuron). Subsequent numerical studies have focused on exploring the effect of power-law degree distributions, hypercubic lattice coupling and loops on the dynamic range [29, 30, 31].

Although the dynamic range of a network of coupled excitable systems is potentially important in applications, a theoretical understanding of how it is affected by the underlying topology of the network has been lacking. Previous work on the dynamic range of interconnected excitable systems has considered analytically only random or regular networks [6, 30, 31], is based on averaged quantities (i.e, the average network branching ratio) [6], or has been limited to numerical studies of specific network features [29]. However, studies of the rat visual cortex have demonstrated that the synaptic circuitry is highly nonrandom, with features characteristic of a complex network structure [32], and that a more coarse grained functional network has a heterogeneous degree distribution characteristic of complex networks [33]. Thus, it is important to understand how this complex topology affects the dynamic range.

Subsequent studies explored this system on networks with power-law degree distributions

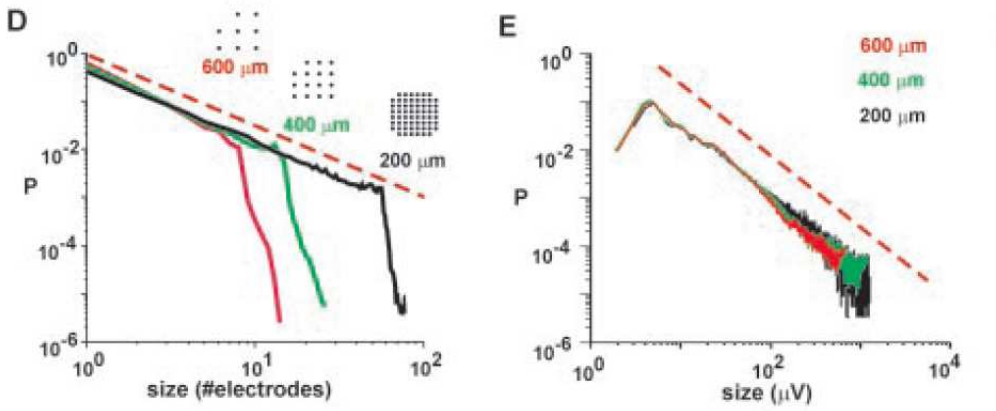

Figure 1.10: Recordings of many cascades of spontaneous activity in slices of neonatal rat cortex show a fascinating organization when viewed as a histogram of cascade sizes, measured both by number of recording electrodes stimulated (D) and by accumulated potential in microVolts (F). On the log-log scale, the red dotted line is a reference for a power law, exponent $-3/2$. The colors correspond to different subsampling of the total number of electrodes, as shown in the diagram inset (D). Figure reproduced from figure 4 of [5].

and hypercubic lattice coupling, and with a varying number of loops [29, 30, 31, 34], showing that the criterion for criticality based on the network mean degree does not hold for networks with a heterogeneous degree distribution. However, these studies do not take into account features that are commonly found in real networks, such as, for example, community structure, correlations between in- and out-degree of a given node, or correlations between the degree of two nodes at the ends of a given edge [35]. Furthermore, they do not consider the effect of transmission delays or a distribution in the number of refractory states. Thus, the previous publications are not applicable to many classes of network structures and variations on the dynamics. The research described in chapters 2 and 3 attempts to provide theoretical coverage for these cases.

In chapters 2 and 3, the largest eigenvalue of the network adjacency matrix plays an important role, characterizing the critical regime in which dynamic range is maximized. Experimentally, this critical regime is linked to so-called *critical avalanches*, cascades of neuronal activity with power-law distributions of duration and size [5, 21, 7, 23, 22]. However, existing theoretical work has not taken into account complex network structure.

Prior theoretical work has been done investigating avalanches in excitable networks with regular structure such as simple branching trees [17], including cases where network structure can not be included explicitly [36, 37, 38, 39]. However, this work is not applicable to the wide variety of complex network structures of interest as listed in the previous paragraph. Furthermore, previous studies are unable to account for differences in avalanches beginning from different nodes in the network. To motivate this point, one might reasonably conceive that an avalanche which begins from a "well-connected" node may be more likely to grow large than an avalanche originating from a "poorly-connected" node. Thus motivated, the research presented in chapter 4 examines the distributions of avalanche size and duration in complex networks, without *a priori* assuming any of the results from chapters 2 and 3. These results also address avalanches originating from specific network nodes, in the process bringing precise meaning to the descriptions of nodes as "well-connected" and "poorly-connected" from the point of view of avalanche dynamics.

The results of all three chapters dovetail without conflict, supporting and explaining each

other nicely, despite originating from significantly different analytical approaches. Chapter 5 makes some concluding remarks, commenting on the unexpected effectiveness of the Greenberg-Hastings cellular automaton, despite its extremely crude approximation of neuron dynamics. Furthermore, it proposes future directions of study to make the Kinouchi-Copelli model more biologically realistic in order to make deeper connection with a growing body of experimental work.

1.3 Publication Note

This Thesis comprises three main chapters. Chapters 2 and 3 have been published as

- [40] "Predicting criticality and dynamic range in complex networks: effects of topology" Larremore, D, Shew, WL, Restrepo, JG, *Physical Review Letters* **106**, 058101 (2011).

- [41] "Effects of network topology, transmission delays, and refractoriness on the response of coupled excitable systems to a stochastic stimulus" Larremore, D, Shew, WL, Ott, E, Restrepo, JG, *Chaos* **21**, 025117 (2011).

Chapter 4 has been submitted to Physical Review E. It is a collaboration with Marshall Y. Carpenter, Edward Ott, and Juan G. Restrepo. It is available at the time of submission of this thesis on the arXiv at http://arxiv.org/abs/1204.3861.

Chapter 2

Predicting criticality and dynamic range in complex networks: effects of topology

The collective dynamics of a network of coupled excitable systems in response to an external stimulus depends on the topology of the connections in the network. Here we develop a general theoretical approach to study the effects of network topology on dynamic range, which quantifies the range of stimulus intensities resulting in distinguishable network responses. We find that the largest eigenvalue of the weighted network adjacency matrix governs the network dynamic range. Specifically, a largest eigenvalue equal to one corresponds to a critical regime with maximum dynamic range. We gain deeper insight on the effects of network topology using a nonlinear analysis in terms of additional spectral properties of the adjacency matrix. We find that homogeneous networks can reach a higher dynamic range than those with heterogeneous topology. Our analysis, confirmed by numerical simulations, generalizes previous studies in terms of the largest eigenvalue of the adjacency matrix.

2.1 Introduction

Numerous natural and social systems are accurately described as networks of interacting excitable nodes. For example, the dendritic branching tree of the mammalian neuron has been modeled using branching trees and chains of excitable nodes [42]. The same excitable nodes on random networks have also been used to model interacting patches of many neurons [6]. Epidemics propagating through social networks have also been successfully modeled using networks of excitable

nodes as well [43]. Interestingly, the collective dynamics of such excitable networks often defy naive expectations based on the dynamics of the single nodes which comprise the network. For example, the collective response of a neural network can encode sensory stimuli that span more than 10 orders of magnitude in intensity, while the response of a single neuron (node) typically encodes a much smaller range of stimulus intensities. More generally, the range of stimuli over which a network's response varies significantly is quantified by *dynamic range* and is a fundamental property, whether the network is comprised of people, cell phones, genes, or neurons. In neural networks, recent in-vitro experiments measuring electrical activity in slices of rat cortex in the presence and absence of various drugs [7] suggest that dynamic range is maximized in a critical regime in which neuronal avalanches [5] occur, confirming earlier theoretical predictions [6]. It has been argued [6, 7] that this critical regime occurs when the effective mean degree of the network is one, i.e. the expected number of additional excited nodes produced by one excited node is one. However, this criterion is invalid for networks with broad degree distributions, particularly in scale-free networks [29, 34]. A general understanding of how dynamic range and criticality depend on complex network structure remains lacking. In this chapter, we present a unified theoretical treatment of stimulus-response relationships in excitable networks, which holds for diverse networks including those with random, scale free, degree-correlated, and assortative topologies.

2.2 Model Dynamics

As a tractable model of an excitable network, here we consider the Kinouchi-Copelli model [6], previously described in section 1.2.2, which consists of N coupled excitable nodes. Here, we restrict the model so that it does not include time delays. To recap: each node i can be in one of m states x_i. The state $x_i = 0$ is the resting state, $x_i = 1$ is the excited state, and there may be additional refractory states $x_i = 2, 3, ..., m-1$. At discrete times $t = 0, 1, ...$ the states of the nodes x_i^t are updated as follows: (i) If node i is in the resting state, $x_i^t = 0$, it can be excited by another excited node j, $x_j^t = 1$, with probability A_{ij}, or independently by an external process with probability η. The network topology and strength of interactions between the nodes is described by

the connectivity matrix $A = \{A_{ij}\}$. In this model, η is considered the stimulus strength. (ii) The nodes that are excited or in a refractory state, $x_i^t \geq 1$, will deterministically make a transition to the next refractory state if one is available, or otherwise return to the resting state (i.e. $x_i^{t+1} = x_i^t + 1$ if $1 \leq x_i^t < m-1$, and $x_i^{t+1} = 0$ if $x_i^t = m-1$). For a diagrammatic representation of these dynamics, see Fig. 1.9.

An important property of excitable networks is the dynamic range, which is defined as the range of stimuli that is distinguishable based on the system's response F. Following [6], we quantify the network response with the average activity $F = \langle f \rangle_t$ where $\langle \cdot \rangle_t$ denotes an average over time and f^t is the fraction of excited nodes at time t. We consider systems that have been subjected to the stimulus for many time steps before an average is calculated in order to avoid including transient behavior in the average. An analysis of transient dynamics in this system with the additional inclusion of time delays on network links is presented in chapter 3. To calculate a system's dynamic range, we first determine a lower stimulus threshold η_{low} below which the change in the response is negligible, and an upper stimulus threshold η_{high} above which the response saturates since each node may be in the excited state at most every other time step, as shown in figure 2.1. Dynamic range (Δ), measured in decibels, is defined as

$$\Delta = 10 \log_{10} \eta_{high}/\eta_{low}. \tag{2.1}$$

To analyze the dynamics of this system, we denote the probability that a given node i is excited at time t by p_i^t. For simplicity, we will consider from now on only two states, resting and excited (m=2) without any refractory states (noting that this restriction is relaxed in the chapter 3). Then, the update equation for p_i^t is

$$p_i^{t+1} = (1 - p_i^t) \left(\eta + (1 - \eta) \left[1 - \prod_j^N (1 - p_j^t A_{ij}) \right] \right) \tag{2.2}$$

which can be obtained by noting that $1 - p_i^t$ is the probability that node i is resting at time t, and the term in large parentheses is the probability that it makes a transition to the excited state. Termwise, η is the probability that the node is stimulated by the external source, $(1 - \eta)$ is the

probability that the node is *not* stiulated by the external source, and the term in square brackets represents the probability that the node is excited by a network neighbor. We note that, in writing this probability, we treat the events of neighbors of node i being excited at time t as statistically independent. As noted before [43, 44, 45, 46], this approximation yields surprisingly good results even when the network has a non-negligible amount of short loops!

In Ref. [6], the response F was theoretically analyzed as a function of the external stimulation probability η using a mean-field approximation in which connection strengths were considered uniform, $A_{ij} = \sigma/N$ for all i, j. It was shown that at the critical value $\sigma = 1$, the network response F changes its qualitative behavior. In particular, $\lim_{\eta \to 0} F = 0$ if $\sigma < 1$ and $\lim_{\eta \to 0} F > 0$ if $\sigma > 1$. In addition, the dynamic range of the network was found to be maximized at $\sigma = 1$. This result is shown below in Fig 2.2, reproduced from [6]. The parameter σ is defined in Refs. [6, 7] as an average branching ratio, written here as

$$\sigma = \frac{1}{N} \sum_{i,j} A_{ij} = \langle k^{in} \rangle = \langle k^{out} \rangle, \tag{2.3}$$

where $k_i^{in} = \sum_j A_{ij}$ and $k_i^{out} = \sum_j A_{ji}$, as in 1.1.2, are the in- and out-degrees of node i, respectively, and $\langle \cdot \rangle$ is an average over nodes. For the network topology studied by Ref. [6] $\sigma = 1$ marks the critical regime in which the expected number of excited nodes is equal in consecutive timesteps. Such critical branching processes result in avalanches of excitation with power-law distributed sizes and durations. Cascades of neural activity with such power-law size distributions have been observed in rat brain tissue cultures [7], awake monkeys [23], and anesthetized rats [47]. We analyze the statistical properties of avalanches on complex excitable networks in detail in chapter 4. While $\sigma = 1$ successfully predicts the critical regime for Erdős-Rényi random networks [6], this prediction fails in networks with a more heterogeneous degree distribution [34, 29]. Perhaps more importantly, previous theoretical analyses [6, 34, 29] do not account for features that are commonly found in real networks, such as community structure, correlation between in- and out-degree of a given node (node degree correlation as discussed in section 1.1.3), or correlation between the degree of two nodes at the ends of a given edge [35] (edge degree correlation as discussed in section 1.1.3).

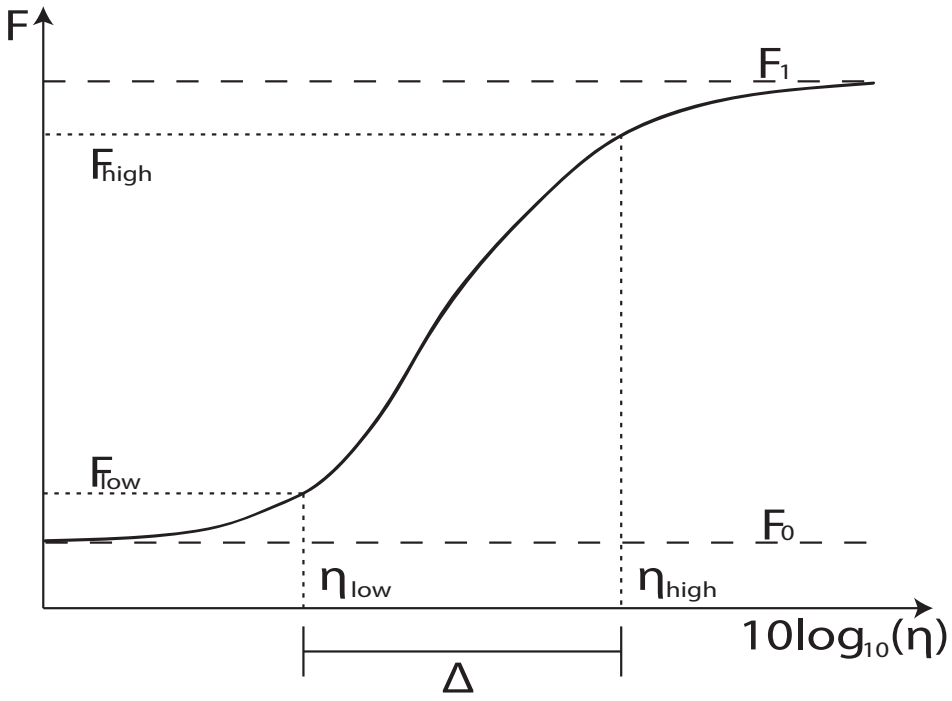

Figure 2.1: Schematic illustration of the definition of dynamic range in the active network case. The baseline and saturation values are F_0 and F_1, respectively. Two threshold values, denoted by F_{low} and F_{high}, respectively, are used to determine the range of values of η defined as the *dynamic range* Δ.

Therefore in what follows, we will generalize the mean-field criterion $\sigma = 1$ to account for complex network topologies.

2.3 Perturbative analysis

To begin, we note that $\lim_{\eta \to 0} F = 0$ corresponds to the fixed point $\vec{p} = 0$ of Eq. (2.2) with $\eta = 0$. This is just to say that if there is no external stimulus, and there is no network activity, then there will be no future network activity spontaneously generated. To examine the linear stability of this fixed point, we set $\eta = 0$ and linearize around $p_i^t = 0$, assuming p_i^t to be small, obtaining

$$p_i^{t+1} = \sum_j^N p_j^t A_{ij}. \tag{2.4}$$

Assuming exponential growth around the fixed point, $p_i^t = u_i \lambda^t$ yields

$$\lambda u_i = \sum_j^N u_j A_{ij}, \tag{2.5}$$

an eigenvalue equation for matrix A with eigenvalue λ. Thus, the stability of the solution $\vec{p} = 0$ is governed by the largest eigenvalue of the network adjacency matrix, λ, with $\lambda < 1$ being stable (perturbations decay back to the fixed point) and $\lambda > 1$ being unstable (perturbations grow away from the fixed point). Therefore, the critical state described in previous literature, occurring at various values of $\langle k \rangle$, should occur at $\lambda = 1$. Importantly, since $A_{ij} \geq 0$, the Perron-Frobenius theorem, discussed in section 1.1.5, guarantees that λ is real and positive [2]. Other previous studies in *random* networks have also investigated spectral properties of A to gain insight on the stability of dynamics in neural networks [48] and have shown how λ could be changed by modifying the distribution of synapse strengths [49]. An important implication of Eq. (2.5) is that, when p and η are small enough, p should be almost proportional to the right eigenvector u corresponding to λ, so we write

$$p_i = C u_i + \epsilon_i, \tag{2.6}$$

where C is a proportionality constant and the ϵ_i error term captures the deviation of actual system behavior from the linear analysis. To first order in p and η, the constant C is related to the network

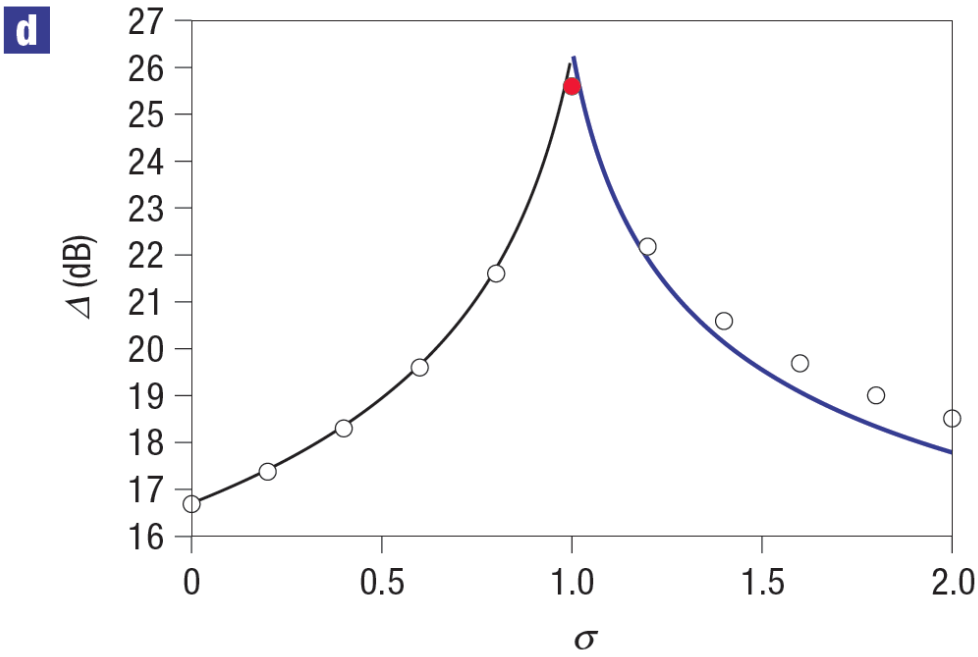

Figure 2.2: Dynamic range (Δ) is maximized when the mean degree (σ, Eq. (2.3)) is equal to one in excitable Erdős-Rényi random networks without degree correlations, reproduced from [6].

response F since, neglecting ϵ, we have

$$F = \langle f \rangle_t = \frac{1}{N} \sum_i p_i \approx \frac{1}{N} \sum_i C u_i = C \langle u \rangle. \tag{2.7}$$

The linear analysis allowed us to identify $\lambda = 1$ as the point at which the network response becomes non-zero as $\eta \to 0$. In what follows, we use a weakly nonlinear analysis to obtain approximations to the response $F(\eta)$ when η is small, a necessary step to eventually analyze dynamic range. As we will show, these approximations depend only on a few spectral properties of A. Assuming $A_{ij} p_j \ll 1$ (which is valid near the critical regime if each node has many incoming connections), we approximate the product term of Eq. (2.2) with an exponential, obtaining in steady state

$$p_i = (1 - p_i) \left(\eta + (1 - \eta) \left[1 - \exp \left(- \sum_j p_j A_{ij} \right) \right] \right) \tag{2.8}$$

which we expand to second order using Eq. (2.6) and $Au = \lambda u$,

$$C u_i + \epsilon_i = (A\epsilon)_i + \eta(1 - C u_i) + (1 - \eta) \lambda C u_i - \left(\lambda + \frac{1}{2} \lambda^2 \right) C^2 u_i^2. \tag{2.9}$$

The approximation of the product $\prod_j^N (1 - p_j^t A_{ij})$ with an exponential $\exp \left(- \sum_j p_j A_{ij} \right)$ is demonstrated in the appendix, 2.7.

To eliminate the error term ϵ_i from Eq. (2.9), we multiply by v_i, the ith entry of the left eigenvector corresponding to λ, and sum over i,

$$\sum_{i=1}^{N} (C u_i v_i + \epsilon_i v_i) = \sum_{i=1}^{N} \left(v_i (A\epsilon)_i + \eta(1 - C u_i) v_i + (1 - \eta) \lambda C u_i v_i - \left(\lambda + \frac{1}{2} \lambda^2 \right) C^2 u_i^2 v_i \right). \tag{2.10}$$

We use the fact that $v^T A \epsilon = \lambda v^T \epsilon$ (first term, right hand side), where v^T denotes the transpose of v, and neglect the resulting small term $(1 - \lambda) \sum_i v_i \epsilon_i$ close to the critical value $\lambda = 1$, obtaining

$$C \langle uv \rangle = \eta(\langle v \rangle - C \langle uv \rangle) + (1 - \eta) C \lambda \langle uv \rangle - \left(\lambda + \frac{1}{2} \lambda^2 \right) C^2 \langle v u^2 \rangle, \tag{2.11}$$

where $\langle \cdot \rangle$ denotes an average over nodes, e.g. $\langle u \rangle = N^{-1} \sum_i u_i$ and $\langle v u^2 \rangle = N^{-1} \sum_i v_i u_i^2$. This equation is quadratic in C [and therefore also in F, via Eq. (2.7)] and linear in η, and may be easily solved for either. For $\eta = 0$ the nonzero solution for F is

$$F_{\eta=0} = \frac{(\lambda - 1)}{(\lambda + \frac{1}{2}\lambda^2)} \frac{\langle uv \rangle \langle u \rangle}{\langle u^2 v \rangle}. \tag{2.12}$$

This equation predicts that while zero is always a solution for $F_{\eta=0}$, it is only stable when $\lambda < 1$. The stable solution for $F_{\eta=0}$ when $\lambda > 1$ is given by Eq. (2.12). This prediction is numerically confirmed in Fig. 2.5, below. A more refined approximation than Eq. (2.11) can be obtained by repeating this process without expanding Eq. (2.8), which yields the linear equation for η

$$C\langle uv\rangle = \sum_{i=1}^{N}(1 - Cu_i)(\eta + (1-\eta)[1 - \exp(-\lambda C u_i)]). \tag{2.13}$$

Before numerically testing our theory, we will explain how it relates to previous results. For a network with correlations between degrees at the ends of a randomly chosen edge (assortative mixing by degree [35]), measured by the correlation coefficient $\rho = \langle k_i^{in} k_j^{out}\rangle_e / \langle k^{in} k^{out}\rangle$ as in Eq. (1.8), with $\langle\cdot\rangle_e$ denoting an average over edges, the largest eigenvalue may be approximated [3] by

$$\lambda \approx \rho\langle k^{in} k^{out}\rangle / \langle k\rangle. \tag{2.14}$$

In the absence of assortativity, when $\rho = 1$, Eq. (2.14) becomes

$$\lambda \approx \langle k^{in} k^{out}\rangle / \langle k\rangle. \tag{2.15}$$

If, in addition, there are no correlations between k^{in} and k^{out} (*node degree correlations*) or if the degree distribution is sufficiently homogenous, then $\langle k^{in} k^{out}\rangle \approx \langle k\rangle^2$ and the approximation of Eq. (2.15) reduces to

$$\lambda \approx \langle k\rangle \tag{2.16}$$

(The reader may be interested in a brief return to Fig. 1.6, which depicts an example network with $\lambda = 1.7693$, in order to calculate that the mean degree is $\langle k\rangle = 1.75$, illustrating a simple example of the potential accuracy of Eq. (2.16). We caution however, that the method of generating the approximations uses an assumption of very large network size to guarantee asymptotic accuracy [3], and so its accuracy in four node case is perhaps more of a convenient novelty.) In the case of Ref. [6], $\lambda \approx \langle d\rangle$ applies, and in the case of Refs. [29, 34], $\lambda \approx \langle k^{in} k^{out}\rangle / \langle k\rangle$ applies.

2.4 Numerical Simulations

We test our theoretical results via direct simulation of the Kinouchi-Copelli model on six categories of directed networks with $N = 10,000$ nodes:

- (category 1) Random networks with no node degree correlation between k^{in} and k^{out}.
- (category 2) Random networks with maximal degree correlation, $k^{in} = k^{out}$.
- (category 3) Random networks with moderate correlation between k^{in} and k^{out}.
- (category 4) Networks with power law degree distribution with power law exponents $\gamma \in [2.0, 6.0]$, with and without node degree correlations.
- (category 5) Networks constructed with $\langle k \rangle = 1$, and assortativity coefficient ρ varying in $[0.7, 1.3]$.
- (category 6) Networks with weights which depend on the degree of the node from which the edge originates, $A_{ij} = \alpha / k_i^{out}$.

We created networks in multiple steps:

(1) We created binary networks ($A_{ij} \in \{0, 1\}$) with target degree distributions as described below.

(2) We assigned a weight to each link, drawn from a uniform distribution between 0 and 1.

(3) We calculated λ for the resulting network and multiplied A by a constant to rescale the largest eigenvalue to the targeted eigenvalue. This is almost certainly *not* the method by which real neuronal networks achieve the critical state, which we freely acknowledge. Here, we use it simply to test our predictions. The field of *self-organized criticality* examines the potential ways in which systems may achieve a critical state spontaneously, but we do not cover it here.

This process was restarted from the first step for every network used in categories 1-4, creating a structurally different network for each simulation. The initial binary networks in categories 1-3 were Erdős-Rényi random networks [9], constructed by linking any pair of nodes with probability $p = 10/N$, resulting in a mean unweighted degree $\langle k \rangle = 10$, as discussed in section 1.1.4. . Maximal degree correlation resulted from creating undirected binary networks and then forcing $A_{ij} = A_{ji}$ for $i < j$ while assigning weights. Moderate degree correlation resulted from making undirected binary networks but allowing $A_{ij} \neq A_{ji}$ when weights were assigned. The algorithms for constructing the initial binary networks of categories 4-6 placed links randomly between nodes with specified in- and out-degrees via the configuration model [50], discussed in section 1.1.4. For this model, we generated in- and out-degree sequences from a power law distribution of desired exponent γ by calculating the expected integer number of nodes with each integer degree, from minimum degree 10 to maximum degree 200. In creating category 5 networks, we initially created one scale free network with power law exponent $\gamma = 2.5$ and $\lambda = 1$. Then, to change the degree of assortativity, we modified this original network by choosing two links at random and swapping them if the resulting swap would change the assortativity in the direction desired. This process was repeated until a desired value of ρ was achieved. Importantly, this swapping makes it possible to leave the degree distributions of the network unchanged, while still changing the assortative or disassortative properties of the network as in [3, 35]. Therefore, by this method we may maintain exactly the same degree distribution and mean degree, yet modify λ by virtue of $\lambda \propto \rho$, Eq. (2.14).

In the six network types tested, results of simulations unanimously confirm the hypothesis that criticality occurs only for largest eigenvalue $\lambda = 1$. We present representative results in Fig. 2.3 (a), noting that each line and set of points corresponds to a single network realization, implying that the effect of the largest eigenvalue on criticality is robust for individual systems. Fig. 2.3 (a) shows the response F as a function of stimulus η for scale-free networks with exponent $\gamma = 2.5$, constructed with no correlation between in- and out-degree, highlighting the significant difference between the regimes of $\lambda < 1$ and $\lambda > 1$, with the critical data corresponding to $\lambda = 1$. The lines were obtained by using Eqs. (2.7) and (2.13). Fig. 2.3 (b) shows Δ as a function of λ, using

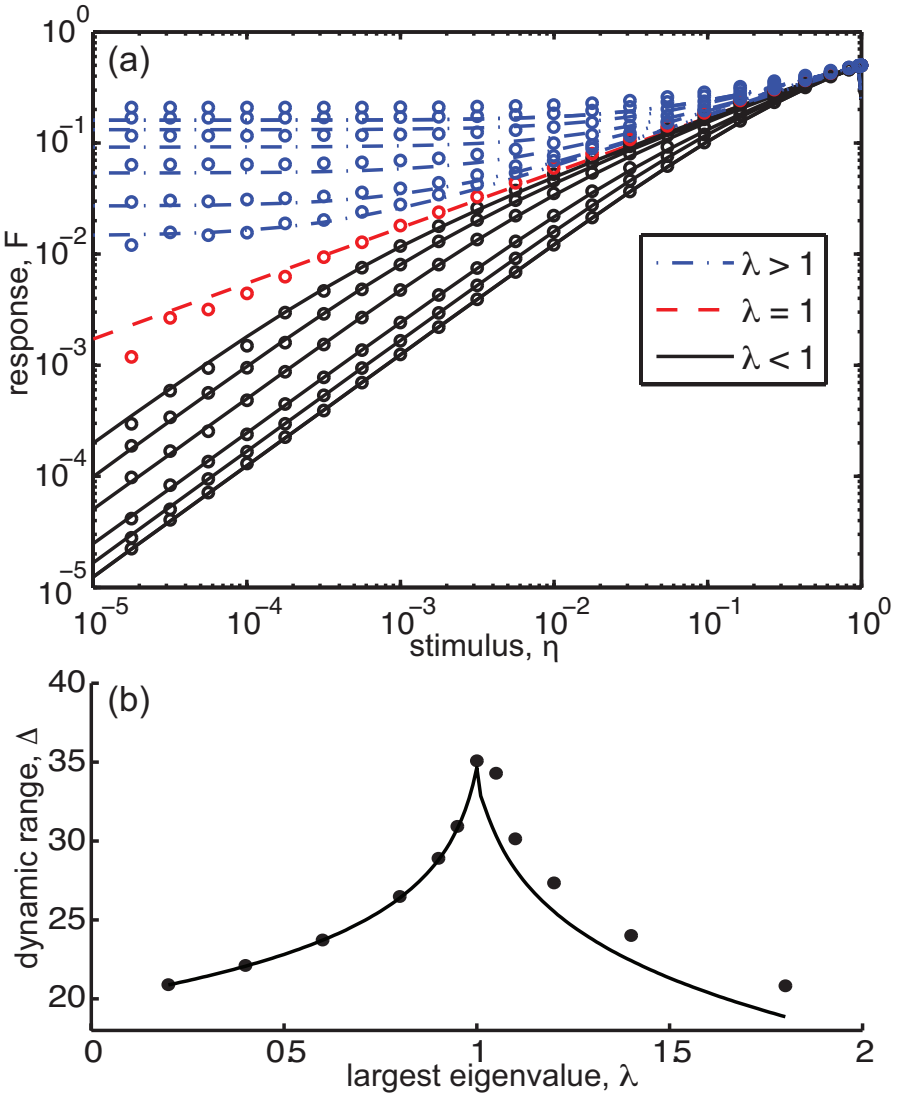

Figure 2.3: (a) Response F vs. stimulus η for power law networks with exponent $\gamma = 2.5$ and no correlation between k^{in} and k^{out}. Eq. (2.13) (lines) captures much of the behavior of the simulation (circles), particularly for low levels of η and F, as expected from approximating Eq. (2.2). (b) Dynamic range Δ is maximized at $\lambda = 1$ in both simulation results (circles) and Eq. (2.11) (line). This result compares quite favorably in trend with the dynamic range result for Erdős-Rényi random networks [6] reproduced in Fig. 2.2 and the dynamic range result for in vitro measurements of the dynamic range of slices of neonatal rat cortex [7] reproduced in Fig. 2.4.

$\eta_{high} = 1$ and $\eta_{low} = 0.01$, with the maximum occurring at $\lambda = 1$. Similar results showing criticality and maximum dynamic range at $\lambda = 1$ are obtained for networks of all categories 1-5, but are not shown here. Fig. 2.3(b) should be compared with Kinouchi and Copelli's result, Fig. 2.2 and Shew *et. al*'s experimental result, Fig. 2.4, noting that the axes are scaled differently yet similarities are striking. We comment on this surprising similarity in chapter 5.

Fig. 2.5 shows $F_{\eta\to 0}$ for networks of categories 3-5, confirming the transition predicted by the leading order analysis in Eq. (2.5). The symbols show the result of direct numerical simulation of the Kinouchi-Copelli model, the solid lines were obtained by iterating Eq. (2.2), and the dashed lines were obtained from Eq. (2.12). Fig. 2.5(a) shows that criticality occurs at $\lambda = 1$ (indicated by a vertical arrow) rather than at $\langle k\rangle = 1$ for a category 3 random network. Fig. 2.5(b) shows that criticality occurs at $\lambda = 1$ for scale-free networks (category 4). Correlations between k^{in} and k^{out} affect the point at which $\lambda = 1$ occurs (vertical arrows). In Fig. 2.5(c), the mean degree was fixed at $\langle d\rangle = 1$, while λ was changed by modifying the assortative coefficient ρ. As predicted by the theory, there is a transition at $\lambda = 1$ even though the mean degree is fixed, differentiating this result from previous work, which does not predict any difference among the simulations shown.

2.5 Impact on Dynamic Range

We now explore the question of what network topology will best enhance dynamic range. In many of the systems we simulate, a majority of the variation in dynamic range from one stimulus-response curve to another occurs due to variation at the low stimulus end of the curve, since most of the systems tend to saturate at around the same high stimulus levels (though this may not be the case for neuronal network experiments [7]). We therefore consider the following approximate measure of dynamic range, Λ, obtained by setting η_{high} to one in the definition of Δ,

$$\Lambda = 10 \log_{10} 1/\eta_*, \tag{2.17}$$

where η_* is the stimulus value corresponding to a lower threshold response F_*. Since dynamic range is maximized at criticality, we set $\lambda = 1$, solve Eq. (2.11) for η_*, substitute it into the definition of

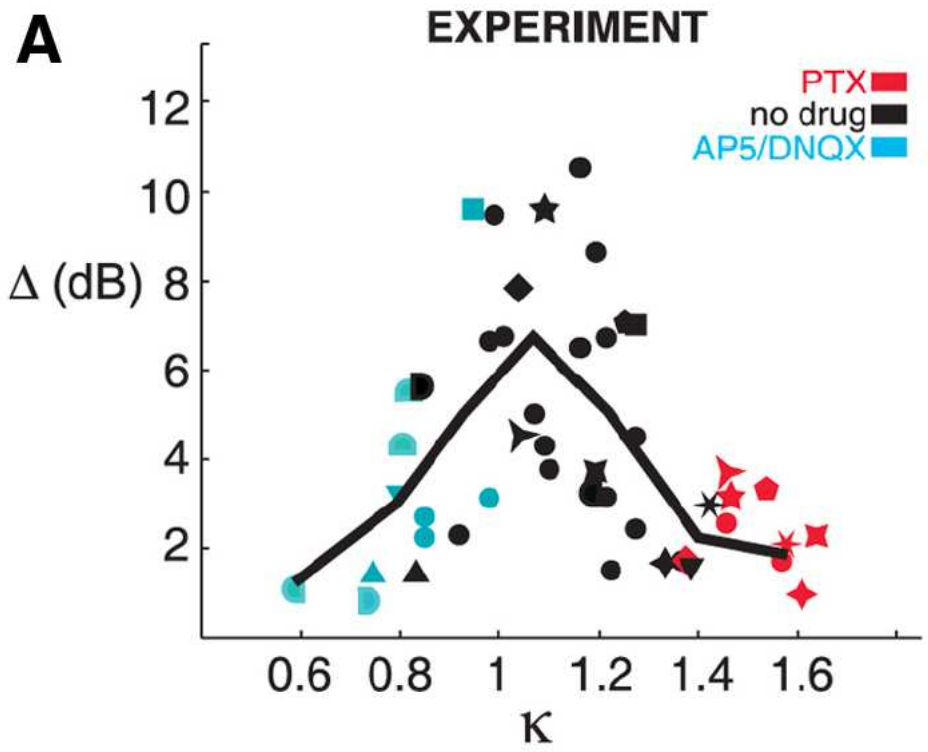

Figure 2.4: Dynamic range (Δ) is maximized when the in vitro neonatal rat cortex is stimulated in the absence of drugs (black symbols). When drugs are added which suppress excitatory neurons, dynamic range decreases (blue symbols). Similarly, dynamic range decreases when drugs are added whic suppress inhibitory neurons (red symbols). The horizontal axis κ is a statistical measure devised *ad hoc* in [7] to measure deviation away from the critical state in which neuronal avalanches occur. Figure reproduced from [7].

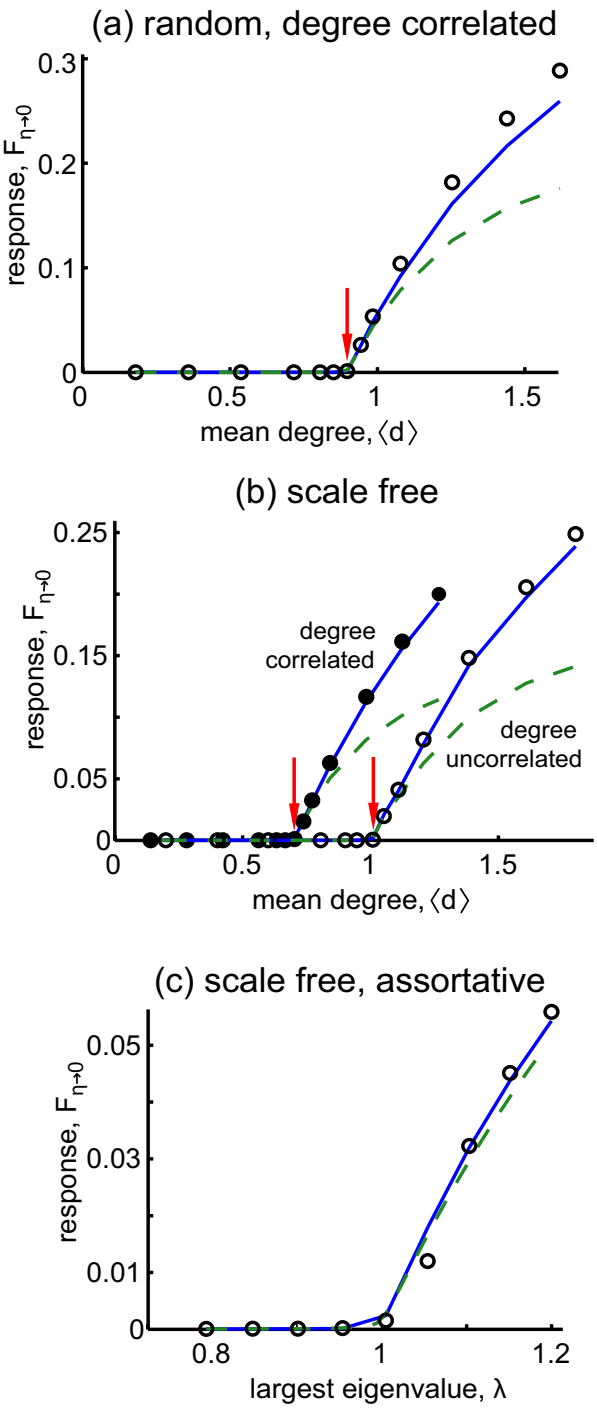

Figure 2.5: $F_{\eta\to 0}$ obtained from direct numerical simulation of the Kinouchi-Copelli model (symbols) plotted against $\langle d\rangle$ (a, b) and λ (c). Blue solid lines result from iterating Eq. (2.2) and green dashed lines result from Eq. (2.12). Small arrows show where $\lambda = 1$ predicts a phase transition. (a) A set of random networks (category 3) showing that criticality occurs at $\lambda = 1$ (arrow), but not $\langle k\rangle = 1$. (b) Criticality in scale free networks (category 4) with node degree correlation also occurs at $\lambda = 1$ (arrow), but not $\langle k\rangle = 1$. (c) Category 5 networks are tuned through criticality by changing assortativity, without changing the degree distributions and fixed $\langle k\rangle = 1$.

Λ using Eq. (2.7), retaining the leading order behavior to get

$$\Lambda_{MAX} = 10\log_{10}\frac{2}{3F_*^2} - 10\log_{10}\frac{\langle vu^2\rangle}{\langle v\rangle\langle u\rangle^2}. \tag{2.18}$$

The first term of this equation shows that Λ_{MAX} depends on F_*, i.e. dynamic range depends on how you measure it. Since the entries of the right (left) dominant eigenvector are a first order approximation to the in-degree (out-degree) of the corresponding nodes [51], the second term suggests that maximum dynamic range should increase (decrease) as the degree distribution becomes more homogenous (heterogeneous). For example, consider the case of an undirected, uncorrelated network, in which $v_i = u_i \approx k^i$. The second term is then approximately $-10\log_{10}(\langle k^3\rangle/\langle k\rangle^3)$, which is maximized when k^i is independent of i. It may be helpful to consider the relationship between this ratio of third moments of the degree distribution and the variance of samples from a distribution K: the variance is the difference of the average of K^2 and the average of K squared, whereas the ratio above is the ratio of the average of k^3 and the average of k cubed. In other words, as the degree distribution becomes more broad, its variance and this similar ratio of third moment to first moment cubed will increase. This corroborates the numerical findings in Refs. [6, 34] that random graphs enhance dynamic range more than more heterogeneous scale free graphs, and that the heterogeneity of the degree distribution affects dynamic range [34]. To test our result, we simulate scale free networks with different power law exponents $\gamma \in [2.0, 6.0]$, yet with $\lambda = 1$ to maximize dynamic range in each case. Results of simulation (circles) plotted against the prediction of Eq. (2.18) (line) are shown in Fig. 2.6.

2.6 Discussion

In summary, we analytically predict and numerically confirm that criticality and peak dynamic range occur in networks with largest eigenvalue $\lambda = 1$. This result holds for diverse network topologies including random, scale-free, assortative, and/or degree-correlated networks, and for networks in which edge weights are related to nodal degree, thus generalizing previous work. Moreover, we find that homogeneous (heterogeneous) network topologies result in higher (lower) dynamic

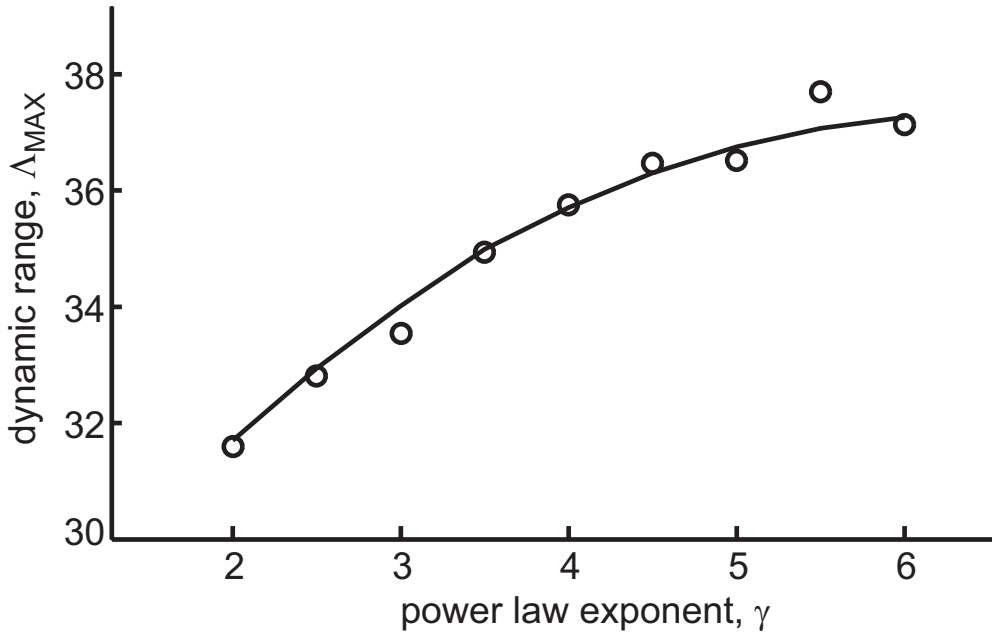

Figure 2.6: For power-law degree distributions with $\lambda = 1$, peak dynamic range increases monotonically with network homogeneity, as measured by power law exponent γ. Simulations (circles) agree well with our predictions [Eq. (2.18); line].

range. Previous demonstrations of how λ governs network dynamics in many other models (see [51] and references therein) suggest that the generality of our findings may extend beyond the particular model studied here. Previous model studies have shown that mutual information between stimulus and response is also maximized at criticality [5]. Our findings suggest that peak mutual information will also be determined by $\lambda = 1$, but verifying this will require additional investigation. Taken together with related experimental findings [7], our results are consistent with the hypotheses that 1) real brain networks operate with $\lambda \approx 1$, and 2) if an organism benefits from large dynamic range, then evolutionary pressures may act to homogenize the network topology of the brain.

This work is extended and made more accurate in the following chapter by including the possibilities of (i) time delays on the network links and (ii) distributions of refractory states other than $m = 2$. It also features analysis of the non-steady state behavior which was not addressed above.

2.7 Appendix: approximation of product by exponential

The approximation of the product by an exponential in Eq. (2.8) may be understood more easily by the following example. For simplicity of notation, consider the product $\prod_i (1 - a_i)$. Expanding the product, we get

$$\prod_i^N (1 - a_i) = 1 - \sum_i a_i + \sum_i \sum_{j<i} a_i a_j + \sum_i \sum_{j<i} \sum_{k<j} a_i a_j a_k + \mathcal{O}(a^4). \tag{2.19}$$

Then, we note that if one considers the space of integers between 1 and N as $\zeta = \{1, 2, ..., N\}$, the first sum is over the whole space ζ. The second is over approximately half of the space of $\zeta \times \zeta$—approximately half and not strictly half because the pairs where $i = j$ are excluded. The third term is a sum over one approximately one sixth of the space ζ^3. As an analogy, consider that the value of the integral in the first octant of $\mathbb{R}^3$ under the plane $i+j+k = 1$ with (i, j, k) cartesian coordinates is one sixth. One can confirm that subsequent terms decrease factorially.

Therefore, we may rewrite the terms on the right hand size of Eq. (2.19) by summing over

all i, j, k, etc. and dividing each subsequent sum by the appropriate factor,

$$\prod_i^N (1-a_i) = 1 - \sum_i a_i + \frac{1}{2!}\sum_i \sum_{j\neq i} a_i a_j + \frac{1}{3!}\sum_i \sum_{j\neq i} \sum_{k\neq i, k\neq j} a_i a_j a_k + \mathcal{O}(a^4). \tag{2.20}$$

where we have converted 1/2 to 1/2! and 1/6 to 1/3! for emphasis. By including the forbidden terms in the sums above, we may then separate the sums,

$$\prod_i^N (1-a_i) \approx 1 - \sum_i a_i + \frac{1}{2!}\sum_i a_i \sum_j a_j + \frac{1}{3!}\sum_i a_i \sum_j a_j \sum_k a_k + \mathcal{O}(a^4). \tag{2.21}$$

and so when N is large, we opt for the following approximation, appealing due to the exponential's many helpful properties,

$$\prod_i^N (1-a_i) \approx \exp(-\sum_i a_i). \tag{2.22}$$

Chapter 3

Effects of network topology, transmission delays, and refractoriness on the response of coupled excitable systems to a stochastic stimulus

We study the effects of network topology on the response of networks of coupled discrete excitable systems to an external stochastic stimulus. We extend results presented in chapter 2 that characterize the response in terms of spectral properties of the adjacency matrix by allowing distributions in the transmission delays and in the number of refractory states, and by developing a nonperturbative approximation to the steady state network response. We confirm our theoretical results with numerical simulations. We find that the steady state response amplitude is inversely proportional to the duration of refractoriness, which reduces the maximum attainable dynamic range. We also find that transmission delays alter the time required to reach steady state. Importantly, neither delays nor refractoriness impact the general prediction that criticality and maximum dynamic range occur when the largest eigenvalue of the adjacency matrix is unity.

Networks of coupled excitable systems describe many engineering, biological and social applications. Recent studies of how such networks respond to an external, stochastic stimulus have provided insight on information processing in sensory neural networks [6, 40], as discussed in the previous chapter. In agreement with recent experiments[7], these studies showed that the dynamic range of neural tissue is maximized in the critical regime, which is precisely balanced between growth and decay of propagating excitation. This regime was studied theoretically for directed random Erdős-Rényi networks in Ref.[6], where it was found to be characterized by a network mean degree equal to one. However, other studies[29, 34] showed that this condition does not

specify criticality for other network topologies. In this chapter, extending results of the previous chapter, we present a general framework for studying the effects of network topology on the response to a stochastic stimulus. With this framework, we derive a requirement for criticality and maximum dynamic range that holds for a wide variety of network topologies. Moreover, we show that this prediction holds when refractory states and transmission time delays are included in the network dynamics, although other aspects of the response do depend on these properties.

3.1 Introduction

Many applications involve networks of coupled excitable systems. Two prominent examples are the spread of information through neural networks and the spread of disease through human populations. The collective dynamics of such systems often defy naive expectations based on the dynamics of their individual components. For example, the collective response of a neural network can encode sensory stimuli that span more than 10 orders of magnitude in intensity, while the response of a single neuron typically encodes a much smaller range of stimulus intensities. Likewise, the collective properties of social contact networks determine when a disease becomes an epidemic.

Recently, a framework to study the response of a network of coupled excitable systems to a stochastic stimulus of varying strength has been proposed. The Kinouchi-Copelli model[6] considers the response of a directed Erdős-Rényi random network of coupled discrete excitable systems to a stochastic external stimulus. A mean-field analysis of this model predicted[6] that the maximum *dynamic range* (the range of stimuli over which the network's response varies signicantly) occurs in the critical regime where an excited neuron excites, on average, one other neuron. This criterion can be stated as the mean out-degree of the network being one, $\langle d^{out} \rangle = 1$, where the out-degree of a node d^{out} is defined as the expected number of nodes an excited node excites in the next time step (Ref.[6] refers to this quantity as the branching ratio).

Subsequent studies explored this system on networks with power-law degree distributions and hypercubic lattice coupling, and with a varying number of loops [40, 29, 30, 31, 34], showing that the criterion for criticality based on the network mean degree does not hold for networks with

a heterogeneous degree distribution. However, these studies (except[40]) do not take into account features that are commonly found in real networks, such as, for example, community structure, correlations between in- and out-degree of a given node, or correlations between the degree of two nodes at the ends of a given edge [35]. Furthermore, they do not consider the effect of transmission delays or a distribution in the number of refractory states.

In a recent report [40], recapitulated in extended form in the previous chapter, we presented an analysis of the Kinouchi-Copelli model that accounts for a complex network topology. We found that the general criterion for criticality is that the largest eigenvalue of the network adjacency matrix is one, $\lambda = 1$, rather than $\langle d^{out} \rangle = 1$. While this improved criterion successfully takes into account various structural properties of networks, our analysis did not address the effect of delays or multiple refractory states, and was based on perturbative approximations to the network response. In this chapter, we will extend the results of Ref.[40] by developing a nonperturbative analysis that accounts for distributions in the transmission delays and number of refractory states.

This chapter is organized as follows. In Section 3.2 we describe previous related work and the standard Kinouchi-Copelli model. In Section 3.3 we present the model to be analyzed and derive a governing equation for its dynamics. In Section 3.4 we present our main theoretical results. In Section 3.5 we apply our results to estimate the dynamic range of excitable networks. In Section 3.6 we present numerical experiments to validate our results. We discuss our results in Sec. 3.7.

3.2 Background

In this Section we describe the Kinouchi-Copelli model [6] and other relevant previous work. In order to focus on the effects of network topology, the dynamics of the excitable systems is taken to be as simple as possible. The model considers N coupled excitable elements. Each element i can be in one of $m+1$ states, x_i. The state $x_i = 0$ is the resting state, $x_i = 1$ is the excited state, and there may be additional refractory states $x_i = 2, 3, ..., m$. At discrete times $t = 0, 1, ...$ the states of the elements x_i^t are updated as follows: (i) If element i is in the resting state, $x_i^t = 0$, it can be excited by another excited element j, $x_j^t = 1$, with probability A_{ij}, or independently by an external

process with probability η; (ii) the elements that are excited or in a refractory state, $x_i^t \geq 1$, will deterministically make a transition to the next refractory state if one is available, or return to the resting state otherwise (i.e., $x_i^{t+1} = x_i^t + 1$ if $1 \leq x_i^t < m$, and $x_i^{t+1} = 0$ if $x_i^t = m$).

For a given value of the external stimulation probability η, which is interpreted as the stimulus strength, the network response F is defined in Ref.[6] as

$$F = \langle f \rangle_t, \tag{3.1}$$

where $\langle \cdot \rangle_t$ denotes an average over time and f^t is the fraction of excited nodes at time t. Of interest is the dependence of the response $F(\eta)$ on the topology of the network encoded by the connection probabilities A_{ij}. In particular, it is found that, depending on the network A, the network response can be of three types[6, 40]: *quiescent*, in which the network activity is zero for vanishing stimulus, $\lim_{\eta \to 0} F = 0$; *active*, in which there is self-sustained activity for vanishing stimulus, $\lim_{\eta \to 0} F > 0$; and *critical*, in which the response is still zero for vanishing stimulus but is characterized by sporadic long lasting avalanches of activity that cause a much slower decay in the response, compared with the quiescent case case, as the stimulus is decreased. Recent experiments [7] suggest that cultured and acute cortical slices operate naturally in the critical regime. Therefore, the network properties that characterize this regime are of particular importance.

In Ref. [6], the response F was theoretically analyzed as a function of the external stimulation probability, η, using a mean-field approximation in which connection strengths were considered uniform, $A_{ij} = \langle d \rangle / N$ for all i, j. It was shown that the critical regime is achieved at the value $\langle d \rangle = 1$, with the network being quiescent (active) if $\langle d \rangle < 1$ ($\langle d \rangle > 1$). For more general networks (i.e., A_{ij} not constant), $\langle d \rangle$ is defined as the mean degree $\langle d \rangle = \frac{1}{N} \sum_{i,j} A_{ij} = \langle d^{in} \rangle = \langle d^{out} \rangle$, where $d_i^{in} = \sum_j A_{ij}$ and $d_i^{out} = \sum_j A_{ji}$ are the in- and out-degrees of node i, respectively, and $\langle \cdot \rangle$ is an average over nodes. Such critical branching processes result in avalanches of excitation with power-law distributed sizes. Cascades of neural activity with power-law size and duration distributions have been observed in brain tissue cultures [5, 7, 22, 52, 53], awake monkeys [23, 22], and anesthetized rats [47, 54, 55]. While $\langle d \rangle = 1$ successfully predicts the critical regime for Erdős-

Rényi random networks [6], it does not result in criticality in networks with a more heterogeneous degree distribution [34, 29]. Perhaps more importantly, previous theoretical analyses [6, 34, 29] are not able to take into account features that are commonly found in real networks, such as, for example, community structure, correlations between in- and out-degree of a given node, or correlations between the degree of two nodes at the ends of a given edge [35]. We will generalize the mean-field criterion $\langle d \rangle = 1$ to account for complex interaction topologies encoded in the matrix A as well as refractoriness and transmission delays.

3.3 Generalized Kinouchi-Copelli model

3.3.1 Description of the model

We will analyze a generalized version of the Kinouchi-Copelli model which includes possibly heterogeneous distributions of delays and refractory periods. The model is as follows:

- There are N excitable elements, labeled $i = 1, \ldots, N$.
- At discrete times $t = 0, 1, ...,$ each element i can be in one of $m_i + 1$ states, x_i^t. The state $x_i^t = 0$ is the resting state, $x_i^t = 1$ is the excited state, and there may be additional refractory states $x_i^t = 2, 3, ..., m_i$.
- If element i is in the resting state at time t, $x_i^t = 0$, it can be excited in the next time step, $x_i^{t+1} = 1$, by another excited element j with delay τ_{ij} (i.e., if $x_j^{t-\tau_{ij}} = 1$) with probability A_{ij}, or independently by an external stimulus with probability η.
- The elements that are excited or in a refractory state, $x_i^t \geq 1$, will deterministically make a transition to the next refractory state if one is available, or return to the resting state otherwise (i.e., $x_i^{t+1} = x_i^t + 1$ if $1 \leq x_i^t < m_i$, and $x_i^{t+1} = 0$ if $x_i^t = m_i$).
- The coupling network, encoded by the matrix with entries A_{ij}, is allowed to have complex topology.

3.3.2 Model dynamics

By considering a large ensemble of realizations of the above stochastic process on the same network, we can define the probability that node i is at state x_i^t at time t as $p_i^t(x)$. The probabilities p_i^t evolve in one time step by

$$p_i^{t+1}(1) = p_i^t(0) r_i^t, \tag{3.2}$$

$$p_i^{t+1}(2) = p_i^t(1), \tag{3.3}$$

$$\cdots \tag{3.4}$$

$$p_i^{t+1}(m_i) = p_i^t(m_i - 1), \tag{3.5}$$

and we also have the normalization condition

$$p_i^t(0) = 1 - \sum_{j=1}^{m_i} p_i^t(j), \tag{3.6}$$

where r_i^t in Eq. (3.2) is the rate of transitions from the ready to the excited state, given by

$$r_i^t = E\left[\eta + (1-\eta)\left\{1 - \prod_j (1 - A_{ij} I_j^{t-\tau_{ij}})\right\}\right], \tag{3.7}$$

where I_j^t is one if node j is excited at time t and zero otherwise, and $E[\cdot]$ denotes an ensemble average. Assuming that the neighbors of node i being excited are independent events, we obtain, letting $p_i^t(1) \equiv p_i^t$,

$$r_i^t = \eta + (1-\eta)\left\{1 - \prod_j (1 - A_{ij} p_j^{t-\tau_{ij}})\right\}. \tag{3.8}$$

We note that the assumption of independence is reasonable if there are few short loops in the network, and has been successfully used in similar situations [44, 46]. However, this assumption is violated if the number of bidirectional links is significant, and therefore we will restrict our attention to purely directed networks. Inserting the expression above in Eq. (3.2) and eliminating $p_i^t(j)$ in terms of p_i^t for $j = 2, \ldots, m_i$, we obtain the governing equation for the dynamics of p_i^t

$$p_i^{t+1} = \left(1 - \sum_{k=1}^{m_i} p_i^{t+1-k}\right)\left(\eta + (1-\eta)\left[1 - \prod_j^N (1 - A_{ij} p_j^{t-\tau_{ij}})\right]\right). \tag{3.9}$$

In the following, we will analyze the response of the network by studying solutions of this equation as a function of η.

3.4 Analysis

In this Section we study the solutions of Eq. (9) and the associated network response. In Sec. IV A, we develop a nonperturbative approximation to the steady state response of the network. In Sec. IV B we analyze limiting cases of the steady-state response that give us additional qualitative insight. In Sec. IV C, we study the effect of a distribution in the transmission time delays on the time scale of relaxation to the steady state solutions. We then discuss in Sec. IV D how our results relate to previous work.

3.4.1 Steady-state response

First, we will study steady-state solutions to Eq. (3.9). To find those, we set $p_i^t = p_i$ in Eq. (3.9), which becomes

$$p_i = (1 - m_i p_i) \left(\eta + (1 - \eta) \left[1 - \prod_j^N (1 - A_{ij} p_j) \right] \right). \tag{3.10}$$

Proceeding as in Ref. [40], by assuming $A_{ij}p_j$ is small, we replace $\prod_j (1 - A_{ij}p_j)$ by $\exp(-\sum_j A_{ij}p_j)$ to get

$$p_i = (1 - m_i p_i) \left(\eta + (1 - \eta) \left[1 - e^{-\sum_j A_{ij} p_j)} \right] \right). \tag{3.11}$$

The assumption that $A_{ij}p_j$ is small is motivated as follows. If the weights A_{ij} are not very different from each other and each node has many incoming connections (such as in neural networks, where the number of synapses per neuron is estimated[56] to be of the order of $10,000$), then near the onset of self-sustained activity one should have $\sum_j A_{ij} \sim 1$ (the mean-field prediction of Ref. [6], which we refine here, states that the node average of $\sum_j A_{ij}$ is one at criticality), implying A_{ij} is small. The quantity $A_{ij}p_j$ is even smaller, especially for low levels of activity where p_j is small.

To proceed further we find convenient to define an alternative network response $\hat{F}$ as

$$\hat{F} = \langle \hat{f} \rangle_t, \tag{3.12}$$

where

$$\hat{f}^t = \frac{\sum_{i,j} A_{ij} I_j^t}{\sum_{i,j} A_{ij}}, \tag{3.13}$$

and $I_j^t = 1$ if node j is excited at time t and 0 otherwise. The variable $\hat{f}^t$ can be interpreted as proportional to the number of excited nodes weighted by their out-degree $d_j^{out} = \sum_i A_{ij}$. In terms of the probabilities p_i, $\hat{F}$ is

$$\hat{F} = \frac{\sum_{i,j} A_{ij} p_j}{\sum_{i,j} A_{ij}}, \tag{3.14}$$

and can be interpreted as the fraction of links that successfully transmit an excitation. This is analogous to the interpretation of F in Eq. (3.1) as the fraction of excited nodes. In principle, the definitions of $\hat{f}$ and $\hat{F}$ preclude their use in comparing directly against commonly used measures of activity since knowledge of the matrix A is required to estimate them. However, we note that in all the numerical experiments discussed below, $\hat{F}$ and F were found to be nearly identical. To develop a nonperturbative approximation to $\hat{F}$, we solve Eq. (3.11) for p_i in terms of $\sum_{j=1}^N A_{ij} p_j$. Multiplying the resulting expression by A_{ki} and summing over i, we obtain

$$\sum_{i=1}^N A_{ki} p_i = \sum_{i=1}^N A_{ki} \frac{1 - (1-\eta) e^{-\sum_{j=1}^N A_{ij} p_j}}{1 + m_i - m_i (1-\eta) e^{-\sum_{j=1}^N A_{ij} p_j}}. \tag{3.15}$$

Now, we use the fact that the largest eigenvalue of A, λ, is typically much larger than the second eigenvalue[3, 57], and thus $Ap \approx su$, where s is a scalar to be determined, and u is the right eigenvector of A corresponding to λ. The validity of this approximation will be discussed in Section 3.6.3. With this substitution, the previous equation reduces to

$$s u_k = \sum_{i=1}^N A_{ki} \frac{1 - (1-\eta) e^{-s u_i}}{1 + m_i - m_i (1-\eta) e^{-s u_i}}. \tag{3.16}$$

Noting that

$$\hat{F} = \frac{\sum_{i,j} A_{ij} p_j}{\sum_{i,j} A_{ij}} \approx \frac{\sum_i s u_i}{\sum_j d_j^{out}} = s \frac{\langle u \rangle}{\langle d \rangle},$$

where $\langle x \rangle \equiv \sum_{i=1}^{N} x_i/N$, we substitute $s \approx \hat{F}\langle d \rangle / \langle u \rangle$ into Eq. (3.16) yielding

$$\frac{\hat{F} u_k \langle d \rangle}{\langle u \rangle} = \sum_{i=1}^{N} A_{ki} \frac{1 - (1-\eta) e^{-\hat{F} u_i \langle d \rangle / \langle u \rangle}}{1 + m_i - m_i (1-\eta) e^{-\hat{F} u_i \langle d \rangle / \langle u \rangle}}.$$

which may now be summed over k, simplified, and solved for $\hat{F}$, yielding the scalar equation

$$\hat{F} = \left\langle \frac{d^{out}}{\langle d \rangle} \frac{1 - (1-\eta) e^{-\hat{F} u \langle d \rangle / \langle u \rangle}}{1 + m - m(1-\eta) e^{-\hat{F} u \langle d \rangle / \langle u \rangle}} \right\rangle. \tag{3.17}$$

We note that in the notation above, the outer average $\langle \cdot \rangle$ corresponds to a sum over the index i in Eq. (3.16). Given the adjacency matrix A, Eq. (3.17) can be solved numerically to obtain the response $\hat{F}$ as a function of η. We call Eq. (3.17) the "nonperturbative approximation" since its derivation does not rely on a perturbative truncation of the product term of Eq. (3.10), and we will numerically test its validity in Sec. 3.6, where we will find that Eq. (3.17) can be a good approximation for all values of η. In order to gain theoretical insight into how some features of the network topology and the distribution of the number of refractory states affect the response, we will use Eq. (3.17) to obtain analytical expressions for the response in various limits.

3.4.2 Perturbative approximations

While the nonperturbative approximation developed in the last section provides information for all ranges of stimulus, it is useful to consider perturbative approximations, for example, to determine what is the transition point from quiescent to active behavior. We will obtain an approximation to $\hat{F}$ which is valid for small η and $\hat{F}$. To do this, we expand the right hand side of Eq. (3.16) to second order in s and first order in η (as we will see, expanding to second order in s is necessary to treat the $\eta = 0$ case) obtaining

$$s u_k = \sum_{i=1}^{N} A_{ki} \left[\eta(1 - s u_i (1 + 2 m_i)) - s^2 u_i^2 \left(\frac{1}{2} + m_i \right) + s u_i \right]. \tag{3.18}$$

Multiplying by the left eigenvector entry v_k and summing over k we obtain, using $\sum_k A_{ki} v_k = \lambda v_i$ and rearranging,

$$\lambda s^2 \left\langle v u^2 \left(\frac{1}{2} + m \right) \right\rangle = \eta \lambda \langle v \rangle - s \eta \lambda \langle v u (1 + 2m) \rangle + (\lambda - 1) s \langle v u \rangle. \tag{3.19}$$

In terms of $\hat{F}$, this equation becomes

$$\hat{F}^2\langle d\rangle^2\left\langle vu^2\left(\frac{1}{2}+m\right)\right\rangle\lambda=\eta\lambda\langle v\rangle\langle u\rangle^2-\hat{F}\langle d\rangle\eta\lambda\langle vu(1+2m)\rangle\langle u\rangle+(\lambda-1)\hat{F}\langle d\rangle\langle vu\rangle\langle u\rangle. \quad (3.20)$$

To find the transition from no activity, $\hat{F}=0$, to self-sustained activity, $\hat{F}>0$, for vanishing stimulus, we let $\eta\to 0^+$ in the previous equation to find

$$\hat{F}_{\eta=0}(\lambda)=\begin{cases}0 & \lambda<1,\\ \frac{(\lambda-1)\langle vu\rangle\langle u\rangle}{\lambda\langle d\rangle\langle vu^2\left(m+\frac{1}{2}\right)\rangle} & \lambda\geq 1,\end{cases} \quad (3.21)$$

where the solution $\hat{F}=0$ was chosen for $\lambda<1$ to satisfy $\hat{F}\geq 0$. This equation shows that the transition from a quiescent network to one with self-sustained activity has, if the response $\hat{F}$ is interpreted as an order parameter, the signatures of a second order (continuous) phase transition. In addition, while the eigenvalue λ determines when this transition occurs (at $\lambda=1$), its associated eigenvectors u and v determine the significance of the observed response past the transition. If $\langle vu^2\rangle\gg\langle uv\rangle\langle u\rangle$, for example, the response might be initially too small to be of importance. One aspect that was not considered in Ref. [40] is how the distribution of refractory periods affects the response. If the refractory periods m_i are strongly positively correlated with the product $v_iu_i^2$, they can significantly increase the term $\langle mvu^2\rangle$ in the denominator, decreasing the response. This can be intuitively understood by noting that this amounts to preferentially increasing the refractory period of the nodes that are more likely to be active (as measured by the approximation $p_i\propto u_i$ valid close to the critical regime), thus removing them from the available nodes for longer times.

The response $\hat{F}$ for small stimulus and response in Eq. (3.21) agrees with the perturbative expression derived for F directly from Eq. (3.9) in Ref. [40] if $m_i=1$ and $\lambda\to 1$, and confirms the findings in Ref. [40] that the critical point is determined by $\lambda=1$. Henceforth, we will refer to networks with $\lambda<1$ as *quiescent*, to networks with $\lambda>1$ as *active*, and to networks with $\lambda=1$ as *critical*.

The behavior of the system for high stimulation is also of interest. When $\eta=1$, node i cycles deterministically through its m_i+1 available states, and so $p_i=(1+m_i)^{-1}$. The question is how this behavior changes as η decreases from 1. This information can be extracted directly

from Eq. (3.11) by linearizing around the solution $\eta = 1$, $\bar{p}_i = (1 + m_i)^{-1}$. Setting $\eta = 1 - \delta\eta$, $p_i = \bar{p}_i - \delta p_i$ with $\delta\eta \ll 1$, $\delta p_i \ll \bar{p}_i$, we obtain

$$\delta p_i \approx \bar{p}_i^2 e^{-\sum_j A_{ij}\bar{p}_j}\delta\eta. \tag{3.22}$$

Thus, the response of the nodes to a decreased stimulus depends on a combination of their refractory period (which determines $\bar{p}_i$) and decays exponentially with the number of expected excitations from its neighbors. In terms of the aggregate response $\hat{F}$, Eq. (3.22) becomes, after multiplying by A_{ki}, summing over k and i, and normalizing,

$$\frac{d\hat{F}}{d\eta} = \frac{\langle d^{out}\bar{p}^2 e^{-A\bar{p}}\rangle}{\langle d\rangle} \tag{3.23}$$

3.4.3 Dynamics near the critical regime

As in Ref. [40], we will study the transition from no activity to self-sustained activity in the limit of vanishing stimulus by linearizing Eq. (3.9) around $p_i^t = 0$ for $\eta = 0$. Assuming p_i^t is small, we obtain to first order

$$p_i^{t+1} = \sum_{j=1}^{N} A_{ij} p_j^{t-\tau_{ij}}. \tag{3.24}$$

Assuming exponential growth, $p_i^t = \alpha^t w_i$, we obtain

$$\alpha w_i = \sum_{j=1}^{N} A_{ij}\alpha^{-\tau_{ij}} w_j. \tag{3.25}$$

The critical regime, determined as the boundary between no activity and self-sustained activity as $\eta \to 0$, i.e, between the solution $p_i^t = 0$ being stable and unstable, can be found by setting $\alpha = 1$, obtaining

$$w_i = \sum_{j}^{N} A_{ij} w_j. \tag{3.26}$$

This implies that the onset of criticality occurs when $\lambda = 1$ and in this case $w = u$. This conclusion agrees with the results in Ref. [40] and those in the previous section. Although the critical regime is not affected by the presence of delays or refractory states, the rate of growth (decay) α of perturbations for the active (quiescent) regime depends on the distribution of delays. To illustrate

this, we consider the case when the network deviates slightly from the critical state, so that the largest eigenvalue of A is $\lambda = 1 + \delta\lambda$ and has right eigenvector u, $Au = (1 + \delta\lambda)u$. Expecting the solution w to Eq. (3.25) to be close to u, we set $w_i = u_i + \delta u_i$ and $\alpha = 1 + \mu$, where the rate of growth μ is assumed to be small. Inserting these in Eq. (3.25), we get to first order

$$\mu u + \delta u \approx u\delta\lambda + A\delta u - \mu\hat{A}u, \tag{3.27}$$

where the entries of the matrix $\hat{A}$ are given by $\hat{A}_{ij} = A_{ij}\tau_{ij}$. To eliminate the term δu, we left-multiply by the left eigenvector of A, v, satisfying $v^T A = (1 + \delta\lambda)v^T$. Canceling small terms, we get

$$\mu \approx \frac{\delta\lambda}{1 + \frac{v^T\hat{A}u}{v^T u}}. \tag{3.28}$$

If the delay is constant, $\tau_{ij} = \tau$, we obtain

$$\mu \approx \frac{\delta\lambda}{1 + \tau}, \tag{3.29}$$

and in this particular case a more general result can be obtained from Eq. (3.25), which implies $\alpha = \lambda^{1/(1+\tau)}$.

3.4.4 Relation to previous results

Here we will briefly discuss how our results for the critical regime agree with previous work in particular cases. Correlations between degrees at the ends of a randomly chosen edge (assortative mixing by degree [35]) can be measured by the correlation coefficient

$$\rho = \langle d_i^{in} d_j^{out}\rangle_e / \langle d^{in} d^{out}\rangle \tag{3.30}$$

defined in Ref. [3], with $\langle\cdot\rangle_e$ denoting an average over edges. The correlation coefficient ρ is greater than 1 if the correlation between the in-degree and out-degree of nodes at the end of a randomly chosen edge is positive, less than one if the correlation is negative, and one if there is no correlation. For a large class of networks, the largest eigenvalue may be approximated[3] by

$\lambda \approx \rho\langle d^{in}d^{out}\rangle/\langle d\rangle$. In the absence of correlations, when $\rho = 1$, the largest eigenvalue can be approximated by $\lambda \approx \langle d^{in}d^{out}\rangle/\langle d\rangle$. If there are no correlations between d^{in} and d^{out} at a node (*node degree correlations*) or if the degree distribution is sufficiently homogeneous, then $\langle d^{in}d^{out}\rangle \approx \langle d\rangle^2$ and the approximation reduces to $\lambda \approx \langle d\rangle$. This is the situation that was considered in Ref. [6], and thus they found that the critical regime was determined by $\langle d\rangle = 1$. In the case of Refs. [29, 34], with more heterogeneous degree distributions, $\lambda \approx \langle d^{in}d^{out}\rangle/\langle d\rangle$ applied, which accounts for their observation that the critical regime did not occur at $\langle d\rangle = 1$.

The situation encountered here is analogous to what occurs in the analysis of the transition to chaos in Boolean networks [46] and in the transition to synchronization in networks of coupled oscillators [58], where it is found that, instead of the mean degree, the largest eigenvalue is what determines the transition between different collective dynamical regimes.

Other previous studies in random networks have also investigated spectral properties of A to gain insight on the stability of dynamics in neural networks[48] and have shown how λ could be changed by modifying the distribution of synapse strengths[49]. In addition, it has been shown recently that the largest eigenvalues in the spectrum of the connectivity matrix may affect learning efficiency in recurrent chaotic neural networks [59].

3.5 Dynamic Range

We have studied the response of the network to stimuli of varying strengths. In particular, we studied in detail the response close to the critical regime. As has been previously noted [6], this regime corresponds to the point where the *dynamic range* Δ is maximized. In our context, the dynamic range can be defined as the range of stimulus η that results in significant changes in response $\hat{F}$. Typically the dynamic range is given in decibels and measured using arbitrary thresholds just above the baseline ($\lim_{\eta\to 0}\hat{F} \equiv \hat{F}_0$) and below the saturation ($\lim_{\eta\to 1}\hat{F} \equiv \hat{F}_1$) values, respectively, as illustrated in Fig. 2.1 for the active network case $\hat{F}_0 > 0$. More precisely, the value of stimulus η_{low} (η_{high}) corresponding to a low (high) threshold of activity $\hat{F}_{low}$ ($\hat{F}_{high}$)

are found and the dynamic range is calculated as

$$\Delta = 10 \log_{10}(\eta_{high}/\eta_{low}). \tag{3.31}$$

Using our approximations to the response $\hat{F}$ as a function of stimulus η, we can study the effect of network topology on the dynamic range. The first approximation is based on the analysis of Sec. 3.4.1. Using Eq. (3.17), the values of η correponding to a given stimulus threshold can be found numerically and the dynamic range calculated.

Another approximation that gives theoretical insight into the effects of network topology and the distribution of refractory states on the dynamic range can be developed as in Ref. [40], by using the perturbative approximations developed in Sec. 3.4.2. In order to satisfy the restrictions under which those approximations were developed, we will use $\hat{F}_{high} = \hat{F}_1$ and $\hat{F}_{low} = \hat{F}_0 \ll 1$. Taking the upper threshold to be $\hat{F}_{high} = \hat{F}_1$ is reasonable if the response decreases quickly from $\hat{F}_1$, so that the effect of the network on the dynamic range is dependent mostly on its effect on $\hat{F}_{low}$. Whether or not this is the case can be established numerically or theoretically from Eq. (3.22), and we find it is so in our numerical examples when the values of $\{m_i\}$ are not large (see Fig. 3.4). Taking $\eta_{high} = 1$ and $\eta_{low} = \eta^*$ we have

$$\Delta = -10 \log_{10}(\eta^*). \tag{3.32}$$

The stimulus level η can be found in terms of $\hat{F}$ by solving Eq. (3.20) and keeping the leading order terms in $\hat{F}$, obtaining

$$\eta = \frac{\hat{F}^2 \langle d \rangle^2 \left\langle v u^2 \left(\frac{1}{2} + m\right) \right\rangle - \hat{F} \langle d \rangle (\lambda - 1) \langle u \rangle \langle uv \rangle}{\lambda \langle v \rangle \langle u \rangle^2}. \tag{3.33}$$

This equation shows that as $\eta \to 0$ the response scales as $\hat{F} \sim \eta$ for the quiescent curves ($\lambda < 1$), and as $\hat{F} \sim \eta^{1/2}$ for the critical curve ($\lambda = 1$). We highlight that these scaling exponents for both the quiescent and critical regimes are precisely those derived in Ref. [6] for random networks, and therefore are robust to the generalization of the criticality criterion to $\lambda = 1$, the inclusion of time delays, and heterogeneous refractory periods. This is particularly important since these exponents could be measured experimentally [6]. Using this approximation for η^* in (3.32), we

obtain an analytical expression for the dynamic range valid when the lower threshold F^* is small. Of particular theoretical interest is the maximum achievable dynamic range Δ_{max} for a given topology. It can be found by setting $\lambda = 1$ in Eq. (3.33) and inserting the result in Eq. (3.32), obtaining

$$\Delta_{\max} = \Delta_0 - 10\log_{10}\left(\frac{\langle d\rangle^2 \left\langle vu^2\left(\frac{1}{2}+m\right)\right\rangle}{\langle v\rangle\langle u\rangle^2}\right), \tag{3.34}$$

where $\Delta_0 = -20\log_{10}(F^*) > 0$ depends on the threshold F^* but is independent of the network topology or the distribution of refractory states. The second term of Eq. (3.34) suggests that a positive correlation between refractoriness m and eigenvector entries u and v will decrease dynamic range, whereas a negative correlation will increase dynamic range. This prediction may be investigated in more depth in future publications. The second term of Eq. (3.34) also suggests that an overall increase in the number of refractory states will lead to an overall decrease in dynamic range. This is in contrast with the result of Ref. [60], which found that there exists a $m > 0$ which maximizes dynamic range in two-dimensional arrays of neurons. We note that the assumption of independence used in deriving Eq. (3.8) is not valid for a two dimensional array.

3.6 Numerical experiments

We tested our theoretical results from section 3.4 by comparing their predictions to direct simulation of our generalized Kinouchi-Copelli model described in section 3.3. Simulation parameters were chosen specifically to test the validity of Eqs. (3.17), (3.23), (3.28) and (3.34). All simulations, except where indicated, were run with $N = 10^4$ nodes for $T = 10^5$ timesteps, over a range of η from 10^{-5} to 1.

3.6.1 Construction of networks

We created networks in three steps: first, we created binary directed networks, $A_{ij} \in \{0, 1\}$, with particular degree distributions as described below, forbidding bidirectional links and self-connections; second, we assigned a weight to each link, drawn from a uniform distribution between

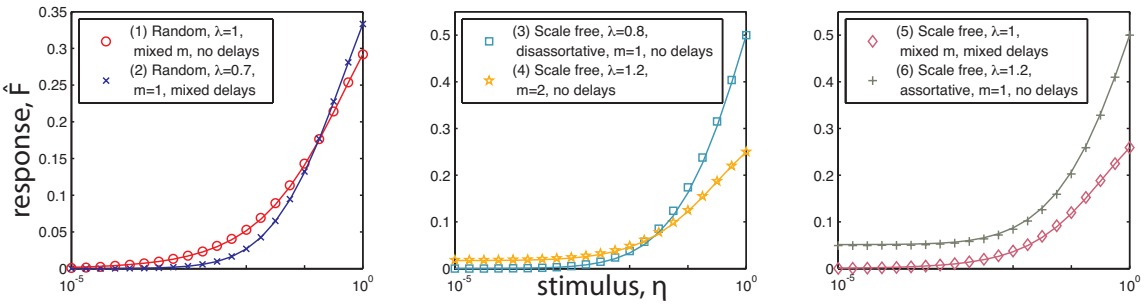

Figure 3.1: Semi-log plots of data from five simulations (symbols) testing a variety of situations in order to show the robustness of Eq. (3.17) (lines) to various sets of conditions: (1) Random network; $\lambda = 1$; mixed refractory states, $m_i \in \{1, 2, 3\}$; no delays; (2) Random network; $\lambda = 0.7$; no refractory states, $m_i = m = 1$; mixed delays, $\tau_{ij} \in \{0, 1, 2, 3\}$; (3) Scale free network; $\lambda = 0.8$; disassortative rewiring; no refractory states, $m_i = m = 1$; no delays; (4) Scale free network; $\lambda = 1.2$; uniform refractory states, $m_i = m = 2$; no delays; (5) Scale free network; $\lambda = 1.0$; mixed refractory states, $m_i \in \{1, 2, 3, 4\}$; mixed delays, $\tau_{ij} \in \{0, 1, 2\}$; (6) Scale free network; $\lambda = 1.2$; uniform refractory states, $m_i = m = 1$; no delays. The plots show excellent agreement between prediction and simulation at many points in parameter space.

0 and 1; third, we calculated λ for the resulting network, and multiplied A by a constant to rescale λ to the targeted eigenvalue. This is almost certainly not the method by which real biological networks tune their connectivity, but provides a theoretical starting point by which we can assess the properties of networks with varying λ, without commenting on how real networks may achieve such connectivities. The two classes of topology considered for simulations were directed Erdős-Rényi random networks and directed networks with power-law degree distributions, where we set the power-law exponent to $\gamma = 2.5$, and enforced a minimum degree of 10 and a maximum degree of 1000. Erdős-Rényi networks[9] were constructed by linking any pair of nodes with probability $p = 15/N$, and networks with power-law degree distribution were constructed by first generating in-degree and out-degree sequences drawn from the power-law distribution described above, assigning those target degrees to N nodes, and then connecting them using the configuration model [50]. In some cases an additional fourth step was used to change the assortativity coefficient ρ, defined in Eq. (3.30), of a critical (i.e., with $\lambda = 1$) network with power-law degree distribution, making this network more assortative (disassortative) by choosing two links at random, and swapping their destination connections only if the resulting swap would increase (decrease) ρ. This swapping allows

for the degree of assortativity (and thereby, λ) to be modified while preserving the network's degree distribution [3, 35].

3.6.2 Results of numerical experiments

We first demonstrate the ability of the non-perturbative approximation to predict aggregate network behavior in a variety of conditions. Fig. 3.1 shows a multitude of simulations (symbols) with the predicted behavior of Eq. (3.17) overlaid (lines). The cases considered in Fig. 3.1 include different combinations of topology, assortativity, largest eigenvalue λ, delays, and number of refractory states. The number of refractory states m_i was chosen either constant, $m_i = m$, or randomly chosen with equal probability among $\{1, 2, \ldots, m_{\max}\}$. Similarly, the delays τ_{ij} were either constant, $\tau_{ij} = \tau$, or uniformly chosen with uniform probability in $(0, \tau_{\max})$. The predictions capture the behavior of the simulations, with particularly good agreement for networks with neutral assortativity, $\rho = 1$. In the assortative and disassortative cases shown [cases (3) and (6) in Fig. 3.1], low and high stimulus simulations are well captured by the prediction, while a small deviation can be observed for intermediate values of η [e.g., in case (6) in the right panel of Fig. 3.1, the crosses have a small systematic error around $\eta = 10^{-2}$]. In Sec. 3.6.3, we will discuss why Eq. (3.17), which assumes $Ap \approx su$, works so well. In particular, we will discuss why this approximation is expected to work well for small and large η.

As reported previously[40], we find in our simulations that networks with $\lambda = 1$ show critical dynamics and exhibit maximum dynamic range. This applies to random networks, networks with power-law degree distribution, and networks with power-law degree distribution with modified assortativity. Networks with $\lambda < 1$ exhibit no self-sustained activity in the absence of stimulus, whereas networks with $\lambda > 1$ exhibit self-sustained activity. Furthermore, in all numerical experiments, with distributed refractory states, and various time delays, the criticality of networks at $\lambda = 1$ was preserved as predicted above. Typical results in Fig. 3.2 (a) show the response $\hat{F}$ as a function of stimulus η for networks with power-law degree distribution with $\gamma = 2.5$, refractory states $m_i = m = 1$, and no time delays, with λ ranging from 0.2 to 1.8. Each symbol in the figure

is generated by a single simulation on a single network realization. Lines show $\hat{F}$ obtained from numerical solution of Eq. (3.17). We note that the simulations with $\lambda = 1$ show a deviation from the theoretically predicted critical curve for values of η less than 10^{-4}. We believe this is due to the fact that for such low values of η, a much longer time average than the one we are doing would be required. For example, with $\eta = 10^{-5}$ we expect that, using 10^5 time steps, a given node will not be excited externally with probability $e^{-1} \approx 0.37$. This might be especially important in the critical regime, where activity is mostly determined by sporadic avalanches propagated by hubs.

Figure 3.2 (b) shows the dynamic range Δ calculated using $F^* = 10^{-2}$ directly from the simulation (circles) and using Eq. (3.17) (dashed line). As demonstrated in Ref.[40], the dynamic range is maximized when $\lambda = 1$. We note that in Ref.[40] the dynamic range was estimated using a perturbative approximation, and as a consequence our prediction had a systematic error in the $\lambda > 1$ regime [cf. Fig. 1 (b) in Ref.[40]]. The nonperturbative approximation Eq. (3.17) results in a much better prediction.

Figure 3.3 shows the transition that occurs at $\lambda = 1$ when $\eta \to 0$ for experiments with a varying number of refractory states, $m = 1$, 3, and 5. Symbols indicate the results of direct simulation using $\eta = 10^{-5}$, and the lines correspond to Eq. (3.17), which describes well the result of the simulations. We found that for this particular network, the perturbative approximation (3.21) only gives correct results very close to the transition at $\lambda = 1$, and its quantitative predictions degrade quickly as $\hat{F}$ grows. [A similar situation can be observed in Fig. 2(b) of Ref.[40].] However, we found that the perturbative approximation is still useful to predict the effect of the refractory states. Eq. (3.21) predicts that the response should scale as $\langle m + 1/2 \rangle^{-1}$. The inset shows how, after multiplication by $\langle m + 1/2 \rangle$, the response curves collapse onto a single curve. Figure 3.3 also depicts a linear relationship, $\hat{F} \sim (\lambda - 1)$ for $\lambda > 1$. Making a connection with the theory of nonequilibrium phase transitions in which $\hat{F} \sim (\lambda - \lambda_c)^\beta$, we derive $\lambda_c = 1$ and the critical exponent $\beta = 1$.

Figure 3.4 shows the response $\hat{F}$ close to $\eta = 1$ calculated for various values of m from the simulation (symbols), and from Eq. (3.23) (solid lines). Eq. (3.23) describes well the slope of $\hat{F}$

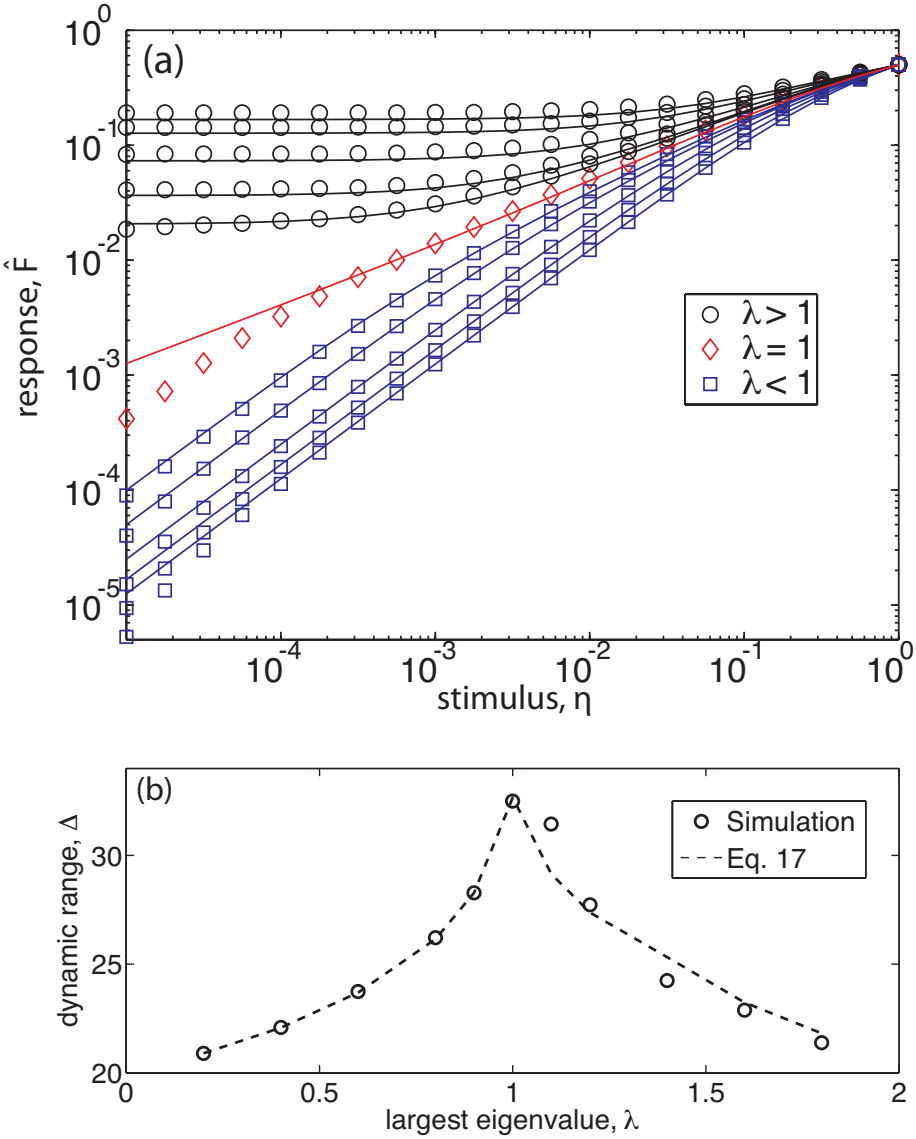

Figure 3.2: Simulation data for networks with power-law degree distribution comprising 10^4 nodes (symbols) and numerical solution of Eq. 3.17 (lines). (a) Stimulus vs response predictions agree well in the regime where $Ap \approx su$, as discussed in section 3.6.3. Eigenvalues range from 0.2 to 0.9 (blue squares), exactly 1.0 (red diamonds), and from 1.1 to 1.8 (black circles). (b) Dynamic range predictions capture maximization at $\lambda = 1$ as well as the non-critical behavior.

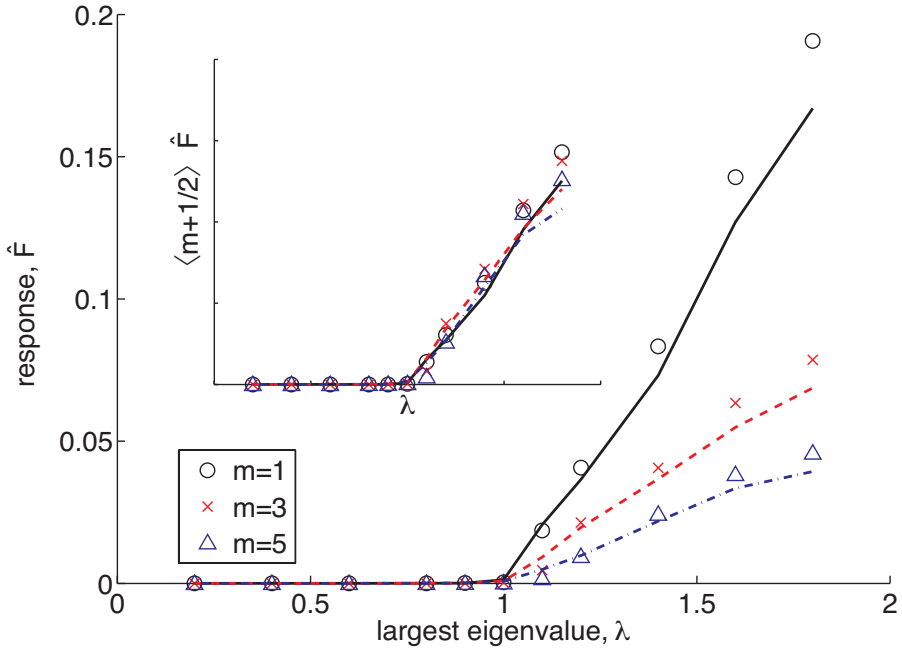

Figure 3.3: Phase transitions of $F_{\eta\to 0}$ for different refractory states, m for simulations (symbols) and Eq. (3.17) (lines). Inset: Eq. (3.21) predicts that phase transitions should scale by $\langle m+1/2\rangle^{-1}$, confirmed by rescaling data from the larger plot accordingly.

close to $\eta = 1$. An important observation is that as m grows, the relative slope $\hat{F}^{-1}d\hat{F}/d\eta$ at $\eta = 1$ decreases. Therefore, if the typical refractory period m is large, the response $\hat{F}$ saturates [e.g., reaching 90% of $\hat{F}(1)$] for smaller values of η.

Transmission delays, as in the analogous system of gene regulatory networks[46], do not modify steady state response. However, delays modify the time scale of relaxation to steady state. We quantified this modification in the growth rate in Eq. (3.28), which determines the growth rate of perturbations from an almost critical quiescent network in terms of a matrix determined from the distribution of delays. In Fig. 3.5 we show time series (solid lines) for the initial growth in the number of excited nodes within four active networks with and without time delays. For comparison, we show the slope that results from the corresponding growth rates obtained from Eq. (3.28) (dotted lines). The timesteps shown on the horizontal axis have been shifted to display multiple results together, but not rescaled or distorted. As shown in Fig. 3.5, Eq. (3.28) is helpful in quantifying the growth rate of signals within the network in the regime during which growth is exponential. In this limited regime, simulation data compare well with time series of excitations, and capture the growth rate's dependence on eigenvalue and time delays. We note here that Eq. (3.28) predicts the growth rate of p_i^t, and therefore the growth rate of both f^t and $\hat{f}^t$. Here we have chosen to show the growth in the number of excited nodes (proportional to f^t) which is more experimentally accessible than $\hat{f}^t$.

3.6.3 Validity of the approximation $Ap \propto u$

Here we will address the question of the validity of our approximation $Ap \propto u$, which was used to develop the nonperturbative approximation Eq. (3.17). First, we note that when η and p are small, the linear analysis of Sec. 3.4.3 and Ref.[40] shows that $p \propto u$, and therefore the approximation $Ap \propto u$ is justified in this regime. As η grows, and for situations where p is not small, one should expect deviations of p from being parallel to u. However, we note that since p_i measures how active node i is, it should still be highly correlated with the in-degree of node i. Since in many situations the in-degree is also correlated with the entries of the eigenvector u, we expect

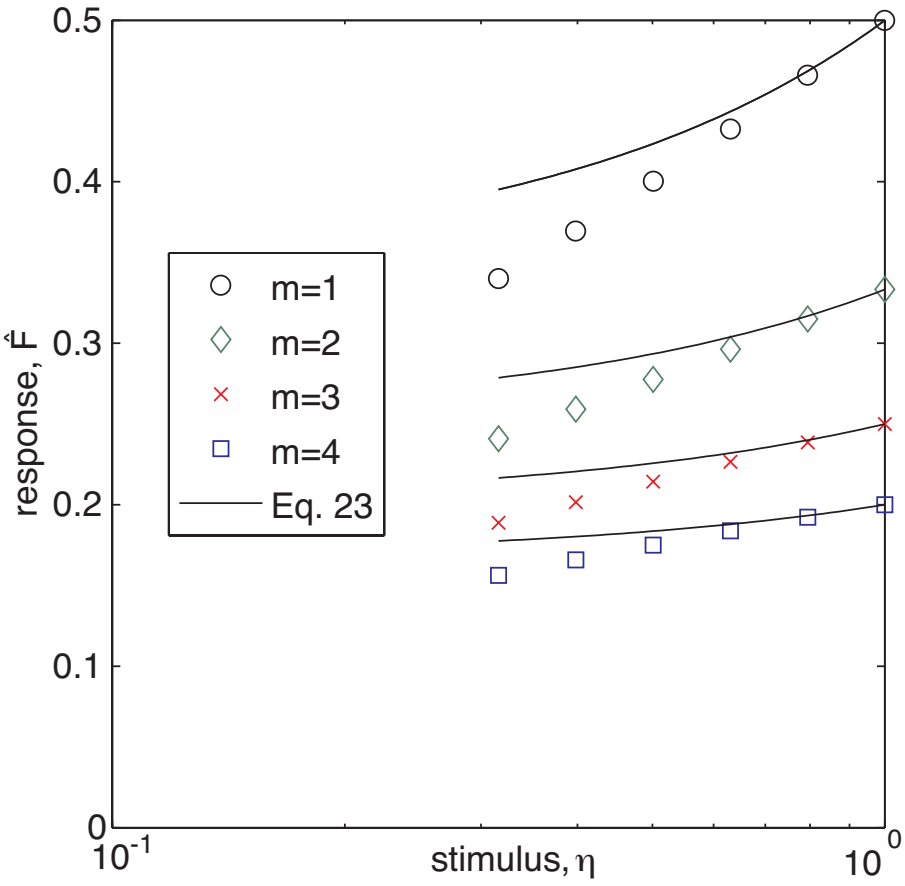

Figure 3.4: Simulation data (symbols) compare reasonably with the prediction of the perturbative approximation close to saturation, Eq. 3.23, for different refractory states. $\delta\eta$ was chosen to be the difference between $\eta = 10^0$ and $\eta = 10^{-0.1}$, corresponding to the two rightmost data points of each simulation.

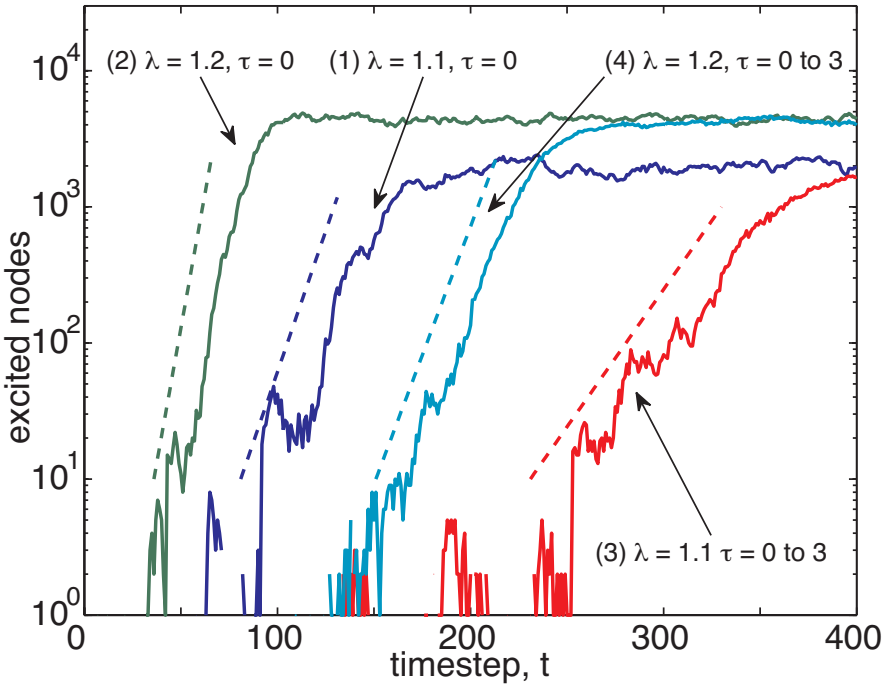

Figure 3.5: Time series (solid lines) for initial growth of signals within four active networks, with growth rates from Eq. (3.23) shown (dotted lines). The timesteps shown on the horizontal axis have been shifted to display multiple results together, but not rescaled or distorted. In less than 100 timesteps, all networks tested exhausted the exponential growth regime. N=100000 nodes and $\eta = 10^{-6}$, for (1) $\lambda = 1.1$, $\tau = 0$, (2) $\lambda = 1.2$, $\tau = 0$, (3) $\lambda = 1.1$, $\tau \in \{0, 1, 2, 3\}$, (4) $\lambda = 1.2$, $\tau \in \{0, 1, 2, 3\}$.

that in those cases p remains correlated with u. After multiplication by A, the approximation can only become better. For the class of networks in which the ratio between the largest eigenvalue λ and the next largest eigenvalue scales as $\sqrt{\langle d \rangle}$ (which include Erdős-Rényi and other networks[57]), we expect that $Ap \propto u$ should be a good approximation.

Another reason why the approximation $Ap \propto u$ works well even when $\hat{F}$ is not small is that the errors introduced by this approximation vanish exactly when $\eta = 1$. To see this, note that for $\eta = 1$, since each node cycles deterministically through its $m_i + 1$ available states, we have $p_i = 1/(1 + m_i)$, which gives $\hat{F} = \sum_{i,j} A_{i,j}(1 + m_j)^{-1} / \sum_{i,j} A_{i,j} = \langle d^{out}(1 + m)^{-1} \rangle / \langle d \rangle$, which agrees exactly with the result of setting $\eta = 1$ in Eq. (3.17). Thus, even as the assumption $Ap \propto u$ may become less accurate as η grows, the importance of the error introduced by it decreases and eventually vanishes at $\eta = 1$.

To illustrate how the assumption $Ap \approx su$ works in some particular examples, Fig. 3.6 compares normalized Ap_i and u_i for a variety of eigenvalues and stimulus levels. Good agreement between them (characterized by a high correlation) indicates that the assumption of section 3.4.1 is valid, whereas more noisy agreement for some cases indicates that the assumption $Ap \propto u$ is invalid (although, as discussed above, this does not necessarily imply that the nonperturbative approach will fail). Low stimulus levels in quiescent networks (top left panel) show relatively low correlation for short simulations, but the correlation improves with more timesteps as relative nodal response increases at well connected nodes and decreases at poorly connected nodes. Assortative networks (bottom panels) show slightly lower correlation as well, corroborating the results shown in Fig. 3.1 where the predictive power of Eq. (3.17) is slightly diminished for the assortative network. As expected, correlation between Ap and u entries is worst at $\eta = 1$ (right panels), but we reiterate that for $\eta = 1$ this error does not affect the predictions of Eq. (3.17).

3.7 Discussion

In this chapter we studied a generalized version of the Kinouchi-Copelli model in complex networks. We developed a nonperturbative treatment [Eq.(3.17)] that allows us to find the re-

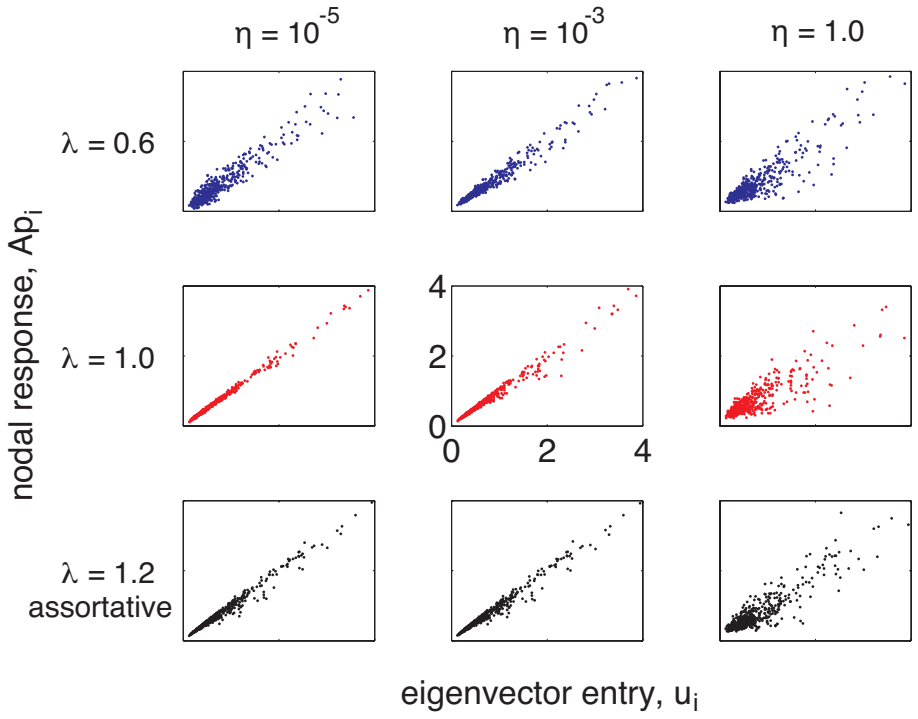

Figure 3.6: Plots of normalized Ap_i vs su_i for scale-free networks, with eigenvalues 0.6 (blue, top row), 1.0 (red, middle row), and 1.2 with assortative mixing (black, bottom row) at stimulus levels $\eta = 10^{-5}, 10^{-3}$,and 1 for the left, middle, and center columns respectively. Agreement is very good for critical and active cases, with more noise in the quiescent case due to less incoming stimuli over the duration of the simulation.

sponse $\hat{F}$ of the network for a given value of the stimulus given a matrix of excitation transmission probabilities A. Our approach includes the possibility of heterogeneous distributions of excitation transmission delays and numbers of refractory states. An important assumption in our theory is that there are many incoming links to every node, which allows us to transform the product in Eq. (3.9) into an exponential. This assumption is very reasonable for neural networks, where the number of synapses per neuron is estimated[56] to be of the order of $10,000$. In addition, in order to obtain a closed equation for $\hat{F}$, we assumed $Ap \propto u$. As discussed in Sec. 3.6.3, this approximation works well in the regime when the response and stimulus are small. Furthermore, the error introduced by this approximation becomes smaller as the probability of stimulus increases and eventually vanishes for $\eta = 1$. The result is that Eq. (3.17) predicts the response $\hat{F}$ satisfactorily for all values of η. While we validated our predictions using scale-free networks with various correlation properties, we did not test them in topologies in which mean-field theories have been shown to fail, such as periodic hypercubes and branching tree networks [31, 42]. This study is left to future research.

Our theory describes how the introduction of additional refractory states modifies the network response by modifying Eq. (3.17). In addition, their effect is captured by the perturbative approximations of Sec. 3.4.2 which, although valid in principle only for very small $\hat{F}$, we have found successfully predict the effect of a distribution in the number of refractory states for a larger range of response values.

We studied the effect of time delays on the time scale needed to reach a steady-state response, and found that Eq. (3.28) determines the growth rate of perturbations from a quiescent, almost critical network. The temporal characteristics of the response could be important in the study of sensory systems, in which the stimulus level might be constantly changing in time. Additionally, delays may be important in studying the phenomenon of synchronization and propagation of wavefronts, which we do not study here. Synchronization in epidemic models similar to the model considered here has been well-described in the absence of time delays [61], and synchronization in Rulkov neurons has been shown to be affected subtly by time delays [62]. However, the effect of

time delays on synchronization in our model remains an open line of inquiry.

An important practical question regarding the application of our theory to neuroscience is how our results can be made compatible with the presence of excitatory and inhibitory connections in neural networks. Considering one excited neuron, and after excitatory and inhibitory connections are taken into account, the important quantity that determines the future activity of the network is how many other neurons are expected to be excited by the originally excited neuron. This number might depend on the overall balance of excitatory and inhibitory connections, but it must be a positive number. The Kinouchi-Copelli model we are using, and similar models used successfully by neuroscientists to model neuronal avalanches[7], have therefore considered only excitatory neurons, while adjusting the probabilities of excitation transmission to account for different balances of excitatory and inhibitory neurons. Nevertheless, we believe a generalization of the Kinouchi-Copelli model that accounts for inhibitory connections should be investigated in the future.

Another important issue is the generality of our findings for more biologically realistic excitable systems. We conjecture that the effect of network topology on the dynamic range of networks of continuous-time, continuous-state coupled excitable systems such as coupled ODE neuron models[15] is qualitatively similar to its effect on the class of discrete-time, discrete-state dynamical systems studied here. However, this remains open to investigation.

Chapter 4

Statistical Properties of Avalanches in Networks

We characterize the distribution of sizes and durations of avalanches propagating in complex networks. We find that the statistics of avalanches can be characterized in terms of the largest eigenvalue and corresponding eigenvector of an appropriate adjacency matrix which encodes the structure of the network. By using mean-field analyses, previous studies of avalanches in networks have not considered the effect of network structure on the distribution of size and duration of avalanches. Our results apply to individual networks (rather than network ensembles) and provide expressions for the distribution of size and duration of avalanches starting at particular nodes in the network. These findings might find application in the analysis of branching processes in networks, such as cascading power grid failures and critical brain dynamics. In particular, our results show that some experimental signatures of critical brain dynamics (i.e., power-law distributions of neuronal avalanches sizes and durations), are robust to complex underlying network topologies. In this chapter we study the statistics of avalanches propagating in complex networks. The study of avalanches of activity in complex networks is relevant to diverse fields, including epidemiology [63, 64], genealogy [17], and neuroscience [23, 7, 65, 6, 40, 41, 66, 5, 22, 39]. The simplest case of an avalanche corresponds to a branching process [67, 68], first studied by Galton and Watson [17]. These branching processes can be considered as avalanches propagating in a tree network. Various generalizations to the case where avalanches propagate in a more general network have been considered recently [37, 38, 39, 36], and related problems such as the distribution of cluster sizes in percolation models [69] and self-organized criticality in the "sandpile" model [70] have been

studied. In contrast to these previous studies, we develop a theory of avalanche size and duration on complex networks that, instead of using some form of mean field analysis, explicitly includes the network topology. This approach allows for an analysis of avalanches starting from arbitrary nodes in the network and the effect of nontrivial network structure on the distribution of avalanche sizes and durations.

While our formalism is general, our analysis was motivated by recent experiments on avalanches of neuronal bursting in the mammalian cortex. When a neuron fires, it stimulates other neurons which may subsequently fire. When this linked activity occurs in a cascade, it is called a *neuronal avalanche* (experimentally, neuronal avalanches are observed propagating in functional networks where each node represents a group of neurons). Recent experiments have studied neuronal avalanches of activity in the brains of awake monkeys [23] and slices of rat cortex [7]. These studies found that when the tissue is allowed to grow and operate undisturbed in homeostasis [65], both the size and temporal duration of neuronal avalanches is distributed according to a power law. In contrast, the application of drugs that selectively decrease the activity of inhibitory or excitatory neurons results in avalanches with different statistics [7]. Based on these observations, it has been argued and demonstrated experimentally that many neuronal networks operate in a critical regime that leads to power-law avalanche distributions [7], maximized dynamic range [7, 40, 41, 6], and maximized information capacity [22, 66, 5]. Therefore, it is of great interest to characterize this critical state and to understand how experimental signatures of criticality may change upon modifications to the underlying network (e.g., such as those induced by the drugs used in the experiment).

We find that the statistical properties of avalanches are determined by spectral properties of the matrix whose entries A_{mn} are the probabilities that the avalanche propagates from node n to node m. In particular, the eigenvalue λ of maximum magnitude (by the Perron-Frobenius theorem λ is real and positive if $A_{mn} > 0$) and its associated eigenvector play a prominent role in determining the functional form and the parameters for the statistical distribution of avalanche sizes and durations. While many of our findings have analogous results in classical Galton-Watson

branching processes [67, 68], we emphasize that our analysis allows us to identify how changes in network structure affect the parameters of the statistical distributions of avalanche sizes and durations. Moreover, our theory allows us to obtain the statistics of avalanches starting at particular network nodes.

This chapter is organized as follows. In Sec. 4.1 we describe our model for avalanche propagation in networks. In Secs. 4.2 and 4.3 we analyze the statistics of avalanche durations and sizes. In Sec. 4.4 we validate our analysis through numerical experiments. Section 4.5 presents further discussion and conclusions.

4.1 Formulation

To model the propagation of avalanches on a network, we consider a network of N nodes labeled $m = 1, 2, ..., N$. Each node m has a state $\tilde{x}_m = 0$ or 1. We refer to the state $\tilde{x}_m = 0$ as the *resting* state and to $\tilde{x}_m = 1$ as the *excited* state. At discrete times $t = 0, 1, ...$, the states of the nodes $\tilde{x}_m^t$ are simultaneously updated as follows: (i) If node m is in the resting state, $\tilde{x}_m^t = 0$, it can be excited by an excited node n, $\tilde{x}_n^t = 1$, with probability $0 \leq A_{mn} < 1$, so that $\tilde{x}_m^{t+1} = 1$. (ii) The nodes that are excited, $\tilde{x}_n^t = 1$, will deterministically return to the resting state in the next time step, $\tilde{x}_n^{t+1} = 0$. We therefore describe a network of N nodes with a $N \times N$ weighted network adjacency matrix $A = \{A_{mn}\}$, where $A_{mn} > 0$ may be thought of as the strength of connection from node n to node m, and $A_{mn} = 0$ implies that node n does not connect to node m.

Starting from a single excited node k ($\tilde{x}_m^0 = 1$ if $m = k$ and $\tilde{x}_m^0 = 0$ if $m \neq k$), we let the system evolve according to the dynamics above, and observe the cascade of activity until there are no more excited nodes. This motivates the following definitions, which are illustrated in Fig. 4.1 : (1) an *avalanche* is the sequence of excitations produced by a single excited node; (2) the *duration* d of an avalanche is defined as the total number of time steps spanned by the avalanche: if the avalanche starts with $\tilde{x}_n^0 = 1$, then

$$d_n = \min_{t \geq 0} \{\tilde{x}_k^t = 0 \text{ for all } k\}. \tag{4.1}$$

An avalanche that continues indefinitely is said to have infinite duration; (3) the *size* x of an avalanche starting at $\tilde{x}_n^0 = 1$ is defined as the total number of nodes excited during an avalanche, allowing for nodes to be excited multiple times:

$$x_n = \sum_{t=0}^{d_n - 1} \sum_{k=1}^{N} \tilde{x}_k^t. \tag{4.2}$$

Note that it is possible for an avalanche to have size larger than the total size of the network (e.g. if $d_n = \infty$, then $x_n = \infty$). Our goal in this chapter is to determine the probability distributions of these variables in terms of the matrix A.

4.2 Distribution of Avalanche Durations

In order to analyze the statistics of avalanche durations, we define $c_n(t)$ as the probability that an avalanche starting at node n has duration less than or equal to t,

$$c_n(t) = \mathrm{P}(d_n \leq t). \tag{4.3}$$

The quantity $c_n(t)$ is the cumulative distribution function (CDF) of the random variable d_n. In what follows, we will restrict our attention to a class of networks that we call **locally tree-like**. By locally tree-like, in this chapter we shall mean that, for any given t not too large, and pair of nodes j and k, if there exists a directed parth of length t from j to k, then it is rarely the case that there will also exist a second such path [71]. Many networks found in applications are of this type, and it has been found that the locally tree-like approximation works very well in describing various dynamical processes while still capturing the effects of network heterogeneity [40, 41, 51, 71, 46]. For these networks, we can approximately treat the avalanches propagating to different neighbors of node n as independent, and write the recursion relation

$$c_n(t+1) = \prod_{m=1}^{N} \Big[(1 - A_{mn}) + A_{mn} c_m(t) \Big], \tag{4.4}$$

together with $c_n(0) = 0$ which follows from the definition (4.3). The right hand side of Eq. (4.4) is the probability that nodes are either not excited by node n, or, if they are, then they generate

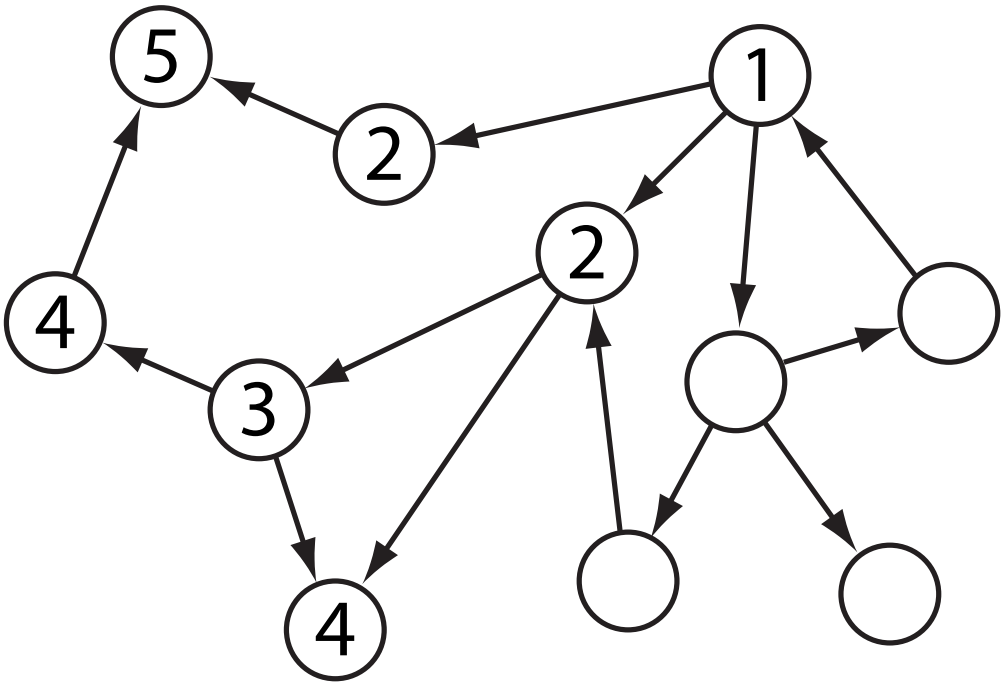

Figure 4.1: An example avalanche is shown, where circles represent nodes, arrows represent links, and numbers inside nodes correspond to the time step at which each node is activated. Starting from a single excited node, labeled 1, the avalanche spreads to two other nodes, labeled 2, and so on. Note that the presence of a link does not guarantee the transmission of excitation. The example avalanche above lasts for five time steps and excited a total of six nodes in addition to the initial node, so $d = 5$ and $x = 7$.

avalanches of duration at most t: $(1 - A_{mn})$ is the probability that an excitation *does not* pass from node n to node m, whereas $A_{mn}c_m(t)$ is the probability that an excitation *does* pass from node n to node m and the resulting avalanche has duration at most t. Note that Eq. (4.4) can treat any node n as the starting node for an avalanche. As discussed above, Eq. (4.4) assumes that the descendent branches of the avalanche are independent. It is, however, possible that an avalanche may branch in such a way that two branches interact at a later time. Nevertheless, for the networks we studied we found that, while these effects do occur for large avalanches, they do not significantly affect our predictions. We show numerical results confirming this in Sec. 4.4.

We are interested in the distribution of long avalanche durations, i.e., in the asymptotic form of $c_n(t)$ for $t \to \infty$. By definition (see also Appendix 4.6), $c_n(t)$ is a bounded, increasing function of t, and therefore it must converge to a value $\lim_{t\to\infty} c_n(t) = b_n \leq 1$ which can be interpreted as the probability that an avalanche starting at node n has finite duration. Our analysis will be based on whether or not this limit is less than or equal to one. As shown in Appendix 4.6, this is determined by the Perron-Frobenius eigenvalue of A, λ: if $\lambda \leq 1$, then $\lim_{t\to\infty} c_n(t) = 1$. The case $\lambda < 1$ will be referred to as the *subcritical* case, and the case $\lambda = 1$ will be referred to as the *critical* case. On the other hand, if $\lambda > 1$, then $\lim_{t\to\infty} c_n(t) = b_n < 1$, which implies that there is a finite probability that an avalanche has infinite duration. This case will be referred to as the *supercritical case*. The asymptotic form of $c_n(t)$ will be analyzed separately for these three cases below.

4.2.1 Subcritical Networks ($\lambda < 1$)

In the subcritical case, $b_n = 1$ is the only fixed point of the system Eq. (4.4) (see Appendix 4.6). To analyze the asymptotic form of $c_n(t)$, we assume it is close to the fixed point and define the small quantity $f_n(t) = 1 - c_n(t)$. Linearizing Eq. (4.4) we obtain

$$f_n(t+1) = \sum_{m=1}^{N} A_{mn} f_m(t). \tag{4.5}$$

Assuming exponential decay (or growth) of perturbations, $f_n(t) = \lambda^t v_n$, we obtain

$$\lambda v_n = \sum_{m=1}^{N} A_{mn} v_m. \tag{4.6}$$

Thus, λ is an eigenvalue of A and $\mathbf{v} = [v_1, v_2, ..., v_N]$ its left eigenvector. We identify λ as the Perron-Frobenius eigenvalue since, having the largest magnitude among all the eigenvalues, $\lambda^t v_n$ will be the dominant term as $t \to \infty$ when compared with the other modes. We note that for finite t, this approximation is good as long as there is a large enough separation between λ and the rest of the spectrum of A. This issue is discussed in [57], where it is found that this separation is typically large in networks without strong community structure. Henceforth, we will assume that λ is well separated from the rest of the spectrum of A. Therefore, $c_n(t)$ approaches 1 exponentially as

$$c_n(t) \approx 1 - \lambda^t v_n, \tag{4.7}$$

where $\mathbf{v}$ is the left eigenvector of A corresponding to λ; $v_n > 0$ by the Perron-Frobenius theorem [2]. The fixed point $b_n = 1$ is linearly stable when $\lambda < 1$.

The probability density function (PDF) of avalanche durations is given by $p_n(t) = P(d_n = t) = c_n(t) - c_n(t-1)$, so

$$p_n(t) = (\lambda^{-1} - 1)\lambda^t v_n, \tag{4.8}$$

which decays exponentially to zero with decay rate $\ln(1/\lambda)$.

In summary, we can draw two predictions from the analysis above for subcritical networks: (i) the PDF of avalanche duration decays exponentially towards zero as λ^t, and (ii) the probability that an avalanche started at node n lasts more than t steps is proportional to the n^{th} entry of the left eigenvector of A, v_n. These predictions are tested in Sec. 4.4.

4.2.2 Supercritical networks ($\lambda > 1$)

A linear stability analysis of the fixed point $b_n = 1$ in the supercritical case shows that this fixed point is linearly unstable. This implies (see Appendix 4.6) that there exists another fixed point b_n to which $c_n(t)$ converges from below, $\lim_{t\to\infty} c_n(t) = b_n < 1$. Thus, there is a positive probability that an avalanche will have infinite duration. Our analysis below characterizes the distribution of finite avalanche durations in supercritical networks. We first note that the fixed

point b_n satisfies

$$b_n = \prod_{m=1}^{N} \Big[(1 - A_{mn}) + A_{mn} b_m\Big]. \tag{4.9}$$

Again, we introduce the quantity $f_n(t) = b_n - c_n(t)$, and consider the limit when t is large and f_n is small. We substitute this into Eq. (4.4) and rewrite it as

$$b_n - f_n(t+1) = b_n \prod_{m=1}^{N} \Big[1 - \frac{A_{mn} f_m(t)}{(1 - A_{mn}) + A_{mn} b_m}\Big]. \tag{4.10}$$

By defining a new matrix D with entries

$$D_{mn} = \frac{A_{mn} b_n}{(1 - A_{mn}) + A_{mn} b_m}, \tag{4.11}$$

and linearizing Eq. (4.10) we find

$$f_n(t+1) \approx \sum_{m=1}^{N} D_{mn} f_m(t) \tag{4.12}$$

As in the subcritical case, we conclude that $f_n(t) \approx \lambda_D^t w_n$, where $\mathbf{w}$ is the left Perron-Frobenius eigenvector of the matrix D and λ_D its Perron-Frobenius eigenvalue. As argued in Appendix 4.7, $\lambda_D < 1$ when $\lambda > 1$, thus ensuring exponential convergence. Therefore, we have

$$c_n(t) \approx b_n - w_n \lambda_D^t. \tag{4.13}$$

As in the subcritical case, the probability density function (PDF) of avalanche durations is given by

$$p_n(t) = (\lambda_D^{-1} - 1)\lambda_D^t w_n, \tag{4.14}$$

which decays exponentially to zero with decay rate $\ln(1/\lambda_D)$.

In summary, for supercritical networks: (i) the PDF of avalanche duration decays exponentially towards zero as λ_D^t, and (ii) the probability that an avalanche started at node n lasts more than t steps is proportional to the n^{th} entry of the left eigenvector of D, w_n. These predictions are tested in Sec. 4.4. We note that these predictions simplify to those drawn from Eq. (4.7) if the network is subcritical, in which case $b_n = 1$, Eq. (4.11) simplifies to $D_{mn} = A_{mn}$, and therefore $\lambda_D = \lambda$ and $\mathbf{v} = \mathbf{w}$.

4.2.3 Critical Networks ($\lambda = 1$)

The analyses above show that if $\lambda = 1$, the fixed point $b_n = 1$ is marginally stable. This fixed point must be an attracting fixed point, since $c_n(t)$ is nondecreasing and $b_n = 1$ is the only fixed point of Eq. (4.4) as shown in Appendix 4.6. To determine the asymptotic form of $c_n(t)$ for large t, we let $c_n(t) = 1 - f_n(t)$. We assume that Eq. (4.4) has a solution whose asymptotic functional form in t (to be determined) can be extended to a differentiable function of a continuous time variable t. Since the convergence of $f_n(t)$ to 0 is slower than exponential, we look for a solution $f_n(t)$ which is slowly varying in t when $f_n(t)$ is small, and approximate

$$f_n(t+1) \approx f_n(t) + f_n'(t). \tag{4.15}$$

The slowly varying assumption implies that $df_n(t)/dt \equiv f_n'(t) \ll f_n(t)$ as $f_n \to 0$, which we note excludes an exponential solution. Substituting Eq. (4.15) into Eq. (4.4), we get

$$1 - f_n(t) - f_n'(t) \approx \prod_{m=1}^{N} \left[1 - A_{mn} f_m(t)\right]. \tag{4.16}$$

Assuming $f_n(t) \ll 1$ and expanding to second order, we get after simplifying and dropping the time notation for clarity,

$$f_n + f_n' \approx \sum_m A_{mn} f_m - \frac{1}{2} \sum_m \sum_{k \neq m} A_{mn} A_{kn} f_m f_k. \tag{4.17}$$

The leading order terms are f_n on the left-hand side and $\sum_m A_{mn} f_m$ on the right-hand side, so for these to balance as $f \to 0$ requires

$$f_n = \sum_m A_{mn} f_m. \tag{4.18}$$

Therefore, in this limit the vector $\mathbf{f}(t) = [f_1(t), f_2(t), \ldots, f_N(t)]^T$ has to be proportional to the normalized left eigenvector $\mathbf{v}$ of A with eigenvalue $\lambda = 1$. Thus, a slowly varying solution only exists for a critical network. Since $\mathbf{v}$ is independent of time, the constant of proportionality must be time dependent, $f_n(t) = K(t) v_n$. Now, for finite f, we expect the solution to deviate by a small error from this limit solution, so we set

$$f_n(t) = K(t) v_n / \langle v \rangle + \epsilon_n(t), \tag{4.19}$$

where we assume $\epsilon_n \ll f_n(t)$, $\epsilon'_n \ll f'_n(t)$, and the term $\langle v \rangle = \sum_{n=1}^{N} v_n/N$ is included to make $K(t)$ independent of the normalization of $\mathbf{v}$. Inserting this in Eq. (4.17), neglecting terms of order ε', ε^2, $f\varepsilon$, and using $\sum_m \sum_{k \neq m} A_{mn} A_{kn} v_m v_k \approx v_n^2$, we obtain

$$\varepsilon_n + K'(t) v_n / \langle v \rangle = \sum_{m=1}^{N} A_{mn} \varepsilon_m - \frac{1}{2} K^2(t) v_n^2 / \langle v \rangle^2. \tag{4.20}$$

To eliminate the unknown error term ε, we multiply by u_n, where $\mathbf{u}$ is the right eigenvector of A satisfying $\mathbf{u}^T A^T = \mathbf{u}^T$, and sum over n. The error term vanishes and we obtain an ordinary differential equation (ODE),

$$K'(t) = -\frac{1}{2} \frac{\langle uv^2 \rangle}{\langle uv \rangle \langle v \rangle} K^2(t), \tag{4.21}$$

where $\langle xy \rangle \equiv \frac{1}{N} \sum_n x_n y_n$. Solving this ODE yields

$$K(t) \approx \frac{1}{\beta + \frac{1}{2} \frac{\langle uv^2 \rangle}{\langle uv \rangle \langle v \rangle} t}, \tag{4.22}$$

where β is an integration constant. In terms of the original variables, we obtain

$$c_n(t) \approx 1 - \frac{v_n}{\beta + \frac{1}{2} \frac{\langle uv^2 \rangle}{\langle uv \rangle \langle v \rangle} t}. \tag{4.23}$$

The PDF, in the continuous time approximation, is given by $p_n(t) = -c'_n(t)$,

$$p_n(t) \propto \frac{v_n}{\left(\beta + \frac{1}{2} \frac{\langle uv^2 \rangle}{\langle uv \rangle \langle v \rangle} t \right)^2}. \tag{4.24}$$

From Eq. (4.24) we make the prediction that as $t \to \infty$, $p_n(t) \sim t^{-2}$. This prediction is tested in Sec. 4.4.

4.3 Distribution of Avalanche Sizes

In order to analyze the distribution of avalanche sizes, we define the random variable x_n as the size of an avalanche starting at node n. Let z_{mn} be a random variable which is 1 if node n excites node m and 0 otherwise, so that $z_{mn} = 1$ with probability A_{mn} and 0 with probability $1 - A_{mn}$. Thus

$$x_n = 1 + \sum_m z_{mn} x_m. \tag{4.25}$$

From Sec. 4.2.2 and Appendix 4.6, we know that there is a finite probability that an avalanche has infinite duration, and therefore infinite size, when $\lambda > 1$. Therefore, we will restrict our attention only to the distribution of avalanches that are finite. To study this distribution, we define the moment generating function

$$\phi_n(s) \equiv E[e^{-sx_n}|x_n < \infty]. \tag{4.26}$$

We now use Eq. (4.25) to derive a relation between the moment generating functions of different nodes. First, we rewrite the condition $x_n < \infty$ for node n in terms of events applicable to its neighbors:

$$x_n < \infty \Leftrightarrow \forall m(z_{mn} = 0 \text{ or } \{x_m < \infty \text{ and } z_{mn} = 1\}). \tag{4.27}$$

Using Eq. (4.25) we can rewrite Eq. (4.26) as

$$\phi_n(s) = e^{-s} E\Big[\prod_m e^{-sz_{mn}x_m} | \forall m(Z_{nm} \text{ and } W_{nm})\Big]. \tag{4.28}$$

Where we have defined the disjoint events $Z_{nm} = \{z_{mn} = 0\}$ and $W_{nm} = \{x_m < \infty \text{ and } z_{mn} = 1\}$. Assuming the independence of the random variables x_m (consistent with the locally tree-like assumption used in the previous Section), we can rewrite $\phi_n(s)$ as

$$\phi_n(s) = e^{-s} \prod_m E\Big[e^{-sz_{mn}x_m} | Z_{nm} \text{ and } W_{nm}\Big]. \tag{4.29}$$

To simplify this expression, we use, denoting by $P(\cdot)$ the probability of an event,

$$E[e^{-sz_{mn}x_m}|Z_{nm} \text{ and } W_{nm}]P(Z_{nm} \text{ and } W_{nm}) = E[e^{-sz_{mn}x_m}|Z_{nm}]P(Z_{nm}) + E[e^{-sz_{mn}x_m}|W_{nm}]P(W_{nm}). \tag{4.30}$$

Using $P(x_m < \infty) = b_m$, $E[e^{-sz_{mn}x_m}|Z_{nm}] = 1$, and the definition of A_{mn} and $\phi_m(s)$, we get

$$E[e^{-sz_{mn}x_m}|Z_{nm} \text{ and } W_{nm}]P(Z_{nm} \text{ and } W_{nm}) = (1 - A_{mn}) + b_n A_{mn}\phi_m(s) \tag{4.31}$$

Finally, using $P(Z_{nm} \text{ and } W_{nm}) = (1 - A_{mn}) + b_m A_{mn}$, we obtain

$$E[e^{-sz_{mn}x_m}|Z_{nm} \text{ and } W_{nm}] = \frac{(1 - A_{mn}) + b_m A_{mn}\phi_m(s)}{(1 - A_{mn}) + b_m A_{mn}}, \tag{4.32}$$

and inserting this into Eq. (4.29) we obtain one of our main results:

$$\phi_n(s) = e^{-s} \prod_m \frac{(1 - A_{mn}) + b_m A_{mn} \phi_m(s)}{(1 - A_{mn}) + b_m A_{mn}}. \tag{4.33}$$

Defining $g_n(s) = \phi_n(s) - 1$, and the matrix H with entries

$$H_{mn} = \frac{b_m A_{mn}}{(1 - A_{mn}) + b_m A_{mn}}. \tag{4.34}$$

we can rewrite this equation as

$$1 + g_n(s) = e^{-s} \prod_m [1 + H_{mn} g_m(s)]. \tag{4.35}$$

Defining the $N \times N$ matrix, $B = \mathrm{diag}(b_1, b_2, ..., b_N)$, we have from Eqs. (4.11) and (4.34), that $HB^{-1} = B^{-1}D$. Thus the matrix H is related to the matrix D by a similarity transformation and thus has the same spectrum. Therefore, we will denote the Perron-Frobenius eigenvalue of H by λ_D. Note that $\lambda_D = \lambda$ when $\lambda \leq 1$, since in that case $b_n = 1$ and $H = A$.

The asymptotic form for the distribution of the sizes of avalanches starting at node n, $p_n(x)$, can be obtained from the asymptotic form of $g_n(s)$ as $s \to 0$. Therefore, we study Eq. (4.35) by assuming $g_n(s)$ is small. In order to obtain an analytic expression for the distribution of sizes we assume, in addition, that the network is close to critical, $(\lambda_D - 1) \ll 1$. Taking logarithms in Eq. (4.35) and using the approximation $\ln(1 + g) \approx g - g^2/2$ we obtain

$$g_n(s) - \frac{1}{2} g_n(s)^2 = -s + \sum_m H_{mn} g_m(s) - \frac{1}{2} \sum_m H_{mn}^2 g_m^2(s). \tag{4.36}$$

As $s \to 0$ and $g_n \to 0$, the leading order terms are $g_n(s) = -s + \sum_m H_{mn} g_m(s)$, or $(H^T - I)\mathbf{g} = s\mathbf{1}$, where $\mathbf{g} = [g_1, g_2, \ldots, g_N]^T$ and $\mathbf{1} = [1, 1, \ldots, 1]^T$. When $|\lambda_D - 1| \ll 1$, and λ_D is well separated from the rest of the spectrum of H, as we are assuming, $\mathbf{g} = s(H^T - I)^{-1}\mathbf{1} \sim \mathbf{v}$, where $\mathbf{v}$ is the left Perron-Frobenius eigenvalue of H (more precisely, we are assuming such a separation for A, but since $A = H$ when $\lambda = 1$ and we are assuming $\lambda - 1 \ll 1$, by continuity the assumption is valid for H as well). Since $\mathbf{v}$ is independent of s, the solution up to first order is approximately $g_n(s) = g(s) v_n / \langle v \rangle$, where the term $\langle v \rangle = \frac{1}{N} \sum_{n=1}^{N} v_n$ is included to make $g(s)$ independent of

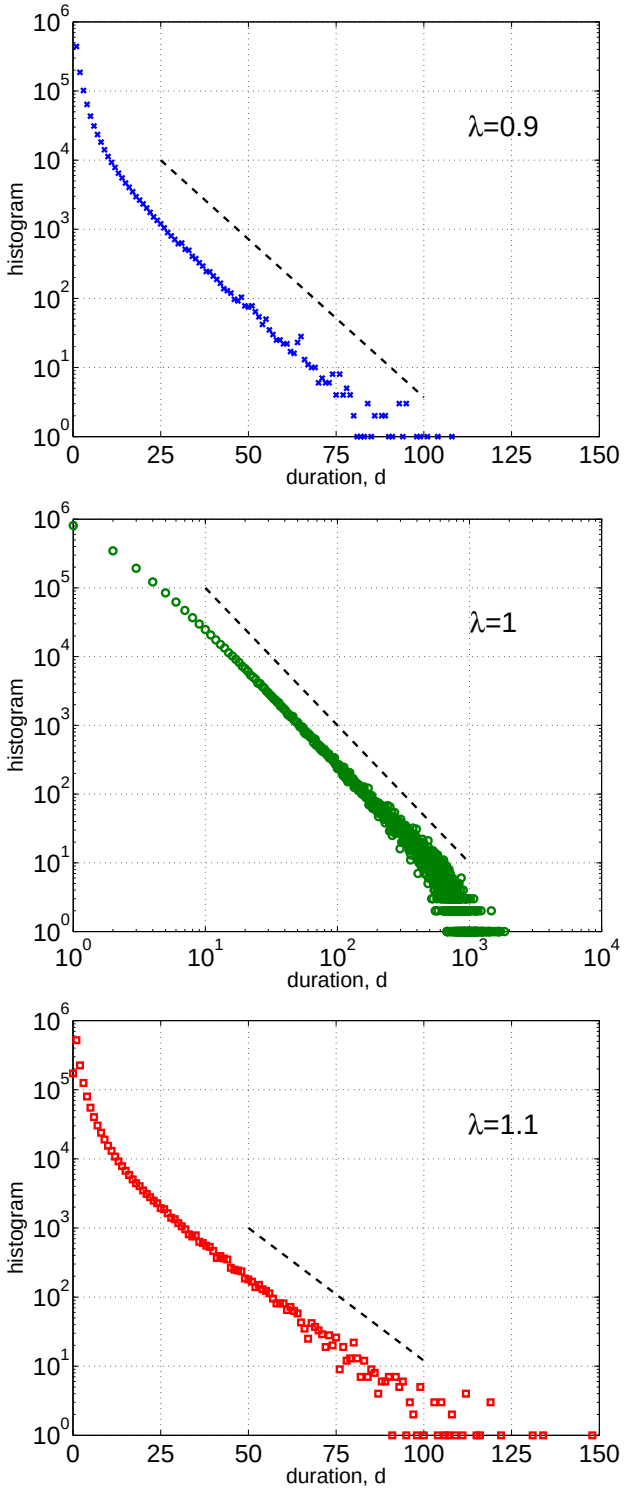

Figure 4.2: Histograms of avalanche durations shown above for networks of $N = 10^5$ nodes with power law degree distribution, exponent $\gamma = 3.5$ with Perron-Frobenius eigenvalues of $\lambda = 0.9$ (left), $\lambda = 1.0$ (center) and $\lambda = 1.1$ (right). Symbols show the number of avalanches having duration d from a single simulation of 10^6, $2 \cdot 10^6$, and 10^6 avalanches, respectively, from left to right. Dashed lines provide a reference for the theoretical predictions described in Eqs. (4.7), (4.23), and (4.13). Note that the vertical position of the dashed lines was chosen arbitrarily. Due to predictions of exponential decay for the sub- and super-critical cases, the left and right plots are plotted on a log-linear scale, while the center plot is plotted on a log-log scale to show the power-law decay. Infinite duration avalanches in the supercritical case (right) are not displayed in the figure.

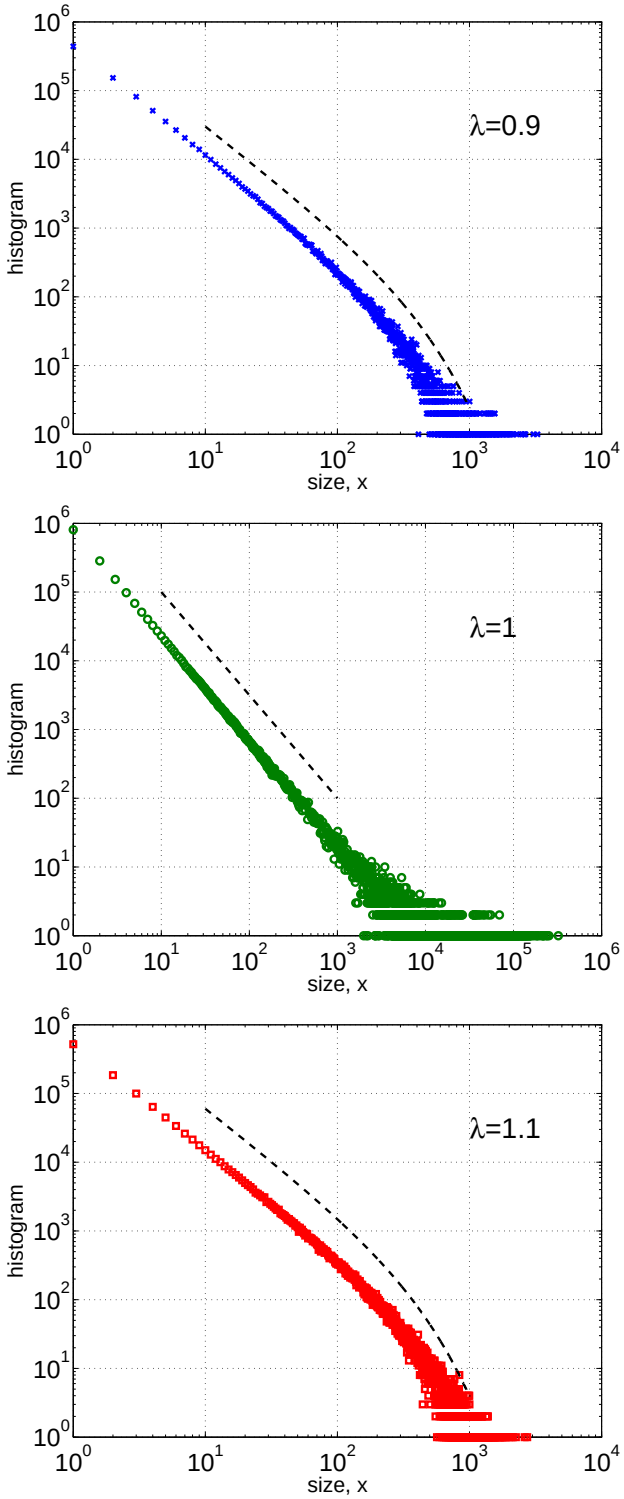

Figure 4.3: Histograms of avalanche sizes shown above for networks of $N = 10^5$ nodes with power law degree distribution, exponent $\gamma = 3.5$ with Perron-Frobenius eigenvalues of $\lambda = 0.9$ (left), $\lambda = 1.0$ (center) and $\lambda = 1.1$ (right) on a log-log scale. Symbols show the number of avalanches having size x from a single simulation of 10^6, $2 \cdot 10^6$, and 10^6 avalanches, respectively, from left to right. Dashed lines provide a reference for the theoretical prediction $x^{-3/2} \exp(-x/x^*)$ described in Eqs. (4.44) and (4.45). Note that the vertical position of the dashed lines was chosen arbitrarily. Infinite size avalanches in the supercritical case (right) are not represented in the data set. Agreement between theoretical prediction and measurement is excellent despite finite sample size noise.

the normalization of $\mathbf{v}$. For small s, and including the nonlinear terms, we expect the solution of Eq. (4.36) to be close to this solution, so we set

$$g_n(s) = g(s)\langle v\rangle^{-1} v_n + \varepsilon_n(s), \tag{4.37}$$

where ε_n is a small unkown error term. Substituting Eq. (4.37) into Eq. (4.36), using $H^T\mathbf{v} = \lambda_D\mathbf{v}$, and neglecting terms of order εg we get

$$g(s)\langle v\rangle^{-1} v_n + \varepsilon_n(s) - \frac{1}{2}g(s)^2\langle v\rangle^{-2} v_n^2 = -s + \lambda g(s)\langle v\rangle^{-1} v_n + \sum_m H_{mn}\varepsilon_m(s) - g(s)^2\langle v\rangle^{-2}\frac{1}{2}\sum_m H_{mn}^2 v_m^2. \tag{4.38}$$

To eliminate the unknown error term ε_n, we multiply by the right eigenvector entry u_n of H and sum over n. We use $H\mathbf{u} = \lambda_D\mathbf{u}$ and neglect $(\lambda_D - 1)\varepsilon_n$ to get

$$g(s)\langle v\rangle^{-1}\langle uv\rangle - \frac{1}{2}g(s)^2\langle v\rangle^{-2}\langle uv^2\rangle = -s\langle u\rangle + \lambda_D g(s)\langle v\rangle^{-1}\langle uv\rangle - g(s)^2\langle v\rangle^{-2}\frac{1}{2N}\sum_n\sum_m u_n H_{mn}^2 v_m^2, \tag{4.39}$$

where $\langle xy\rangle \equiv \frac{1}{N}\sum_n x_n y_n$. Equation (4.39) is a quadratic equation for $g(s)$, $ag^2 + bg + c = 0$, with

$$a = \frac{\sum_n\sum_m u_n(1 - H_{mn}^2)v_m^2}{2N\langle uv\rangle\langle v\rangle}, \tag{4.40}$$

$$b = (\lambda_D - 1), \tag{4.41}$$

$$c = -s\frac{\langle u\rangle\langle v\rangle}{\langle uv\rangle}. \tag{4.42}$$

Solving for $g(s)$ and substituting back into $g_n(s) = \phi_n(s) - 1$ we find, choosing the root that guarantees $g_n < 0$,

$$\phi_n(s) = 1 + \frac{-(\lambda_D - 1) - \sqrt{(\lambda_D - 1)^2 + 4sa\frac{\langle u\rangle\langle v\rangle}{\langle uv\rangle}}}{2a}\frac{v_n}{\langle v\rangle} \tag{4.43}$$

The moment generating function in Eq. (4.26) can be interpreted as the Laplace transform of the distribution of sizes. Taking the inverse Laplace transform we obtain that for large x, the distribution of sizes $p_n(x)$ is approximately given by

$$p_n(x) \propto x^{-3/2}\exp(-x/x^*)v_n, \tag{4.44}$$

where the characteristic size x^* is given by

$$x^* = 4a\frac{\langle v\rangle\langle u\rangle}{\langle vu\rangle}(\lambda_D - 1)^{-2}. \tag{4.45}$$

The distribution of sizes is asymptotically an exponential multiplied by a power law with exponent $-3/2$. Such a functional form describes the distribution of the sizes of connected clusters near the percolation threshold in some network percolation models [69]. In the critical case, when $\lambda = \lambda_D = 1$, x^* diverges and we recover a power-law distribution with exponent $-3/2$, which is the well known exponent for critical branching processes [67]. It is interesting to note that this exponent, in our model, does not depend on the structure of the network, as opposed to related percolation models where all nodes with the same degree are considered statistically equivalent [69]. Also note that the quantity a in Eq. (4.45) depends implicitly on λ_D.

4.4 Numerical Experiments

In this section, we test the theoretical predictions of the previous sections by directly simulating the process described in Sec. 4.1 on computer-generated networks. We first describe the processes used to construct networks and simulate avalanches.

Networks were constructed in two steps. First, binary networks (with adjacency matrix entries $\hat{A}_{mn} \in \{0, 1\}$) were constructed via an implementation of the configuration model [50], using $N = 10^5$ nodes, with nodal degrees drawn from a power-law distribution with exponent 3.5, i.e., the probability that a node has degree k is proportional to $k^{-3.5}$. Second, each nonzero entry $\hat{A}_{mn}$ was given a weight, drawn from a uniform distribution $\mathcal{U}[0, 1]$. We then calculated the Perron-Frobenius eigenvalue of this weighted matrix $\hat{\lambda}$, and multiplied the matrix A by $\lambda/\hat{\lambda}$, resulting in a matrix A with the desired eigenvalue λ. We simulated avalanches for networks with λ between 0.5 and 1.5, sampling more finely for values close to 1.

Each simulated avalanche was created by first exciting a single network node, chosen uniformly at random, and then calculating the size and duration of the resulting avalanche as defined in Eqs. (4.1) and (4.2). If the resulting avalanche lasted for more than 10^6 time steps, we considered

it as having infinite duration and infinite size. In all cases, the initial excitation was included so that the minimum size was $x = 1$ and the minimum duration was $d = 1$. For each subcritical ($\lambda < 1$) and supercritical ($\lambda > 1$) case, 10^6 avalanches were simulated, and for $\lambda = 1$, we simulated $2 \cdot 10^6$ avalanches to better sample the very broad distribution of avalanche sizes at criticality.

A brief summary of the predictions of Secs. 4.2 and 4.3 is as follows.The probability of an avalanche of duration d will decay as λ^d for subcritical networks ($\lambda < 1$), as d^{-2} for critical networks ($\lambda = 1$), and as λ_D^d for supercritical networks ($\lambda > 1$), where λ_D is the Perron-Frobenius eigenvalue of matrix (4.34). For avalanche size distributions, when $|\lambda_D - 1| \ll 1$,. the probability of a finite avalanche of size x will decay as $x^{-3/2} \exp(-x/x^*)$, where x^* is a network-specific constant, given in Eq. (4.45).

In Figs. 4.2 and 4.3 we compare histograms of avalanche durations and sizes obtained from direct numerical simulations for $\lambda = 0.9$ (left), 1.0 (center), and 1.1 (right) with our theoretical predictions described in the previous paragraph (dashed lines). Note that, since our predictions allow for an unspecified proportionality constant, the vertical position of the dashed lines was chosen arbitrarily. In general, we find good agreement between the theoretical predictions of avalanche duration and size distributions with the histograms observed in the simulations. While the dashed lines in Figs. 4.2 and 4.3 are appealing to the eye, more quantitative measures of agreement between theory and experiment are shown in Figs. 4.4 and 4.5.

To numerically test the agreement between theory and experiment for the distribution of avalanche durations, in Fig. 4.4 we compare the best fit $\hat{\lambda}$ of the data to $p(t) \propto \hat{\lambda}^t$, calculated through a nonlinear least-squares exponential regression on the simulated PDF of avalanche duration, to our theoretical predictions in Eqs. (4.8) and (4.14) (solid line). The agreement is excellent, though not exact, over the entire range of λ values simulated.

As a partial test of our theory for the distribution of avalanche sizes, we assume that the form of the distribution is $x^{-3/2} \exp(-x/x^*)$, and estimate x^* from the data, which we then compare with our theoretical prediction in Eq. (4.45). Noting that as $\lambda \to 1$, x^* will diverge, we estimated $1/x^*$ via a nonlinear least-squares using Brent's minimization on the cumulative histogram of the

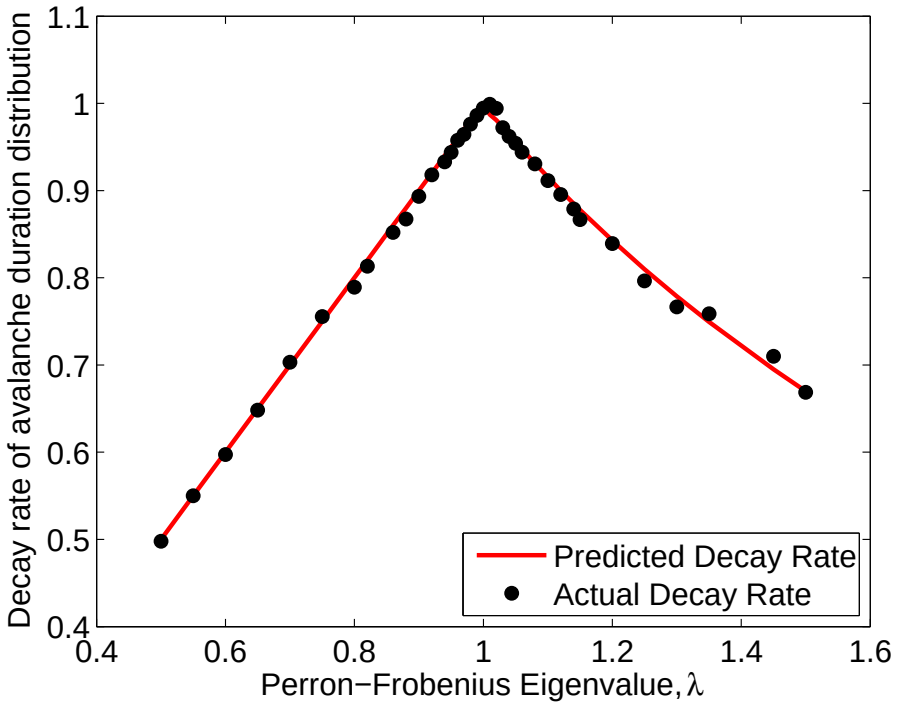

Figure 4.4: A comparison of predicted duration decay rates (Eq. (4.7) and Eq. (4.13)) (solid line), and numerical simulations (solid circles) plotted against λ, the largest eigenvalue of the network adjacency matrix. Agreement is excellent for both the subcritical and supercritical numerical simulations.

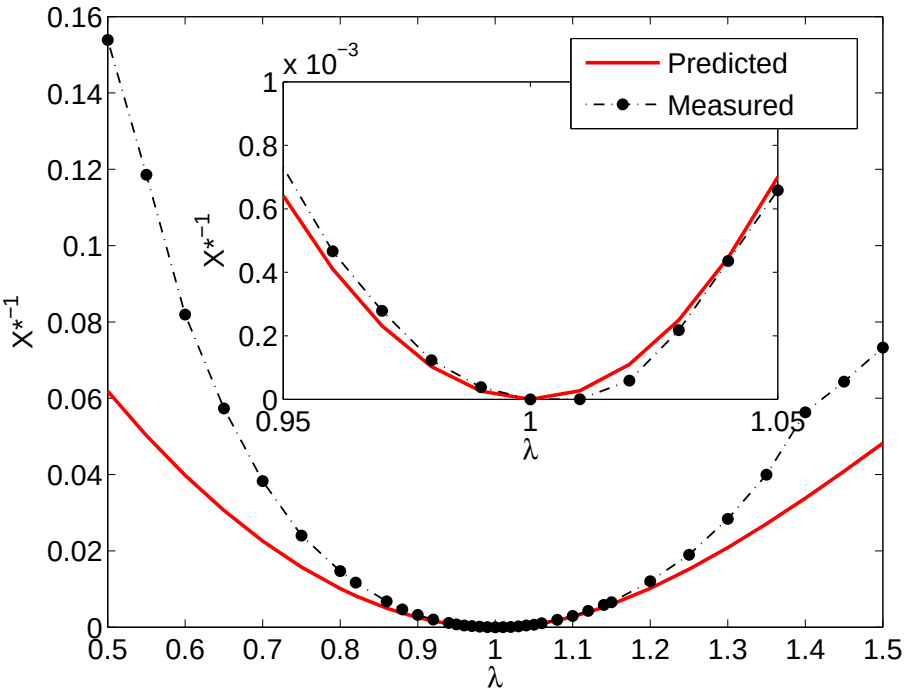

Figure 4.5: Testing the prediction that avalanche size x is distributed as $x^{-3/2}\exp(-x/x^*)$, we compare the theoretical prediction of x^* (solid line) with x^* estimated via regression on the largest 10% of avalanches from numerical simulations (solid circles, dashed line). Inset, identical data on a magnified domain around $\lambda = 1$. Agreement is excellent for λ near 1, and decreasingly accurate for much larger or smaller λ.

avalanche size data. Since our theory describes only the asymptotic form of the distribution, this estimate was performed only on the largest 10% of measured data. [Similar results were obtained using the largest 5%, 1% and 0.1% of data (not shown), but when using more than the largest 10%, the minimizing x^* value diverged, suggesting that we fit the power-law portion of data at the expense of the exponential tail.] Figure 4.5 shows our theoretical prediction (solid line) and the result of the numerical fit to the data (solid circles; the lines are to aid the eye). As shown, agreement is quite good close to $\lambda_D = 1$ (see the inset of Fig. 4.5), but less accurate for very subcritical or supercritical networks. The latter is reasonable since the assumption that $|\lambda_D - 1|$ is a small quantity was used in the derivation of Eq. (4.45).

Although Figs. 4.4 and 4.5 demonstrate agreement between theory and measurement for supercritical networks, that analysis was restricted to finite avalanches. To complement this result, we compare the predicted fraction of infinite avalanches with the measured fraction, for various values of λ_D. The quantity b_n in Eq. (4.9) is the fraction of avalanches originating at node n which will have finite duration and size. In Fig. 4.6, we show the fraction of avalanches that decay in finite time, averaged over nodes, comparing theory (solid line) with experiment (solid circles). The theoretical fraction of avalanches is calculated by numerically solving Eq. (4.9) to find $b_n, n = 1 \ldots, N$, and then plotting $\sum_{n=1}^{N} b_n/N$ as a function of λ. The numerical fraction of finite avalanches was calculated by simulating 10^6 avalanches, each one starting at a random node (out of $N = 10^5$ nodes). If an avalanche lasts more than 10^6 steps, we counted it as an infinite avalanche. Then, an estimate of b_n was calculated as the fraction of finite avalanches starting at node n. The symbols in Fig. 4.6 show $\sum_{n=1}^{N} b_n/N$ as a function of λ. Agreement is excellent over the entire range of λ values tested.

Beyond aggregate statistics, we also test a more subtle prediction of Eq. (4.7). In Sec. 4.2, we concluded that $f_n(t) = 1 - c_n(t)$, the probability that an avalanche started at node n lasts more than t steps, scales for large t as $f_n(t) \propto \lambda^t v_n$, where $\mathbf{v}$ is the left Perron-Frobenius eigenvector of A. Other research in the network adjacency matrix literature has noted that the vector of nodal out-degrees (in-degrees) is a good approximation for the right (left) dominant eigenvector of A in

the absence of degree correlations [3]. In this light, our prediction above is understandable: when there are not degree correlations in the network, a node with a larger right eigenvector entry (and thus larger out-degree) will tend to produce longer avalanches. Therefore, in order to fully test our prediction, we created networks with *assortative (disassortative) mixing by degree* [35], a type of degree correlation which we measure using the coefficient ρ [3],

$$\rho = \frac{\langle k_n^{in} k_m^{out} \rangle_e}{\langle k_n^{in} \rangle_e \langle k_m^{out} \rangle_e}, \tag{4.46}$$

where $\langle \cdot \rangle_e$ denotes an average over all edges and k are weighted nodal degrees defined as $k_n^{in} = \sum_m A_{mn}$ and $k_n^{out} = \sum_m A_{nm}$. In the absence of degree correlations between connected nodes $\langle k_n^{in} k_m^{out} \rangle_e = \langle k_n^{in} \rangle_e \langle k_m^{out} \rangle_e$ and $\rho = 1$. In assortative networks, there exists a positive correlation ($\rho > 1$) between the in-degree at node n and the out-degree at node m at the ends of a directed link from n to m. When the correlation is negative ($\rho < 1$), the network is called disassortative. Thus we created Erdős-Rényi random networks with $N = 10^4$ nodes, and rewired the network via a link-swapping process (as described in Ref. [3]) until we had very assortative and disassortative networks ($\rho = 1.2$ and $\rho = 0.8$, respectively). Eq. (4.7) implies that in such networks, the tails of the CDF of avalanches originating at node n will be proportional to the corresponding entry of the right eigenvector, which may differ significantly from the nodal out-degree. For the a subcritical network $\lambda = 0.95$ with assortativity $\rho = 0.8$ we plot $f_n(30)$ and its corresponding entry in the right dominant eigenvector v_n for each node n, in Fig. 4.7, showing that proportionality is excellent. In the inset of the same figure we plot $f_n(30)$ and against corresponding out-degree k_n^{out} for each node n, showing that proportionality to out-degree does not hold. Assortative networks produce the same effect, but are not shown here.

4.5 Discussion

We have presented an analysis of the asymptotic distributions of the duration and sizes of avalanches in complex networks. This work is of interest in various applications, most notably neuroscience and the analysis of power-grid failure cascades. While some of our results, such as

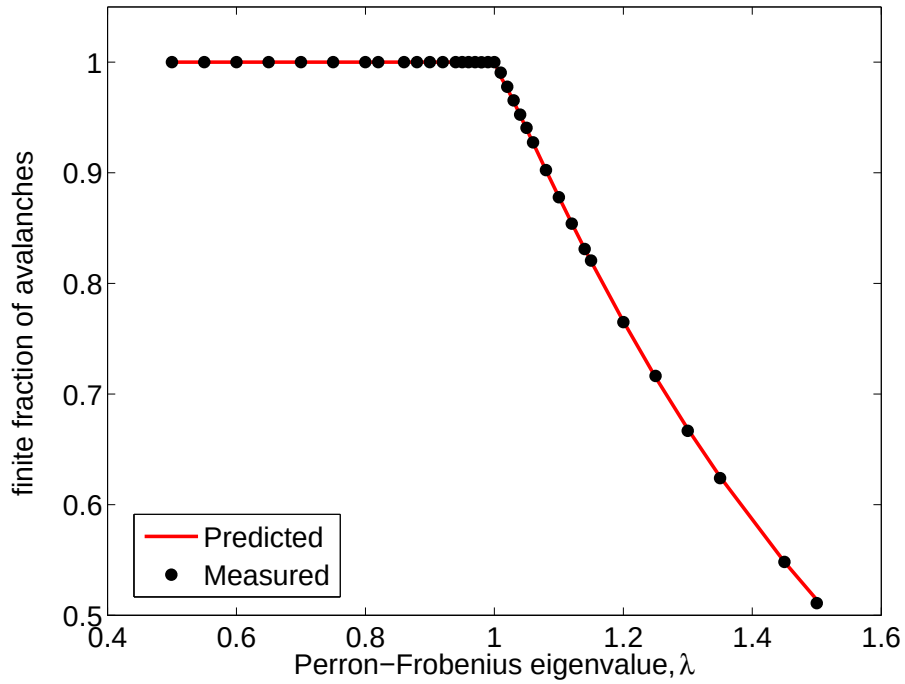

Figure 4.6: When the Perron-Frobenius eigenvalue λ is larger than one, there is a non-zero probability of an avalanche starting at node n having infinite duration, as predicted by Eq. (4.9). Here we average the finite fraction of avalanches originating from node n over all nodes, showing excellent agreement between the fraction predicted by averaging Eq. (4.9) (solid line) and fraction measured from simulation (solid circles).

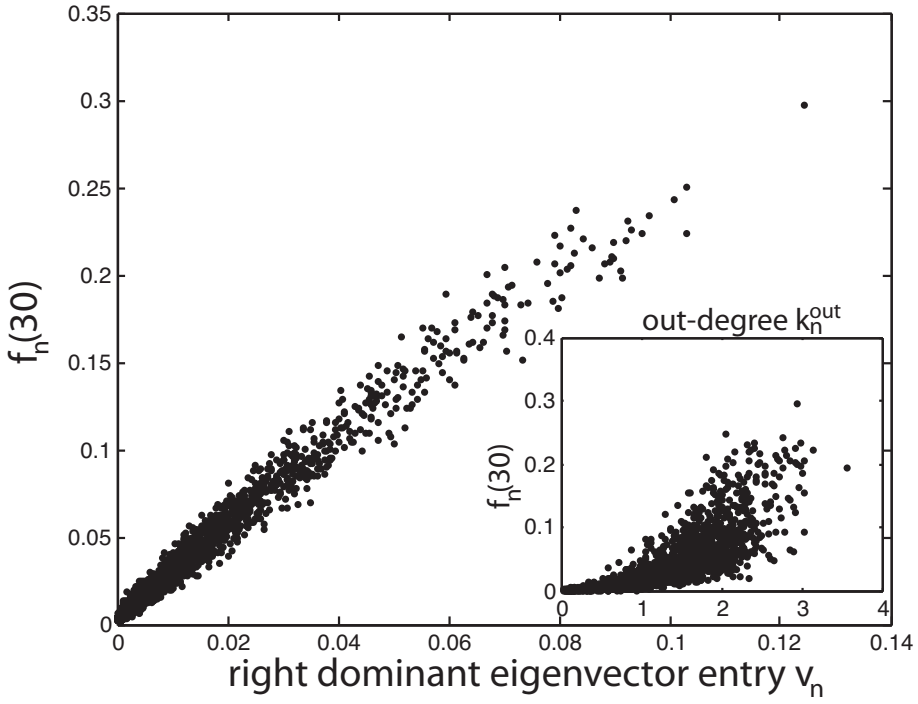

Figure 4.7: Testing the node-specific prediction of Eq. (4.7), avalanches were simulated on a subcritical ($\lambda = 0.95$) and disassortative ($\rho = 0.8$) Erdős Rényi random network with $N = 10^4$ nodes. In the large plot, the fraction of avalanches originating at node n that last longer than 30 time steps, $f_n(30)$ is plotted against the corresponding entry in the right Perron-Frobenius eigenvector, v_n. In the inset, the same values $f_n(30)$ are plotted against the corresponding out-degree k_n^{out}. The eigenvector entry v_n does a significantly better job than out-degree k_n^{out} of predicting the duration of avalanches originating at node n in disassortative networks (shown) and for assortative networks (not shown).

the functional forms for the distributions, are analogous to those found in classical Galton-Watson branching processes [67] or in mean-field models [69], we emphasize the distinguishing aspects of our results: (i) We generalize the criterion for criticality to $\lambda = 1$, which depends on the topology of the network in ways that previous mean-field results do not capture; (ii) The parameters of the asymptotic distributions in the various regimes are affected by the network topology, and our results allow us to predict how various factors (e.g., network degree distributions, degree-degree correlations) affect these parameters [e.g., the parameter x^* in Eq. (4.45) or λ_D in Eq. (4.13)]. (iii) In contrast to previous studies, our results allow us to predict the statistics of avalanches generated at a particular node. This might be of critical importance in certain applications where the adjacency matrix is known or can be inferred (such as the power grid or the Autonomous System network of the Internet) since one can then allocate resources to prevent avalanches, if so desired, that start at the nodes which tend to generate the largest avalanches. As shown in Fig. 4.7, the naive prediction that the nodes with the largest out-degree generate the largest avalanches is not necessarily true when the networks have nontrivial structure, such as degree-degree correlations.

In developing our theory, we made some assumptions which we now discuss. First, we assumed that the network was locally tree-like. This allowed us to treat avalanches propagating to the neighbors of a given node as independent of each other. While this is a good approximation for the networks we used, it is certainly not true in general. In particular, avalanches propagating separately from a given node might excite the same node as they grow. The result is that the number of nodes that the avalanches excite in simulation may be less than what the theory would predict. In running our simulations, we addressed this issue in two ways: first, we kept track of the number of times two branches of the same avalanche simultaneously excited the same node n, finding it to be an increasing function of avalanche size and Perron-Frobenius eigenvalue, yet still negligible when compared to the total number of excitations. In addition, each time such an event occurred, we separately generated an avalanche starting from the doubly excited node n and corrected both the size and duration of the original avalanche by incorporating these additional avalanches. We found that doing this had no appreciable effect on the measured distributions,

and so all figures shown in this chapter are produced from simulation data *without* the additional compensating avalanches included. This, and the fact that the numerical simulations are described well by the theory, suggest that the interaction of avalanches propagating to different neighbor nodes can be safely neglected in the networks studied. The performance of our theory in networks that are not locally tree-like, such as networks with a high degree of clustering, is left for future research. Another approximation we used is that the Perron-Frobenius eigenvalue λ is well separated from the rest of the spectrum. This is a good approximation in networks without well defined communities, but can break down in networks with strong community structure [57].

Finally, we note that our results show that the experimental signatures of criticality in neural systems (characterized by a power-law distribution of avalanche sizes and durations with exponents $-3/2$ and -2, respectively [5, 7, 23, 22]) are robust to complex underlying network topologies.

4.6 Appendix: probability of finite avalanche durations

In this Appendix we establish that the probability of finite avalanches, under our assumptions, is always one when $\lambda \leq 1$ (critical and subcritical networks), and becomes less than one when $\lambda > 1$ (supercritical networks). These probabilities, $b_n = \lim_{t\to\infty} c_n(t)$, satisfy the equation

$$b_n = \prod_{m=1}^{N} \Big[(1 - A_{mn}) + A_{mn} b_m \Big]. \tag{4.47}$$

First, we show that if $\lambda \leq 1$, where λ is the Perron-Frobenius eigenvalue of A, then the only solution to the equation above is $b_n = 1$. Letting $b_n = 1 - f_n$, we have for all n

$$1 - f_n = \prod_{m=1}^{N} \Big[1 - A_{mn} f_m \Big]. \tag{4.48}$$

The Weierstrass product inequality, which can be proved by induction on N, states that if $c_n \in [0, 1]$ for $n = 1, 2, \ldots, N$, then $\prod_{n=1}^{N}(1 - c_n) + \sum_{n=1}^{N} c_n \geq 1$, with equality only if all the c_n are zero, or all the c_n are zero except one of them, which is equal to one. Using the Weierstrass product inequality,

$$\sum_{m=1}^{N} A_{mn} f_m \geq 1 - \prod_{m=1}^{N} \Big[1 - A_{mn} f_m \Big] = f_n, \tag{4.49}$$

with equality only if (i) $A_{mn}f_m = 0$ for all m, or (ii) $A_{mn}f_m = 0$ for all $m \neq k$ and $A_{kn}f_k = 1$ for some k. If u is the right Perron-Frobenius eigenvector of A, this implies, since $\mathbf{u}^T A^T = \lambda \mathbf{u}^T$,

$$\mathbf{u}^T A^T \mathbf{f} = \lambda \mathbf{u}^T \mathbf{f} \geq \mathbf{u}^T \mathbf{f}. \tag{4.50}$$

If there is a nonzero f_n, then $\mathbf{u}^T \mathbf{f} > 0$ since the Perron-Frobenius eigenvector has positive entries for irreducible A. Therefore, if $\lambda < 1$ we must have $f_n = 0$ for all n. If $\lambda = 1$, Eq. (4.50) implies equality in Eq. (4.49), which implies either (i) $A_{mn}f_m = 0$ for all m, and thus $f_n = 0$ by (4.49), or (ii) $A_{mn}f_m = 0$ for all $m \neq k$ and $A_{kn}f_k = 1$ for some k, which is impossible since we assumed that the entries of A are strictly less than one and f_k is a probability. Therefore, we must have $f_n = 0$ if $\lambda = 1$, and this argument is valid for any n. Together with the previous argument above, we conclude that $b_n = 0$ for all n if $\lambda \leq 1$.

Now, we show that if $\lambda > 1$ then $\lim_{t\to\infty} c_n(t) = b_n < 1$. To show this, we view Eq. (4.4) as a dynamical system, and note that the analysis of Sec. 4.2.1, applied to the case $\lambda > 1$, shows that the fixed point $b_n = 1$ is linearly unstable. If we show that $c_n(t)$ are nondecreasing with t, then their limit b_n must be less than one. We will prove by induction that $c_n(t+1) \geq c_n(t)$ for all n. First, we have $c_n(0) = 0$ and $c_n(1) = \prod_m (1 - A_{nm}) \geq 0$, so the statement is valid for $t = 0$. Then, asume $c_m(t) \geq c_m(t-1)$ for all m and consider $c_n(t+1)/c_n(t)$ (assuming $c_n(t) > 0$):

$$\begin{aligned}
\frac{c_n(t+1)}{c_n(t)} &= \prod_{m=1}^{N} \frac{(1 - A_{mn}) + A_{mn}c_m(t)}{(1 - A_{mn}) + A_{mn}c_m(t-1)}. \\
&= \prod_{m=1}^{N} \left[1 + \frac{A_{mn}(c_m(t) - c_m(t-1))}{(1 - A_{mn}) + A_{mn}c_m(t-1)}\right] \\
&\geq 1,
\end{aligned} \tag{4.51}$$

which proves the desired statement. Note that, although from the definition (4.3), it follows that $c_n(t)$ are nondecreasing, this proof is necessary since Eq. (4.4) is an approximation.

4.7 Appendix: $\lambda > 1 \rightarrow \lambda_D < 1$

In this Appendix we argue that the Perron-Frobenius eigenvalue of the similar matrices H and D is less than one when the Perron-Frobenius eigenvalue of A is greater than one: $\lambda > 1 \rightarrow \lambda_D < 1$. Recall that the matrix D was defined as

$$D_{mn} = \frac{b_n A_{mn}}{(1 - A_{mn}) + b_m A_{mn}}, \tag{4.52}$$

where b_n, the probability that an avalanche starting at node n is finite, satisfies

$$b_n = \prod_{m=1}^{N} \Big[(1 - A_{mn}) + A_{mn} b_m \Big]. \tag{4.53}$$

Now, suppose that A is such that $\lambda > 1$, and introduce a parameter $\alpha \leq 1$ by defining $b_n(\alpha)$ as the b_n corresponding to the matrix αA, which satisfies

$$b_n(\alpha) = \prod_{m=1}^{N} \Big[(1 - \alpha A_{mn}) + \alpha A_{mn} b_m(\alpha) \Big]. \tag{4.54}$$

Now, calculate the derivative of $b_n(\alpha)$ with respect to α,

$$\frac{db_n(\alpha)}{d\alpha} = b_n(\alpha) \sum_{m=1}^{N} \frac{-A_{mn} + A_{mn} b_m(\alpha) + \alpha A_{mn} \frac{db_m(\alpha)}{d\alpha}}{(1 - \alpha A_{mn}) + \alpha A_{mn} b_m(\alpha)}. \tag{4.55}$$

Letting $\mu_n = \frac{db_n}{d\alpha}\big|_{\alpha=1}$, and evaluating the expression above at $\alpha = 1$, we get

$$\mu_n = b_n \sum_{m=1}^{N} \frac{-A_{mn} + A_{mn} b_m + A_{mn} \mu_m}{(1 - A_{mn}) + A_{mn} b_m} \tag{4.56}$$

$$= \sum_{m=1}^{N} D_{mn}(b_m - 1) + \sum_{m=1}^{N} D_{mn} \mu_m. \tag{4.57}$$

In matrix form,

$$(D^T - I)\mu = D^T(\mathbf{1} - \mathbf{b}), \tag{4.58}$$

where $\mathbf{1} = [1, 1, \ldots, 1]^T$, $\mathbf{b} = [b_1, b_2, \ldots, b_n]^T$, and $\mu = [\mu_1, \mu_2, \ldots, \mu_n]^T$. Now, left multiply the last equation by $\mathbf{u}^T$, where $\mathbf{u}$ is the right Perron-Frobenius eigenvector of D, satisfying $\mathbf{u}^T D^T = \lambda_D \mathbf{u}^T$, to get

$$(\lambda_D - 1)\mathbf{u}^T \mu = \lambda \mathbf{u}^T (\mathbf{1} - \mathbf{b}). \tag{4.59}$$

If $\lambda > 1$, the previous appendix shows that the entries of $(\mathbf{1} - \mathbf{b})$ are all positive. Since the Perron-Frobenius eigenvector $\mathbf{u}$ has positive entries as well (assuming A is irreducible), the right hand side is positive. Now, we argue that the vector μ has nonpositive entries: as α increases, the probability of an excitation passing between any pair of nodes increases, and thus the probability of having a finite avalanche can not increase, i.e., $db_n/d\alpha \leq 0$. Therefore, the term $\mathbf{u}^T\mu$ on the left hand side must be nonpositive and, since the right hand side is nonzero, it must be negative. Thus, the term $\lambda_D - 1$ must be negative, that is, $\lambda_D < 1$.

Chapter 5

Concluding Remarks

5.1 Summary of Main Results

Chapters 2, 3, and 4 present original research on the subject of critical dynamics in excitable networks, covering dynamics driven by an external stimulus (chapters 2 and 3) and avalanches resulting from a single nodal excitation (chapter 4). In each, the role of the Perron-Frobenius eigenvalue λ is prominent, and we find many interesting properties related to $\lambda = 1$:

(1) $\lambda = 1$ characterizes a critical state in which the excitable network exhibits (i) maximal dynamic range, regardless of the presence of time delays on network links or varied refractory states, and (ii) avalanches of activity with no characteristic size or duration scale, with size x decaying as $x^{-3/2}$ and duration d decaying as d^{-2}.

(2) For $\lambda < 1$, activity under external stimulus tends to decay toward zero, and in the absence of stimulus, cascades of network activity die out in finite time with probability one. Subcritical avalanche size decays as $x^{-3/2}\exp(-x/x^*)$, where x^* is a characteristic size that depends on spectral properties of the network adjacency matrix A, and duration decays as λ^d.

(3) For $\lambda > 1$, activity under external stimulus may be self-sustaining, and the probability that cascades of network activity last for infinite time is non-zero. Of those avalanches which are finite, avalanche size decays as $x^{-3/2}\exp(-x/x^*)$, where x^* is a characteristic size that depends on spectral properties of a modified network adjacency matrix (H), and duration decays as λ_H^d, the largest eigenvalue of H.

5.2 Key assumptions and their roles

These results were obtained primarily through techniques from dynamical systems, statistical physics, and network science. In particular, perturbative techniques played a key role in many results, which dovetailed often with projecting dynamics into the dominant eigenspace of the network adjacency matrix. As an example from each chapter, refer to the arguments that led to Eqs (2.10), (3.19), and (4.39). Such techniques rely heavily on the large separation between λ and the rest of the spectrum of A, Fig. 1.7.

There exist cases when we can not rely on λ to be well-separated from the rest of the spectrum. In particular, networks with strong community structure have been shown to have multiple large eigenvalues [57]. If one considers two disconnected networks indexed under a common adjacency matrix, the spectrum of the matrix is the union of the spectra of each network's adjacency matrix. Since eigenvalues are a continuous function of perturbations to the matrix, adding a small number of connections between these two separate networks, which we could then call "communities," results in a combined spectrum with two large eigenvalues. The work presented in this thesis has not been tested under these conditions, but we speculate that extensions may be possible.

The results in each chapter were also generated under the assumption that networks were "locally tree-like." In fact, we may be certain that some short loops exist in the networks that we generated for simulation. However, there are not many, and the results shown do not seem to be affected by this deviation, as is the case with many other systems analyzed using tree-based theory [71]. It is possible to construct pathological examples, however. For instance, consider dynamics where every node has many refractory states, and for every pair of nodes for which there exists a link from node m to node n, there is a corresponding link from node n to m. If an excitation passes from m to n, it can not return immediately in the opposite direction from n back to m, since node m is unavailable while in a refractory state. In this example, the dynamics is blind to the presence of the short loops, yet λ is affected by each link regardless, increasing monotocially with each additional link. Such a system would not be described accurately by the research in this

thesis.

5.3 Opportunities for future research

Of particular interest is the following puzzle: critical avalanche dynamics are claimed to occur when the actions of excitatory and inhibitory neurons are balanced [5, 7, 22, 23], yet the models in this thesis (and other publications [6]) reproduce much of the observed dynamics using only excitatory nodes. The most straightforward explanation is that the electrodes in experiment are each in contact with thousands of neurons or more, and therefore each Greenberg-Hastings cellular automaton corresponds to a population of neurons. As an alternative explanation, there is experimental evidence that neurons in the cortex operate in functional groups called *microcolumns*, so called because each microcolumn spans multiple cortical layers [8]. Figure 5.1 shows a diagram of a microcolumn, with different cell types labeled in different colors. Figure 5.2 shows a slice of Nissl-stained cortex in which the striations are microcolumns. Perhaps the cellular automata considered here correspond to microcolumns. There exist interesting opportunities to investigate this in more details for both theoreticians and experimentalists.

Although the explanations above may be convincing to some, the work in this thesis could be extended considerably to explicitly include inhibitory nodes and directly investigate the balance of excitation and inhibition. When a quiescent node receives stimuli from multiple other excited nodes, it must decide whether to fire. When inhibition is included in the model, a neuron could accomodate combinations of excitatory and inhibitory inputs by aggregating them according to some rule, and subsequently deciding whether to fire. One approach is to let excitatory nodes emit impulses with positive sign, let inhibitory nodes emit impulses with negative sign, and for a node that receives impulses to simply add them. The sigmoidal function which takes the sum of inputs and maps it to an output is called a *transfer function* [15], commonly occurring in the artificial neural network literature as well. The effect of different transfer functions in this scenario may also be of interest.

Finally, we leave open the problem of extension of this work to other neuron models—ideally

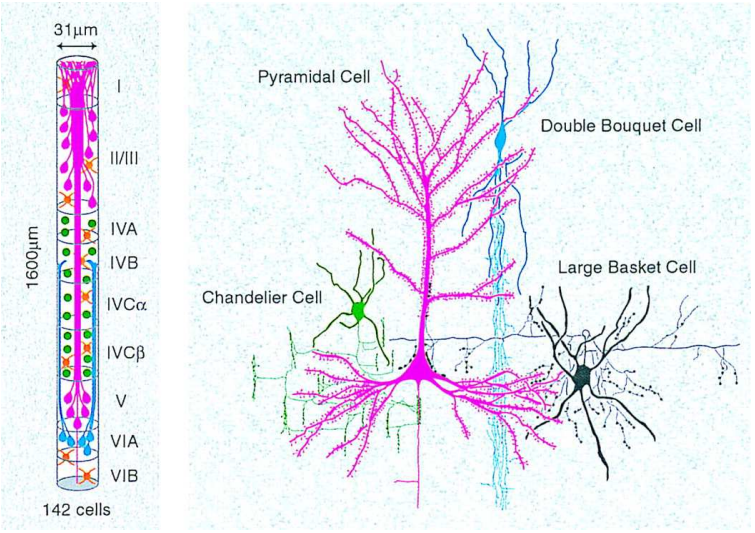

Figure 5.1: Diagram of a cortical "microcolumn" (left) and cell types with diagram of their differing structure (right), reproduced from [8]. Roman numerals (left) correspond to layers of the cortex. This particular microcolumn diagram can be found in the primary visual cortex of macaque monkeys.

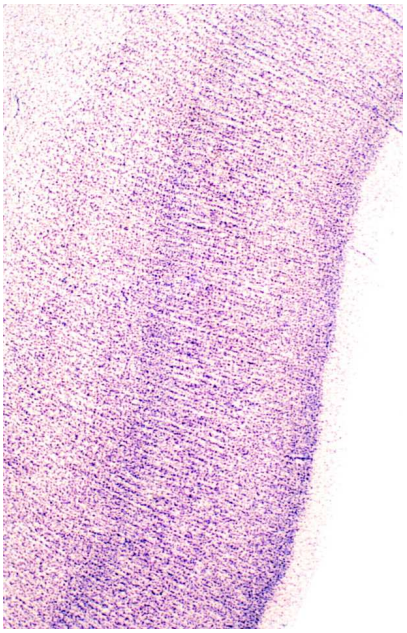

Figure 5.2: A Nissl-stained slice of human cortex (upper bank of superior temporal sulcus) shows striations which correspond to microcolumns spanning multiple cortical layers, reproduced from [8]. Magnification is $\times 40$.

those with more biological realism. If the interpretation of the cellular automata considered here as microcolumns or groups of neurons is correct, then perhaps this extension would be difficult, since individual neurons can exhibit a wide variety of dynamics such as periodic oscillation and repeated rapid firing ("bursting") [15], whereas large groups of cells may not. If the microcolumn interpretation is incorrect and cellular automata may be used to model individual neurons, the techniques developed in this thesis and associated publications may be of particular use to that line of research.

Bibliography

[1] Restrepo, J. G., Dynamics on Networks, class notes, Fall 2011.

[2] MacCluer, C., "The Many Proofs and Applications of Perron's Theorem," SIAM Review, Vol. 42, No. 3, 2000, pp. 487–498.

[3] Restrepo, J., Ott, E., and Hunt, B., "Approximating the largest eigenvalue of network adjacency matrices," Physical Review E, Vol. 76, 2007, pp. 056119.

[4] Hodgkin, A. and Huxley, A., "A quantitative description of membrane current and its application to conduction and excitation in nerve." Journal of Physiology, Vol. 117, 1952, pp. 500–544.

[5] Beggs, J. and Plenz, D., "Neuronal Avalanches in Neocortical Circuits," Journal of Neuroscience, Vol. 23, No. 35, 2003, pp. 11167–11177.

[6] Kinouchi, O. and Copelli, M., "Optimal dynamical range of excitable networks at criticality," Nature Physics, Vol. 2, 2006, pp. 348–351.

[7] Shew, W., Yang, H., Petermann, T., Roy, R., and Plenz, D., "Neuronal avalanches imply maximum dynamic range in cortical networks at criticality," Journal of Neuroscience, Vol. 29, 2009, pp. 15595.

[8] Jones, E., "Microcolumns in the cerebral cortex," Proceedings of the National Academy of Sciences USA, Vol. 97, No. 10, 2000, pp. 5019–5021.

[9] Erdős, P. and Rényi, A., "On random graphs I," Publicationes Mathematicae, Vol. 6, 1959, pp. 290–297.

[10] Erd˝ os, P. and Gallai, T., "Graphs with Prescribed Degrees of Vertices," Mat. Lapok., Vol. 11, 1960, pp. 264–274.

[11] Borobia, A. and Trías, U. R., "A geometric proof of the Perron-Frobenius Theorem," Revista Matematica de la Universidad Complutense de Madrid, Vol. 5, No. 57, 1992.

[12] Keynes, R., "John Zachary Young," Proceedings of the American Philosophical Society, Vol. 143, No. 4, 1999.

[13] Fitzhugh, R., "Impulses and physiological states in theoretical models of nerve membrane," Biophysical Journal, Vol. 1, 1961, pp. 445–466.

[14] Nagumo, J.-i., Arimoto, S., and Yoshizawa, S., "An active pulse transmission line simulating nerve axon," Proc. IRE., Vol. 50, 1962, pp. 2061–2070.

[15] Izhikevich, E., The geometry of excitability and bursting, MIT Press, 2007.

[16] Pastor-Satorras, R. and Vespignani, A., "Epidemic dynamics and endemic states in complex networks," Phys. Rev. E, Vol. 63, May 2001, pp. 066117, 10.1103/PhysRevE.63.066117.

[17] Watson, H. and Galton, F., "On the Probability of the Extinction of Families," Journal of the Anthropological Institute of Great Britain, Vol. 4, 1875, pp. 138–144.

[18] Greenberg, J. and Hastings, S., "Spatial patters for discrete models of diffusion in excitable media," SIAM Journal on Applied Mathematics, Vol. 34, No. 3, 1978, pp. 515–523.

[19] Dowling, J., Neurons and Networks, Harvard University Press, 2001.

[20] Vogels, T., Rajan, K., and Abbott, L., "Neural network dynamics," Annual Review of Neuroscience, Vol. 28, 2005, pp. 357376.

[21] Beggs, J. and Plenz, D., "Neuronal avalanches are diverse and precise activity patterns that are stable for many hours in cortical slice cultures," Journal of Neuroscience, Vol. 24, No. 22, 2004, pp. 5216–5229.

[22] Shew, W., Yang, H., Yu, S., Roy, R., and Plenz, D., "Information Capacity and Transmission Are Maximized in Balanced Cortical Networks with Neuronal Avalanches," Journal of Neuroscience, Vol. 31, No. 1, 2011, pp. 55–63.

[23] Petermann, T., Thiagarajan, T., Lebedev, M., Nicolelis, M., and Chialvo, D., "Spontaneous cortical activity in awake monkeys composed of neuronal avalanches," Proceedings of the National Academoy of Sciences USA, Vol. 106, No. 37, 2009, pp. 15921–15926.

[24] Eurich, C., Herrmann, J., and Ernst, U., "Finite-size effects of avalanche dynamics," Physical Review E, Vol. 66, No. 6, 2002.

[25] Haldeman, C. and Beggs, J., "Critical branching captures activity in living neural networks and maximizes the number of metastable states," Physical Review Letters, Vol. 94, No. 5, 2005.

[26] Beggs, J., "The criticality hypothesis: how local cortical networks might optimize information processing," Philosophical Transactions of the Royal Society A-Mathematical Physical and Engineering Sciences, Vol. 366, No. 1864, 2008, pp. 329–343.

[27] Angioy, A., Desogus, A., Barbarossa, I., Anderson, P., and Hansson, B., "Extreme sensitivity in an olfactory system," Chemical Senses, Vol. 28, No. 4, 2003, pp. 279–284.

[28] Camalet, S., Duke, T., Julicher, F., and Prost, J., "Auditory sensitivity provided by self-tuned critical oscillations of hair cells," Proceedings of the National Academy of Sciences of the United States, Vol. 97, No. 7, 2000, pp. 3183–3188.

[29] Copelli, M. and Campos, P., "Excitable Scale Free Networks," European Physical Journal B, Vol. 56, 2007, pp. 273.

[30] Ribeiro, T. and Copelli, M., "Deterministic excitable media under Poisson drive: Power law responses, spiral waves, and dynamic range," Phys. Rev. E, Vol. 77, 2008, pp. 051911.

[31] Assis, V. and Copelli, M., "Dynamic range of hypercubic stochastic excitable media," Phys. Rev. E, Vol. 77, 2008, pp. 011923.

[32] Song, S., Sjostrum, P., Reigl, M., Nelson, S., and Chkloskii, D., "Highly nonrandom featurs of synaptic connectivity in local cortical circuits," Public Library of Science Biology, Vol. 3, No. 3, 2005, pp. 507–519.

[33] Eguiluz, V., Chialvo, D., Cecchi, G., Baliki, M., and Apkarian, A., "Scale-free brain functional networks," Physical Review Letters, Vol. 67, 2005, pp. 026126.

[34] Wu, A., Xu, X., and Wang, Y., "Excitable Greenberg-Hastings cellular automaton model on scale-free networks," Physical Review E, Vol. 75, 2007, pp. 032901.

[35] Newman, M., "Mixing patterns in networks," Physical Review E, Vol. 67, 2003, pp. 026126.

[36] Hacket, A., Melnik, S., and Gleeson, J., "Cascades on a class of clustered random networks," Physical Review E, Vol. 83, No. 5, 2011, pp. 056107.

[37] Samuelsson, B. and Socolar, J., "Exhaustive percolation on random networks," Physical Review E, Vol. 74, No. 3, 2006, pp. 036113.

[38] Gleeson, J., "Mean size of avalanches on directed random networks with arbitrary degree distributions," Physical Review E, Vol. 77, No. 5, 2008, pp. 057101.

[39] Benayoun, M., Cowan, J., van Drongelen, W., and Wallace, E., "Avalanches in a Stochastic Model of Spiking Neurons," PLoS Computational Biology, Vol. 6, No. 7, 2010, pp. e1000846.

[40] Larremore, D., Shew, W., and Restrepo, J., "Predicting Criticality and Dynamic Range in Complex Networks: Effects of Topology," Physical Review Letters, Vol. 106, 2011, pp. 058101.

[41] Larremore, D., Shew, W., Ott, E., and Restrepo, J., "Effects of network topology, transmission delays, and refractoriness on the response of coupled excitable systems to a stochastic stimulus," Chaos, Vol. 21, 2011, pp. 025117.

[42] Gollo, L., Kinouchi, O., and Copelli, M., "Active Dendrites Enhance Neuronal Dynamic Range," PLoS Computational Biology, Vol. 5, No. 6, 2009, pp. e1000402.

[43] Gomez, S., Arenas, A., Borge-Holthoefer, J., Meloni, S., and Moreno, Y., "Discrete-time Markov chain approach to contact-based disease spreading in complex networks," Europhysics Letters, Vol. 89, 2010, pp. 38009.

[44] Restrepo, J., Ott, E., and Hunt, B., "Weighted Percolation on Directed Networks," Physical Review Letters, Vol. 100, 2008, pp. 058701.

[45] Ott, E. and Pomerance, A., "Approximating the largest eigenvalue of the modified adjacency matrix of networks with heterogeneous node biases," Physical Review E, Vol. 79, 2009, pp. 056111.

[46] Pomerance, A., Ott, E., Girvan, M., and Losert, W., "The effect of network topology on the stability of discrete state models of genetic control," Proceedings of the National Academoy of Sciences USA, Vol. 106, No. 20, 2009, pp. 8209–8214.

[47] Gireesh, E. and Plenz, D., "Neuronal avalanches organize as nested theta- and beta/gamma-oscillations during development of cortical layer 2/3," PNAS, Vol. 105, No. 21, 2008, pp. 7576–7581.

[48] Gray, R. and Robinson, P., "Stability and spectra of randomly connected excitatory cortical networks," Neurocomputing, Vol. 70, 2007, pp. 1000–1012.

[49] Rajan, K. and Abbott, L., "Eigenvalue Spectra of Random Matrices for Neural Networks," Physical Review Letters, Vol. 97, 2006, pp. 188104.

[50] Newman, M., "The Structure and Function of Complex Networks," SIAM Review, Vol. 45, No. 2, 2003, pp. 167–256.

[51] Restrepo, J., Ott, E., and Hunt, B., "Characterizing the Dynamical Importance of Network Nodes and Links," Physical Review Letters, Vol. 97, 2006, pp. 094102.

[52] Pasquale, V., Massobrio, P., Bologna, L., Chiappalone, M., and Martinoia, S., "Self-organization and neuronal avalanches in networks of dissociated cortical neurons," Neuroscience, Vol. 153, No. 4, 2008, pp. 1354–1369.

[53] Tetzlaff, C., Okujeni, S., Egert, U., Wörgötter, F., and Butz, M., "Self-Organized Criticality in Developing Neuronal Networks," PLoS Computational Biology, Vol. 6, No. 12, 2010, pp. e1001013.

[54] Ribeiro, T., Copelli, M., Caixeta, F., Belchior, H., Chialvo, D., Nicolelis, M., and Ribeiro, S., "Spike Avalanches Exhibit Universal Dynamics across the Sleep-Wake Cycle," PLoS ONE, Vol. 5, 2010, pp. e14129.

[55] Hahn, G., Petermann, T., Havenith, M., Yu, S., Singer, W., and Plenz, D., "Neuronal Avalanches in Spontaneous Activity In Vivo," Journal of Neurophysiology, Vol. 104, No. 6, 2010, pp. 3312–3322.

[56] Braitenburg, V. and Shuz, A., Cortex: Statistics and geometry of neuronal connectivity, Springer-Verlag, 1991.

[57] Chauhan, S., Girvan, M., and Ott, E., "Spectral properties of networks with community structure," Physical Review E, Vol. 80, 2009, pp. 056114.

[58] Restrepo, J., Ott, E., and Hunt, B., "Onset of synchronization in large networks of coupled oscillators," Phys. Rev. E, Vol. 71, 2005, pp. 036151.

[59] Sussillo, D. and Abbott, L., "Generating Coherent Patterns of Activity from Chaotic Neural Networks," Neuron, Vol. 63, No. 4, 2009, pp. 423–425.

[60] Copelli, M. and Kinouchi, O., "Intensity coding in two-dimensional excitable neural networks," Physica A, Vol. 349, No. 3–4, 2005, pp. 431–442.

[61] Girvan, M., Callaway, D., Newman, M., and Strogatz, S., "Simple model of epidemics with pathogen mutation," Physical Review E, Vol. 65, 2002, pp. 031915.

[62] Wang, Q., Perc, M., Duan, Z., and Chen, G., "Synchronization transitions on scale-free neuronal networks due to finite information transmission delays," Physical Review E, Vol. 80, 2009, pp. 026206.

[63] Allard, A., Noel, P., Dube, L., and Pourbohloul, B., "Heterogeneous bond percolation on multitype networks with an application to epidemic dynamics," Physical Review E, Vol. 79, No. 3, 2009, pp. 036113.

[64] Miller, J., "Percolation and epidemics in random clustered networks," Physical Review E, Vol. 80, No. 2, 2009, pp. 020901.

[65] Stewart, C. and Plenz, D., "Homeostasis of neuronal avalanches during postnatal cortex development in vitro," Journal of Neuroscience Methods, Vol. 169, 2008, pp. 405–416.

[66] Tanaka, T., Kaneko, T., and Aoyagi, T., "Recurrent infomax generates cell assemblies, neuronal avalanches, and simple cell-like selectivity," Neural Computing, Vol. 21, 2009, pp. 1038–1057.

[67] Harris, T., The Theory of Branching Processes, Springer Verlag, 1963.

[68] Athreya, K. and Ney, P., Branching Processes, Springer Verlag, 1972.

[69] Cohen, R., ben Avraham, D., and Havlin, S., "Percolation critical exponents in scale-free networks," Physical Review E, Vol. 66, No. 3, 2002, pp. 036113.

[70] Lee, D., Goh, K., Kahng, B., and Kim, D., "Branching Process Approach to Avalanche Dynamics on Complex Networks," Journal of the Korean Physical Society, Vol. 44, No. 3, 2004, pp. 633–637.

[71] Melnik, S., Hackett, A., Porter, M., Mucha, P., and Gleeson, J., "The unreasonable effectiveness of tree-based theory for networks with clustering," Physical Review E, Vol. 83, 2011, pp. 036112.

[72] Castellano, C. and Pastor-Satorras, R., "Non-Mean-Field Behavior of the Contact Process on Scale-Free Networks," Physical Review Letters, Vol. 96, 2006, pp. 038701.

[73] Jensen, H., Self-organized criticality: emergent complex behavior in physical and biological systems, Cambridge University Press, 1998.

[74] Zapperi, S., Lauritsen, K., and Stanley, H., "Self-Organized Branching Processes: Mean-Field Theory for Avalanches," Physical Review Letters, Vol. 75, No. 22, 1995, pp. 4071.

[75] Lyons, R. and Peres, Y., Probability on Trees and Networks, unpublished, 2011.

[76] Volz, E., "SIR dynamics in random networks with heterogeneous connectivity," Journal of Mathematical Biology, Vol. 56, 2008, pp. 293–310.